Analysis of Variation in Retinal Vascular Assessment

A thesis submitted in fulfilment of the requirements for the degree of Doctor of Philosophy

Hao Hao

M.Eng

School of Electrical and Computer Engineering

College of Science Engineering and Health

RMIT University

July 2014

Declaration

I certify that except where due acknowledgement has been made, the work is that of the author alone; the work has not been submitted previously, in whole or in part, to qualify for any other academic award; the content of the thesis/project is the result of work which has been carried out since the official commencement date of the approved research program; any editorial work, paid or unpaid, carried out by a third party is acknowledged; and, ethics procedures and guidelines have been followed.

Hao Hao

July 2014

Acknowledgment

It has been a great journey over the last four years where I have experienced a lot of joy and some pain. I would like to thank everyone who joined me on my journey, providing me with their help and support.

Firstly, I would like to express my great appreciation to Professor Dinesh Kant Kumar. His professional knowledge guided me in the right direction and his understanding encouraged me during some difficult times. I would also like to thank Professor Henry Wu for his supervision and valuable advices.

I am particularly grateful for the companionship and support given to me by all of my colleagues at RMIT Biosignals Lab, especially Mohd Zulfaezal Che Azemin, Behzad Aliahmad and Sridhar Poosapadi Arjunan. Technical support provided by David Latter, Rob Michael and Sam Pender is also greatly appreciated

I would like to offer my thanks to my co-authors, Muhammad Bayu Sasongko, Ryo Kawasaki, Tien Yin Wong, Lauren Hodgson, Jie Jin Wang and Carol Yim-lui Cheung. Their expertise and comments were valuable to the papers.

I wish to acknowledge the help provided by the Centre for Eye Research Australia (CERA) and all personnel involved, including Ryan Man, Yumiko Kawasaki, Annie McAuley and Jing (Sophia) Xie.

I would also like to extend my thanks to all volunteers who participated in the retinal photography and RMIT School of Electrical and Computer Engineering for offering me the scholarship.

Finally, special thanks should be given to my parents, Chaoqun Hao and Qizheng Wu, and my sister Wei Hao and her family for their support. I am particularly grateful for the help given by my friends, especially Mark Harris who helped me with proofreading.

Publications

H. Hao, M. B. Sasongko, T. Y. Wong, M. Z. C. Azemin, B. Aliahmad, L. Hodgson*, et al.*, "Does Retinal Vascular Geometry Vary with Cardiac Cycle?," *Investigative Ophthalmology & Visual Science,* vol. 53, pp. 5799-5805, 2012.

H. Hao, D. K. Kumar, B. Aliahmad, and M. Z. C. Azemin, "Improved retinal photography method and visualization of multiple retinal images," in *Computer Applications and Industrial Electronics (ICCAIE), 2011 IEEE International Conference on*, pp. 274-277, 2011.

H. Hao, D. K. Kumar, and B. Aliahmad, "Measure the change of vessel edges across time series retinal images," *AIP Conference Proceedings,* vol. 1559, pp. 80-89, 2013.

H. Hao, D. K. Kumar, R. Kawasaki, M. Z. C. Azemin, and B. Aliahmad, "Normal distribution of cardiac variation in retinal image measurement," in *Biosignals and Biorobotics Conference (BRC),* 2012

H. Hao, D. K. Kumar, B. Aliahmad, M. Z. C. Azemin, and R. Kawasaki, "Mathematical verification of summary formula in retinal vessel diameter measurement," in *Biosignals and Biorobotics Conference, ISSNIP*, 2013

H. Hao, D. K. Kumar, R. Kawasaki, and B. Aliahmad, " Measured Vessel Length in Retinal Vessel Diameter Measurement," in *Biosignals and Biorobotics Conference (BRC),* 2014

H. Hao, D. K. Kumar, M. Z. C. Azemin, and B. Aliahmad, "The measurement of multiple retinal images," in *Medical Measurements and Applications Proceedings (MeMeA), 2011 IEEE International Workshop on*, pp. 345-348, 2011.

H. Hao, D. K. Kumar, B. Aliahmad, M. Z. C. Azemin, and R. Kawasaki, "Using color histogram as the trait of retina biometric," in *Biosignals and Biorobotics Conference (BRC),* 2013

D. K. Kumar, B. Aliahmad, and H. Hao, "Retinal Vessel Diameter Measurement Using Unsupervised Linear Discriminant Analysis," *ISRN Ophthalmology,* vol. 2012, p. 7, 2012.

D. K. Kumar, B. Aliahmad, H. Hao, M. Z. C. Azemin, and R. Kawasaki, "A Method for Visualization of Fine Retinal Vascular Pulsation Using Nonmydriatic Fundus Camera Synchronised with Electrocardiogram," *ISRN Ophthalmology,* vol. 2013, p. 9, 2013.

B. Aliahmad, D. K. Kumar, S. Janghorban, M. Z. C. Azemin, H. Hao, and R. Kawasaki, "Automatic retinal vessel profiling using multi-step regression method," *Conf Proc IEEE Eng Med Biol Soc,* vol. 2011, pp. 2606-9, Aug 2011.

M. Z. C. Azemin, D. K. Kumar, B. Aliahmad, and H. Hao, "Loss of calibre information during vessel segmentation," in *Biomedical Engineering and Sciences (IECBES), 2012 IEEE EMBS Conference on*, pp. 668-672, 2012.

B. Aliahmad, D. K. Kumar, H. Hao, and R. Kawasaki, "Does fractal properties of retinal vasculature vary with cardiac cycle?" in *Biosignals and Biorobotics Conference (BRC), 2013 ISSNIP*, pp. 1-4, 2013.

B. Aliahmad, D. K. Kumar, S. Janghorban, M. Z. C. Azemin, H. Hao, and R. Kawasaki, "Retinal vessel diameter measurement using multi-step regression method," in *Biosignals and Biorobotics Conference (BRC), 2012 ISSNIP*, pp. 1-4, 2012.

Abstract

Changes in retinal vascular parameters have been shown to be associated with systemic vascular diseases. The current assessment of retinal vascular parameters is based on a solo captured image and computer assisted measurement. The solo image assessment ignores the short term, dynamic change of the retinal vessel and its impact on the measurement. Variation in retinal vessel diameter during the cardiac cycle has been debated in the past, while other retinal vascular parameters have never been verified if affected by the cardiac cycle. There is a lack of comprehensive study on the various sources of variation. This thesis has comprehensively studied the variations from the various sources: (i) human cardiac cycle; (ii) multiple graders; (iii) different software; (iv) repeated photographs; (v) region of interest; (vi) the summary method and (vii) measurement protocol. The results showed there was significant change of retinal individual vessel diameters during the cardiac cycle while this change became non-significant after the individual vessel diameters were summarised using a summary method. Other retinal vascular parameters, such as tortuosity, branching angle, LDR and fractal dimension, had little to no variation over the cardiac cycle. Significant variations were found between graders and different measurement software.

This thesis has shown that variation due to the cardiac cycle can be minimised using the ECG synchronised retinal photographs. The work has also suggested that the significant variations between different graders and the measurement software should be considered in all future studies when comparing their results. Number of strategies such as minimum length of measured vessel that reduce the variability in the measurement have also been identified, and these should be considered when developing new methodologies.

To summarise, this thesis has identified variations and their sources in retinal vascular assessment that will contribute to reduce the variability of vessel measurements leading to improved clinical assessment and identified techniques to mitigate some of these.

List of Tables

List of Figures

List of Abbreviations

AVR: Arteriolar-to-Venular diameter Ratio

CI: Confidence Interval

CRAE: the Central Retinal Arteriolar Equivalent

CRVE: the Central Retinal Venular Equivalent

CPDM: Centreline perpendicular diameter Measurement

DVA: Dynamic Vessel Analyser

D (used in 1D, 2D, 3D): Dimension

ECG: electrocardiogram

FA: Fluorescein Angiography

FD: Fractal Dimension

FD_{BC}: Box-counting Fractal Dimension

$FD_{H:}$ Higuchi Fractal Dimension

FPCM: Fixed Point Cross-section Measurement

ICA: Independent Component Analysis

ICG: Indocyanine Green Angiography

IVAN: Retinal vascular diameter measurement software

LDR: Length to Diameter Ratio

OD: Optic Disc

OCT: Optical Coherence Tomography

ROI: Region of Interest

RR: R-R interval; R-wave to R-wave interval

RVA: Retinal Vessel Analyser

SLO: Scanning Laser Ophthalmoscopy

SIVA: Singapore “I” Vessel Assessment (Retinal Vascular Measurement software)

SLR: Single-Lens Reflex

SVP: Spontaneous Venous Pulsation

Contents

Chapter One

Introduction

1.1 Introduction

Retinal imaging provides the only non-invasive visualisation of the microvascular system. Retinal vascular parameters, such as vessel diameter, tortuosity, branching angle, length to diameter ratio (LDR), optimality deviation and fractal dimensions (Wong et al., 2002a, Cheung et al., 2011a, Witt et al., 2006, Sasongko et al., 2010, Kawasaki et al., 2011), are useful measurements of the retinal vasculature. These parameters are associated with disease conditions such as hypertension, stroke, diabetes, coronary heart disease, glaucoma and aging (Wong et al., 2006b, Kaushik et al., 2007, Lindley et al., 2009, Wong et al., 2006a, Kifley et al., 2007, Sasongko et al., 2010, Klein et al., 2007, Amerasinghe et al., 2008).

Retinal vascular assessment methods have evolved with advancement of computers, and image acquisition and analysis techniques. Digital cameras replaced the film camera and the captured image can be displayed directly on screen and stored digitally. Computer assisted analysis has made the measurements more reliable (Couper et al., 2002) and retinal imaging is now a routine ophthalmic examination.

The diameter measurement of the retinal vessels has been widely studied and the changes in diameters have shown association with systemic diseases, genetic and environmental factors (Wong et al., 2006b, Wong et al., 2006a, Xing et al., 2006). There are individual differences in human retinal vasculature, such as vessel size, vessel distribution pattern and number of vessels (Liew et al., 2008). The summary method has been developed to measure retinal vessel diameters quantitatively and to eliminate the variations caused by the individual differences. The individual measures of retinal arterioles and venules are paired and summarised into the central retinal arteriolar equivalent (CRAE) and the central retinal venular equivalent (CRVE) using the summary formulas developed in 1974 and 1999 (Parr and Spears, 1974, Hubbard et al., 1999) and revised in 2003 (Knudtson et al., 2003). The term retinal vessel summary diameter is referred as CRAE and CRVE in this thesis.

The issues of variation in retinal vascular assessment have been raised earlier and a number of sources of variation have been proposed. Retinal pulsation and retinal vascular change during the cardiac cycle have been considered to be one cause of variation, though the extent and origin of retinal pulsation is not accepted by all (Legler and Jonas, 2009, Kain et al., 2010). Chen et al (1994) reported on the variation in the individual vessel diameter during the human cardiac cycle, with retinal arterial and venous diameters varying 3.46% and 4.82% respectively and following the rhythm of the cardiac cycle. Similar or larger variations were reported in retinal arterioles and venules measured at different points in the cardiac cycle by Dumskyj et al (1996) and Knudtson et al (2004) using ECG synchronised retinal photography. Reshef (1999) studied the variation during the human cardiac cycle (termed 'cardiac variation' in this thesis) and its impact on retinal vessel summary diameters using ECG synchronised retinal photographs. Large variations were found and assessment results were different when using and not using ECG synchronisation.

Another source of variation in the retinal vessel is the choice of vessels and the difference between repeated imaging. Significant variations in the summary diameters were noticed in images taken on different days at different locations (Kofoed et al., 2009) despite the strict rule of vessel selection process (Neubaruer et al., 2008). Reshef (1999) reported a significant variation between different photographs taken at the same point in the cardiac cycle, 3.9% for CRVE and 5.6% for CRAE.

Other sources of variation were found due to difference between graders (Sherry et al., 2002) and different software programs (Yip et al., 2012). Studying the variations in retinal vascular measurements is essential to improve the clinical outcomes of the modality, and develop the basis for universal guidelines and for reporting comparable studies.

1.2 Problem Statement

The current method of retinal photography method in retinal vascular assessment is to take an image of the human retina manually and instantaneously at a random time, though cardiac cycle synchronised retinal photography was suggested for accurate assessment results (Dumskyj et al., 1996). Few studies have investigated different sources of variation in retinal vascular measurement and assessment. However, there are a number of limitations in these studies such as experimental equipment, protocol and size. The effect size was questionable in a study where an experiment was conducted on one subject with 30 repeated photographs (Knudtson et al., 2004). Accurate cardiac cycle synchronisation with photography is critical for the assessment of cardiac variation but has not been described (Chen et al., 1994, Reshef, 1999). The manual triggering in other studies (Dumskyj et al., 1996, Knudtson et al., 2004), such as foot switch depression and observation of R-wave, induced uncertain time delays and is questionable. None of the previous studies has considered heart rate variability.

Another concern is that recent advancement in retinal image analysis has resulted in a number of features of the vasculature other than the vessel diameter used in current retinal vascular assessments, such as tortuosity, branching angle and LDR. No study has examined the variability of these parameters over the cardiac cycle.

Apart from the cardiac variation, the dependency of the measurement on the expertise of graders (Couper et al., 2002, Sherry et al., 2002) has been of concern. There is also differences between the protocols of different measurement software (Yip et al., 2012), such as the region of interest, and this may also cause concern for interpreting the results. While previous researchers have studied individual sources of variations; however, no study has comprehensively measured all of the factors simultaneously and determined the combined influence.

Progressing to determine the variability in the retinal vasculature over the cardiac cycle, continuous retinal vessel diameter assessment has been proposed for enhancing

the physiological information (Heitmar et al., 2010). Multiple frames of retinal images are expected to provide a more reliable measure of diameter change (Dumskyj et al., 1996). However, the methodology needs to be developed.

1.3 Hypotheses

This thesis aims to assess the sources of variation in retinal vascular assessment. This thesis has tested the following hypothesis:

i. There are significant variations in retinal vascular assessment due to factors such as the cardiac cycle, repeated photographs, different graders and differences in the software and measurement protocols.

ii. ECG synchronised retinal photographs are able to reduce the cardiac variation.

1.4 Aim and Objectives

The aim of this thesis is to examine the variations and their sources in retinal vascular assessment and to improve the precision of measurement. The objectives are to:

i. Develop proper methodology to study variations in retinal vascular assessment.

ii. Investigate the variations in retinal vascular parameters over the cardiac cycle.

iii. Investigate the variations caused by differences between graders, software and measurement protocols.

iv. Examine the effect of the summary method on variation elimination in retinal vessel diameter measurement.

v. Identify techniques to minimise the systemic error and human bias in the measurement.

vi. Develop methods to assess the variability of retinal vessels in time series retinal images for future study of retinal vessel dynamic change.

This research comprehensively studies the variations and their sources in retinal vascular assessment. It reports the impact of the cardiac cycle on retinal vascular parameters that are used in clinical assessment. This analysis has a direct impact on the clinical application of these techniques. ECG synchronised retinal photography is redesigned and the study suggests the variation reduction in retinal vascular measurement using improved ECG synchronised photography and identified measurement.

1.5 Outline of the Thesis

The chapters of the thesis are organized as follows:

Chapter 1 describes the overall thesis with introduction, problem statement, the hypothesis and the aims, and objectives of the work.

Chapter 2 presents a brief introduction to the human retina, history of retinal imaging, retinal imaging devices, retinal image analysis, retinal vascular assessment and currently used retinal vascular parameters.

Chapter 3 describes the methodology and experiment details, including retinal image acquisition and retinal vascular measurement methods.

Chapter 4 reports the analysis of the impact of the cardiac cycle on retinal vascular parameters.

Chapter 5 investigates the variations in repeated photographs and the effects of graders and software. The issue of minimising cardiac variation using ECG synchronisation is discussed.

Chapter 6 studies the summary methods for variation elimination and discusses the advantages and disadvantages. The impact of different measurement protocols is also discussed. A number of improvements to minimise the variations are suggested.

Chapter 7 presents the methodology of the visualisation and measurement of retinal vessel dynamic change.

Chapter 8 concludes the findings of this thesis and discusses future studies to be undertaken.

Chapter Two

Literature Review

2.1 Human Retina

The retina lines the inner surface of the eye with multiple layered structures, as shown in Figure 2.1. The photoreceptor cells in the retina layers sense the light and the signals are then transferred to the brain via the optic nerve. The retina is considered a part of the central nervous system. Retinal blood supply includes two circulations - uveal and retinal circulations. The uveal circulation supplies blood to the eye uvea layer and outer and middle layers of the retina, while the retinal circulation supplies the inner layer of the retina. The central arteriole and venule bifurcate several times and form the blood supply network with a unique structure pattern. The retina is the only part of the human body where the central nervous system and microcirculation system can be visualised non-invasively (Encyclopaedia, 1987).

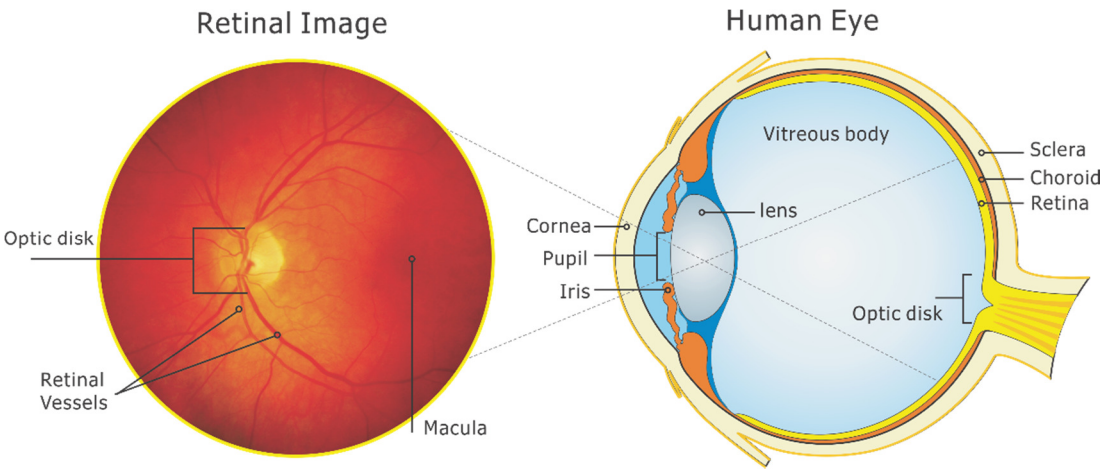

Figure 2.1 Human eye structure and retinal image captured through pupil.

2.2 Retina (Fundus) Imaging

The retina can be visualised with the aid of devices. Czech scientist Jan Evangelista Purkinje invented the principles of ophthalmoscope and his sketches of retinal vasculature were published in 1823 (Jan Evangelista Purkyně, 1823). The first image

of the retina was published by the Dutch ophthalmologist Van Trigt in 1853 after the ophthalmoscope was reinvented and improved by several ophthalmologists (Von Helmholtz, 1851). The ophthalmoscope allows the ophthalmologist a direct view of a patient's retina using external lighting. Since then, retinal examination became routine for ophthalmologists. In 1910, Gullstrand developed the fundus camera and won the Nobel Prize for his invention. His concept of the fundus camera is still used for retinal imaging today (Gullstrand, 1910). The fundus camera builds an optical path between the retina and a camera body. The internal electronic flash sharing the optical path with a reflex mirror provides maximum illumination to the retina and best photography angle. Photography using the fundus camera requires direct illumination to the eye through a relatively small sized pupil. Operation of the pupil dilation by an ophthalmic professional was required.

With the development of digital imaging technology, digital imaging was quickly adapted for retinal imaging. The instant feedback of digital imaging ensures high image quality and the operator is able to adjust exposure settings and camera alignment instantly. In addition, it enhances communication with patients. Digital retinal imaging is believed to be the future as hardware and software continue to evolve and improve in quality (Saine et al., 2002).

Some examples of retinal imaging modalities and techniques are briefly introduced as follows (Saine et al., 2002):

- Ophthalmoscope

An ophthalmoscope provides a direct view of the retina with external illumination at an angle. There is no recording device attached to capture an image or video. The view of the retina is narrow. The advanced Panoptic® ophthalmoscope can have 15 degrees angle of view.

- Retinal Camera

The retinal camera is a low-power microscope with an internal electronic flash and mounted with a 35mm single-lens reflex (SLR) camera or digital SLR camera body. The focus of the retinal camera lens can be adjusted to compensate for refractive errors in the patient's eye. Illumination to the retina is delivered axially and shares the optical path using a reflective mirror box. Most retinal cameras require manual adjustment of the focus and alignment by the operator. The operator can preview the retina on the screen with built-in infrared illumination before the image is captured.

Retinal camera techniques have developed in the aspects of: (i) higher image resolution; (ii) non-mydriatic. Dilatation of the pupils is not required; and (iii) wider angle of view. Retinal camera has a replaceable digital camera body that can be updated to higher resolution. Current retinal cameras have a 30 to 60 degree view of retina without pupil dilation. The larger angle of view can be achieved using wide-angle retinal cameras that often need to illuminate a broader area of retina and require a more-widely dilated pupil. Because of its safety, convenience and cost-effectiveness, the digital retinal camera has remained the primary method of retinal imaging in clinical settings.

- Scanning Laser Ophthalmoscopy (SLO)

The scanning laser ophthalmoscope induces a monochromatic laser beam and scans point-by-point across the retina in a raster pattern (Woon WH et al., 1990). The combination with a confocal optical system produces sole colour and high-contrast images. SLO requires pupil dilation and the angle of view is wide (55 degrees or more; 150 degrees using Ocular Staurenghi 230 SLO retina lens). SLO offers high-speed continuous recording on a digital video format with adjustable frames per second. SLO recordings are rectangular images while retinal camera records the circular images. SLO with narrow wavelength band laser has more efficient excitation of fluorescence and no aerial-image focusing is required. Therefore, it is more suitable for monitoring the flow dynamics, such as Indocyanine Green Angiography or Fluorescein

Angiography, and for calculating the retinal flow velocity (Clark, 2002). The digital systems and SLO's are highly specialised and expensive.

- Stereo Retinal Photography

Stereo retinal photography was first described by Allen Lee (Allen, 1964) to depict three-dimensional (3D) shape of retina using multi-angle images. Stereo separation is achieved by laterally shifting the recording device a few millimeters between sequential photographs. Hyperstereoscopic effect allows brain to fuse the sequential pair of stereo photographs when they are viewed by each eye of the viewer simultaneously but independently. Both SLO and retinal camera can be used for stereo retinal photography.

- Retinal Vessel Analyser(RVA, also called Dynamic Vessel Analyser or DVA)

RVA is a retinal camera attached with a CCD camera and used for online measurement of the retinal vessel diameter in relation to time and locations along the vessel (Seifertl and Vilser, 2002). Continuous illumination and pupil dilation are required. RVA was later developed to record the response of retinal vessel diameter to flicker (Gugleta et al., 2006b). It has been used in studies of retinal blood flow and retinal pulsations (Gugleta et al., 2006a, Paques et al., 2008, Garhofer et al., 2010, Lim et al., 2013). RVA measures the local changes on a paired retinal arteriole and venule from lower resolution video frames.

- Fluorescein Angiography (FA)

A small amount of sodium fluorescein dye is injected into a vein in the patients arm. The dye glows in a yellow-green colour under the blue light. The blood flow in the retinal arterioles and venules can be captured using the retinal camera with a special filter or SLO.

- Indocyanine Green Angiography (ICG)

Different from fluorescein angiography, ICG is able to photograph the choroid that is the layer of the posterior part of the eye and contains a unique network of blood

vessels. ICG use indocyanine dye that fluoresces in the infrared spectrum (Elsner et al., 1994). The images can be recorded on infrared film, a digital camera or SLO.

- Optical Coherence Tomography (OCT)

Retinal OCT was achieved for the first time in 1993 (Swanson et al., 1993) based on OCT tissue-imaging techniques. OCT uses low coherence interferometry to generate cross sectional images of ocular tissue. It analyses the time delay and magnitude change of low coherence light backscattered by ocular tissue. The newest technology of Fourier Domain OCT provides greater tissue resolving power, higher scan density, and faster data acquisition compared to Time Domain OCT (Saine et al., 2002). Retinal imaging is often defined as the two-dimensional (2D) representation of 3D retinal tissues projected on the imaging plane (Ryan et al., 2012). Therefore, OCT imaging is not considered as retinal imaging.

2.3 Retinal Vascular Parameters

Retinal vascular parameters are the features extracted and measured from the retinal image. The technical details of currently used parameters in retinal vascular assessment are briefly provided below:

i. Individual vessel diameter is the diameter measurement of a single vessel at a specific location. The measures are often averaged from multiple cross-sections that are vertical to the vessel direction vector. This parameter was often used in early retinal image analysis (Newsom et al., 1992) or in specific analysis, such as Dynamic Vessel Analyser (Seifertl and Vilser, 2002).

ii. Vessel summary diameter is represented by the central retinal arteriolar equivalent (CRAE) and the central retinal venular equivalent (CRVE) for which the individual vessel diameters are summarised using a summary method (Hubbard et al., 1999, Knudtson et al., 2003).

The summary method was developed to measure the retinal vessel size quantitatively. Parr-Hubbard formulas were developed by Parr et al in 1974 (Parr and Spears, 1974) and Hubbard et al in 1999 (Hubbard et al., 1999) based on experimental data and shown in Eq(1)& Eq(2).

$$Arterioles\ W_c = (0.87W_a^2 + 1.01W_b^2 - 0.22W_aW_b - 10.76)^{1/2} \ldots \text{Eq(1)}$$

$$Venules\ W_c = (0.72W_a^2 + 0.91W_b^2 + 450.05)^{1/2} \ldots \text{Eq(2)}$$

where W_a and W_b are the paired retinal vessel diameters. W_c is the estimate of summary arteriole or venule. With the consistent in Parr-Hubbard formulas, spurious variability was found in the calculation. The revised formulas (Knudtson et al., 2003) were developed to reduce the spurious variability, shown below:

$$Arterioles\ \hat{W} = 0.88 * (w_1^2 + w_2^2)^{1/2} \ldots \qquad \text{Eq(3)}$$

$$Venules\ \hat{W} = 0.95 * (w_1^2 + w_2^2)^{1/2} \ \ldots \qquad \text{Eq(4)}$$

where w_1 and w_2 are the paired retinal vessel diameters. $\hat{W}$ is the estimate of the summary, arteriole or venule.

The branching coefficients 0.88 and 0.95 were estimated based on experimental approximation of Hubbard's experiment, following the formula:

$$Branching\ Coefficient = (w_1^2 + w_2^2)/W^2 \ \ldots. \qquad \text{Eq(5)}$$

where w_1 and w_2 are the widths of the narrower and wider branch, and W is the parent trunk.

After the arterioles and venules are separated and selected, the biggest six arterioles or venules are paired and summarised into CRAE and CRVE using the revised formulas. The pairing process is to pair the largest vessel with the smallest vessel and next largest vessel with next smallest vessel until all vessels are paired. The odd number of vessel will be carried on to the next round of pairing.

iii. Vessel tortuosity, a reflection of the shape of the vessel, is expressed as a tortuosity index (Hart et al., 1999). Vessel tortuosity often has two measures, simple and curvature. Simple tortuosity is a ratio between the actual length of a vessel segment and the shortest distance within the same segment. Curvature tortuosity is calculated from the integral of the total squared curvature along the path of the vessel, divided by the total arc length (Hart et al., 1999). Automatic grading of retinal vessel tortuosity has been studied previously (Grisan et al, 2008).

iv. Branching angle (in degrees) represents the angle between two daughter vessels (Zamir et al., 1979).

v. Length to diameter ratio (LDR) is calculated as the length from the midpoint of the first branch to the midpoint of the second branch divided by the diameter of the parent vessel at the first branch (Sasongko et al., 2010).

vi. Optimality deviation reflects the deviation of the vessel branching from the optimal configuration. Optimality of the vessel network at branching (x, junctional exponent) is determined by the diameter sizes of two daughter vessels relative to the parent vessel (Zamir et al., 1979) and calculated as

$$d_1^x + d_2^x = d_0^x \quad \ldots \quad \text{Eq(6)}$$

where d_0, d_1, and d_2 are diameters of the parent, larger and smaller daughter vessels respectively (Stanton et al., 1995). The greater the value of x, the larger the daughter arterioles are relative to the parent vessel. It has been proposed that in an optimal state, the value of junctional exponent is 3 (Zamir et al., 1979, Patton et al., 2005) and optimality deviation represent the deviation from this value.

vii. Fractal Dimension (FD or D(f)): Retinal vasculature shows a self-similar structure (de Mendonca et al., 2007, Masters, 2004) and fractal dimension of the retinal vasculature is a global measure of the branching pattern complexity. Box-

counting Fractal Dimension (FD_{BC}) and Higuchi Fractal Dimension (FD_H) are investigated in this thesis.

The basic procedure of calculating the FD_{BC} is to cover a binary image with square boxes of decreasing side length L=1/512, 1/ 256, 1/128, …, 1 of the image side length and the number of boxes N(L) containing at least one white pixel are counted. The absolute value of the least squares regression slope of the plot is considered as

$$FD_{BC} = \frac{\log N(L)}{\log L} \quad . \qquad \ldots \qquad \text{Eq(7)}$$

Higuchi Fractal Dimension measures a set of 1D signals (Higuchi, 1988). It overcomes the limitation of Box-counting by calculating the FD in a specific direction and/or in an irregular ROI (Ahammer, 2011). The procedure of calculating FD_H is to convert 2D grayscale images to 1D signals in a specific direction, such as horizontal, vertical or radial. Assuming a set of N discrete observed gray values $s(1),\ s(2),\ ...,\ s(N)$ on each scanning path with fixed regular intervals k, the subsets of new data series $S_k^1,\ S_k^2,\ ...,\ S_k^k$ are defined as $S_k^m : s(m),\ s(m+k),\ s(m+2k),\ ...,\ s\left(m+\left[\frac{N-m}{k}\right]k\right)$ where integer $m = 1,2,...,k$ and [ ] denotes the *floor* function (the largest previous integer). Then the curve length is calculated as

$$L_m(k) = \frac{A}{k}\left(\sum_{i=1}^{\left[\frac{N-m}{k}\right]} \left| s(m+ik) - s(m+(i-1)k) \right|\right) \qquad \ldots \qquad \text{Eq(8)}$$

where $A = \frac{N-1}{k\left[\frac{N-m}{k}\right]}$. The total curve length is obtained by averaging the k sets of $L_m(k)$.

The Higuchi fractal dimension is calculated as

$$FD_H = \frac{\log L(k)}{\log k} \quad \ldots \quad \text{Eq(9)}$$

2.4 Retinal Image Processing and Analysis

Retinal image analysis methods have been developed over the last two decades. Initially, a negative film of a retina photograph was displayed on a light box and the parameters were manually measured using a ruler (Newsom et al., 1992). Computer assisted analysis has been used in recent years and proven more reliable compared to manual measurements (Couper et al., 2002). Due to low contrast and low brightness of retinal photographs, computer assisted retinal image analysis requires image-processing techniques, briefly introduced as follows.

- Retinal Image Enhancement

Retinal images are captured with the light reflected through a small pupil and gel-like vitreous body. The big retinal vessels are approximately several hundred micrometers in diameter; for example, the diameter of the central retinal artery is approximately 160 micrometers. The low light condition induces noise and low contrast of retinal vessels to the background. In order to extract and analyse the features from an image, contrast enhancement and artefacts removal are necessary.

Colour information in the retinal images is useful for vessel classification and some disease identification. However, most features can be extracted from grayscale images (Che Azemin, 2012). Grayscale retinal image can be converted from RGB colour image or extracted from the green channel that shows more contrast than other or combined channels.

Depending on the study objective (e.g. retinal vessels, hemorrhage, optic disc or fovea), the enhancement methods and algorithms are specialised, for example, domain knowledge based enhancement for regional hemorrhage detection (Joshi and Sivaswamy, 2008), contourlet based enhancement for segmentation of blood vessel

(Rezatofighi et al., 2008), model based vessel enhancement using Independent Component Analysis (ICA) (Hani and Nugroho, 2009), and other common image processing techniques (e.g., histogram equalization and Gaussian noise removal).

- Optic Disc (OD) Identification

The optic disc (also called: optic nerve head) is the beginning of the optic nerve and the entry point of major blood vessels which supply the retina. It is often called 'the blind spot' because there are no light sensitive cells at this spot. In a retinal image, OD is often a disk shape and brighter than other areas, though this may not be true in some eyes, especially with some medical conditions (Quigley et al., 1990). Difference in the brightness is often used for OD identification. The retinal images analysed in this thesis are OD centred, though some retinal vascular assessments use fovea or another region as the centre or reference.

OD identification and OD diameter calculation provide the references for the study region and vessel locations. It is also used for the conversion between the image pixels and real value of size (measurement unit: micrometer, μm or micron).

There are a number of algorithms to implement automatic OD identification (Walter and Klein, 2001, Muramatsu et al., 2011, Xu et al., 2007, Niemeijer et al., 2008, Zhu et al., 2010). Most OD identifications draw a circle around the OD. However, this may not reflect the real shape of OD (Quigley et al., 1990). Optic disc can be flat or have a certain amount of cupping.

- Retinal Vessel Segmentation, Tracking and Classification

The accurate extraction of retinal vessels and vascular tree forms the backbone for future tracking and classification of arterioles and venules in computer assisted measurements. Due to the complexity of retinal vessel structures and the individual differences in person and vessel, automated retinal vessel segmentation remains challenging in current retinal image analysis. The edges of retinal vessels are not clear and often have artefacts, especially when the vessel is tiny or lighting noise is

induced. For example, the vessels can be misidentified due to low contrast in intensity or colour; the discontinuous vessel edges are difficult for vessel tracking process; a vessel with the centre reflex caused by the reflection of flash may be misidentified as two vessels (Sofka et al, 2006). A survey on multiple retinal vessel segmentation algorithms (Fraz et al., 2012) compared a number of methods, such as supervised approaches, unsupervised approaches, matching filtering and model based approaches. The performance of supervised classification is better in general than the other segmentation algorithms. Though many promising techniques and algorithms have been developed, current retinal assessment often uses semi-automated computer assisted systems, with manual intervention from a grader.

2.5 Retinal Vascular Assessment and Diseases

Semi-automated computer assisted retinal vascular assessment systems have found that a number of retinal vascular parameters are associated with systemic diseases and other factors.

Among a number of retinal vascular parameters, the measurement and analysis of the retinal vessel diameter is the most used method for the assessment of diseases. Google scholar search (scholar.google.com.au, 2013) shows 15000+ results related to retinal diameter and this is more than any other retinal vascular parameters being studied. Population-based studies compare the case and control groups to identify the retinal arteriolar or venular narrowing or widening. Retinal vessel summary diameters have been reported to exhibit association with human systemic abnormality, such as aging and ethnicity (Wong et al., 2003, Kawasaki et al., 2006, Cheung et al., 2007), blood pressure/hypertension (Ikram et al., 2006, Liew et al., 2006b, Wong et al., 2006b, Kaushik et al., 2007), diabetes (Ronald et al., 2006, Wong et al., 2006a, Wong et al., 2005a), stroke (Wong, 2004, Baker et al., 2008, Lindley et al., 2009), coronary heart disease (Wong et al., 2002b, Wang et al., 2006a, Kim et al., 2011), inflammation and

endothelial dysfunction (Hecke et al., 2006, Wong et al., 2006a), renal dysfunction (Wong et al., 2004d, Sabanayagam et al., 2009), Metabolic Syndrome and obesity (Wong et al., 2004a, Wang et al., 2006b), and ophthalmic diseases (Ikram et al., 2005, Amerasinghe et al., 2008, Pluhacek and Pospisil, 2010). The differences caused by environmental factors, such as alcohol consumption (Ikram et al., 2004, Wong et al., 2006a), smoking (Klein et al., 2006, Wong et al., 2006b), medication (Klein et al., 2001, Wong et al., 2005b, Liew et al., 2006a), pollution (Louwies et al., 2012) and genetic factors (Taarnhøj et al., 2006, Xing et al., 2006, Lee et al., 2004), have also been found in retinal vessel summary diameter.

The associations of other retinal vascular parameters with disease have been investigated. Fractal analysis of retinal image has shown association with stroke (Cheung et al., 2010, Doubal et al., 2010, Kawasaki et al., 2011), heart disease mortality (Liew et al., 2011) and diabetes (Grauslund et al., 2010). Tortuosity, LDR and branching angle are related to systemic diseases (Cheung et al., 2011b, Cheung et al., 2011a, Sasongko et al., 2010).

2.6 Retinal Pulsation and Cardiac Variation

Retinal pulsation has been known since 1853, but the origin of this phenomenon is still under debate. Arterial pulsation was initially considered to be pathological while venous pulsation was regarded as being physiological (Weinstein, 1939). Theories have been developed over the years to attempt to discover the origin of spontaneous venous pulsation (SVP). The wave of arterial pulsation was believed to transpire through the capillaries into the vein, thus inducing SVP. This was rejected when Serr's experiment excluded transmission of the trans-capillary pulse (Serr, 1937). Classic theory was accepted by latter researchers, that the difference between intraocular pressure and retinal venous pressure causes the vein to pulsate (Bailliart, 1918, Williamson-Noble, 1952). However, Levine (1998) found that classic theory was inconsistent in postulating

and not in accordance with experimental data. Levine presented the alternative theories that venous pressure is always higher than intraocular pressure and both fluctuate in phase. The maximum amplitude of the pulsation occurs at the exit point and then decreases proximally to small amplitude relative to the diameter of the vein. The extent of large amplitude pulsations is influenced uniformly by pulse rate, venous resistance and venous capacitance. This theory offers insight into individual variability of spontaneous retinal venous pulsation. Currently, the presence of spontaneous retinal venous pulsation is believed to be due to the increased central retinal venous pressure and intracranial pressure (Legler and Jonas, 2009). Intracranial pulse pressure may be of equal importance to intraocular pulse pressure in producing retinal venous pulsation (Kain et al., 2010).

The assessment of SVP has clinical importance. The presence of SVP is less common in glaucoma eyes and is useful for the diagnosis of glaucomatous optic neuropathy and retinal vein occlusions (Morgan et al., 2004).

Retinal venous pressure, intraocular pressure and intracranial pressure vary with the rhythm of the cardiac cycle (Levine, 1998). Retinal vessel diameter has been found to vary during the cardiac cycle. Chen et al (1994) found that retinal arterial and venous diameters vary 3.46% and 4.82% respectively during the cardiac cycle and follow its rhythm. Dumskyj et al (1996) and Knudtson et al (2004) reported similar or larger variation at different points in the cardiac cycle using ECG synchronised retinal photography, though changes did not follow the rhythm of the cardiac cycle.

2.7 Summary

This chapter has described the anatomy of the human eye, the history of retinal imaging and the development of retinal imaging devices. A review of the literatures on retinal vascular assessment with association of diseases has been provided. The review

focused on the impact of cardiac cycle and other sources on currently used analysis methods and retinal vascular parameters.

Further to the investigation of variations and their sources in retinal vascular assessment, this thesis has proposed the followings:

i. Design a system to capture retinal images at different time frame of the cardiac cycle and identify the methods to analyse the captured images (Chapter 3).
ii. Study the effects of the cardiac cycle on retinal vascular parameters (Chapter 4).
iii. Investigate other sources of variation and their impacts on retinal vascular assessment (Chapter 5 and 6).

Chapter Three

Methodology

3.1 Introduction

This chapter details the methodology used in this thesis, including retinal image acquisition, experiment design and retinal image measurement and analysis methods. A novel Electrocardiogram (ECG) synchronised retinal photography method has been designed to capture time series retinal images during the cardiac cycle. The retinal camera can be triggered electronically and automatically at the designated time delays based on real-time calculated R-wave to R-wave (R-R) intervals. This chapter describes experiment design and image acquisition using ECG synchronised retinal photography and introduces the retinal vascular parameter measurement and related software.

3.2 Automatic ECG Synchronised Retinal Photography

Previous studies of the cardiac variation showed limitations in the methodology of accurate cardiac cycle (mostly ECG) synchronisation (Dumskyj et al., 1996, Knudtson et al., 2004). Manual triggering of the retinal camera, such as the trigger activated by foot switch depression or activated after the observation of ECG R-wave, induced an unpredictable time delay. Furthermore, when calculating the triggering time delay at each cardiac cycle point, fixed time delay or the computation based on fixed R-R interval were used. Heart rate variability, where heart rate and R-R interval exhibit random variations, was ignored. In addition, previous studies did not consider the system and camera time delay when referring the triggering points to the cardiac systole and diastole.

Reliable and accurate ECG synchronised retinal photography is essential for the studies. A specially designed ECG synchronisation unit was built to connect retinal camera with minimum modification to the system, with only the camera trigger push button replaced, as shown in Figure 3.1.

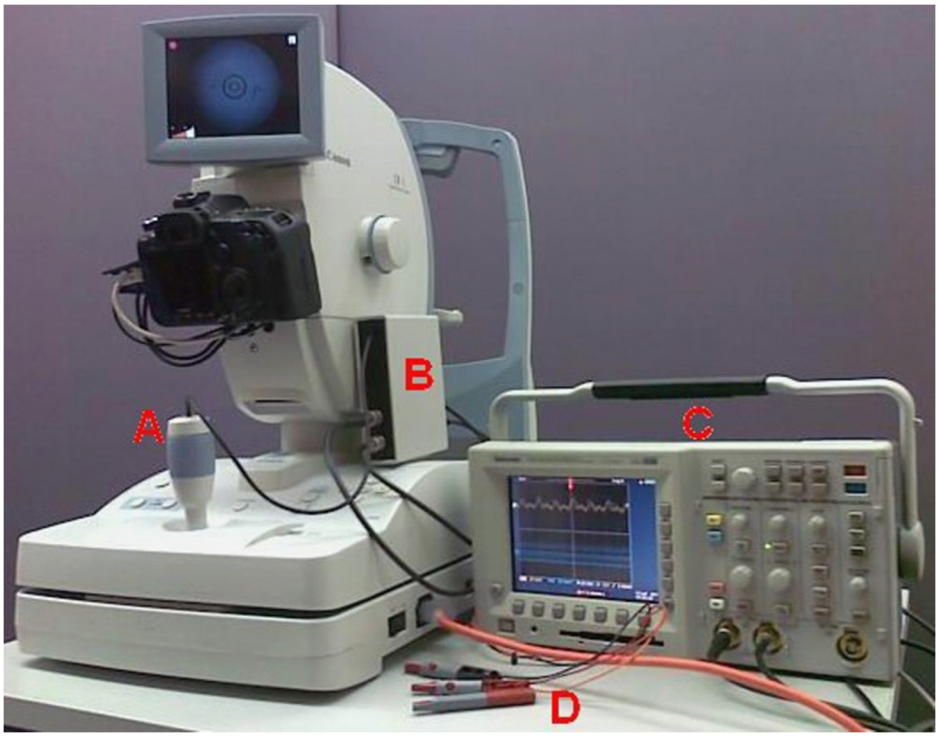

Figure 3.1 ECG synchronised retinal camera photography system used in this thesis. (A) Retinal camera trigger button with connection to ECG synchronisation unit. (B) ECG synchronisation unit. (C) Battery powered oscilloscope (D) ECG Electrodes.

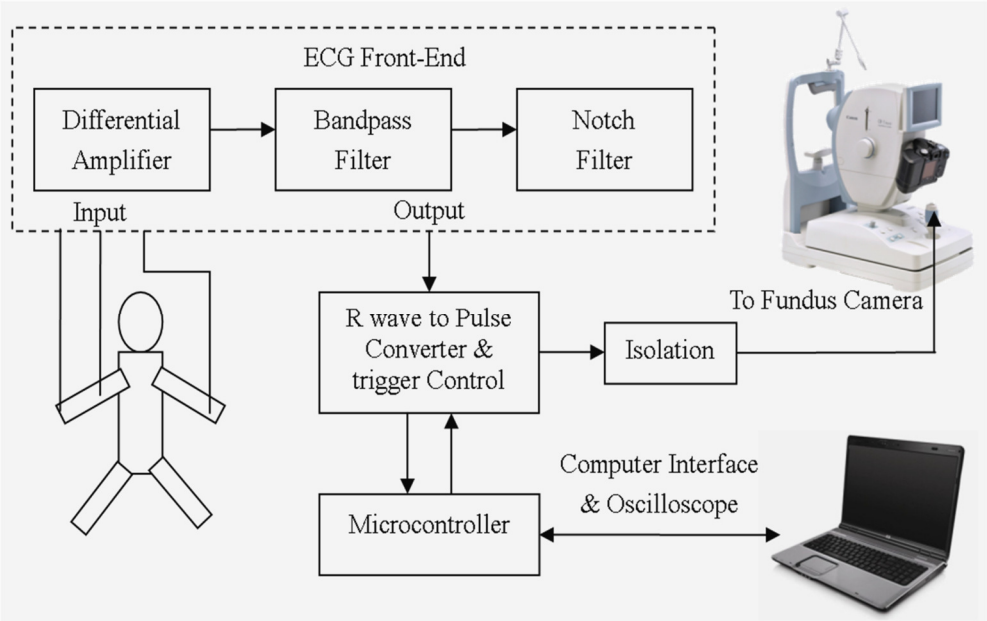

Figure 3.2 ECG synchronised retinal photography system diagram

A 3-lead ECG monitoring unit along with a purpose built microcontroller (Arduino Uno, www.arduino.cc) was used to identify the R-wave and obtain the R-R interval in real time, and to generate a trigger pulse for acquiring the retinal image, as shown in Figure 3.2. R-R interval detection and R-wave identification were parallel-processed in microcontroller analog and digital channels simultaneously. The hardware-based approach avoided unpredictable time delay. The overall system time delay, including those from ECG synchronisation unit and retinal camera system, was 68 milliseconds after manual measurement on the oscilloscope. This ensured correct reference to the cardiac systole and diastole. The triggering mechanism was electronically connected with the ECG synchronisation unit and this allowed for automatic triggering of the camera. The ECG signal and triggering pulse were monitored on an oscilloscope by the examiner during the experiment, and recorded along with the retinal images on the laptop computer with a timestamp. This ensured that the retinal photograph was synchronised with the cardiac cycle.

Based on the typical resting heart rate of 60–100 beats/minute in adults, R-R interval was considered to be abnormal if the detected R-R interval was larger than 1000 or less than 600 milliseconds. No retinal image was taken in such a case and an alarm was raised for the examiner. The validation algorithm for this purpose is shown in Figure 3.3.

3.3 Experiment and Data Acquisition

3.3.1 Ethics

The ethics application (ASEHAPP 54 – 10) was approved on 19 August 2010 by RMIT Research Ethics Committee (CHEAN, College Human Ethics Advisory Network). The amendment and extension were approved on 15 May 2012. This study was conducted in accordance with the principles of the Declaration of Helsinki of 1975, as revised in 2008.

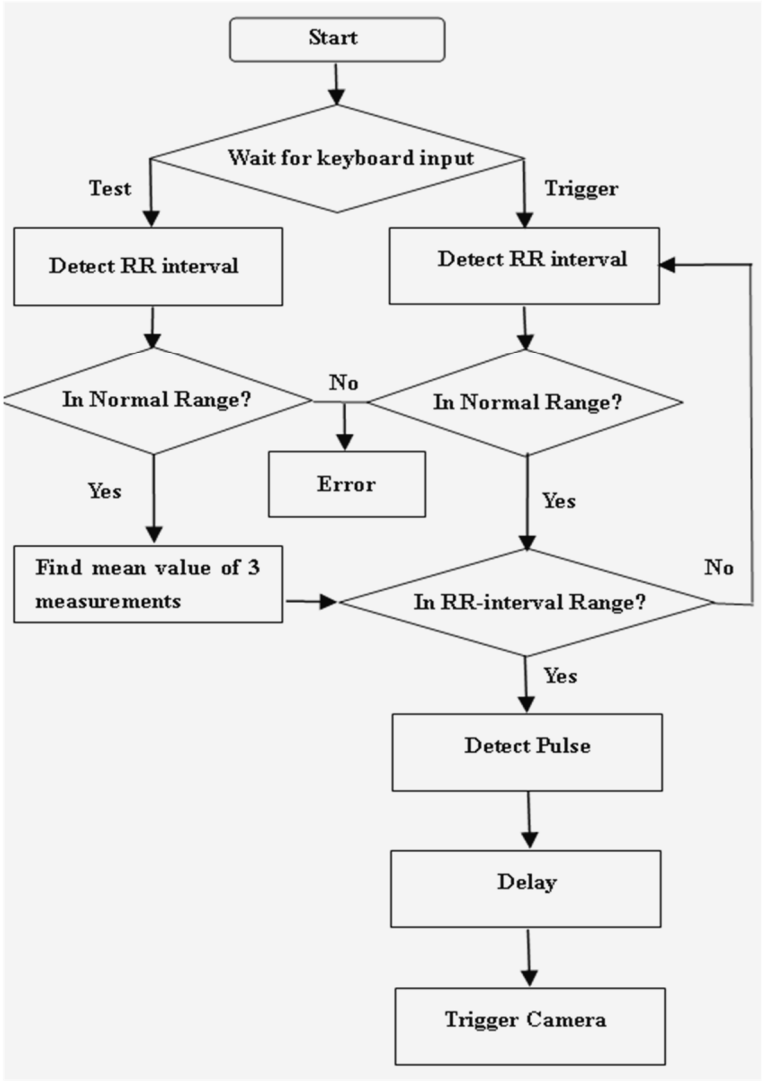

Figure 3.3 Flow chart of real time R-R interval detection and validation

Volunteer participants with a minimal age of 18 were recruited domestically within the state of Victoria, Australia. Written consent was obtained and a questionnaire administrated to each participant prior to the experiment. The questionnaire included information of the participant's age, gender, height, weight, medical history, medication, smoking status and information on glasses wearing if applicable. The medical history was limited to cardiovascular disease, diabetes, ophthalmic disease and eye surgery. The participant's blood pressure was measured before and after retinal photography using a standard cuff blood pressure measurement device.

Participants could request their own retinal photos to be sent to their email box before their identification information was removed to ensure privacy. The individuals were only identified using numerical ID, for example subject '001'.

3.3.2 Data Acquisition

Canon non-mydriatic retinal camera CR-I equipped with Canon EOS 50D digital SLR camera body was used in this thesis. An ECG synchronisation unit was connected to the retinal camera. ECG electrodes were the round shape 3M® electrodes with conductive touch in the middle. After connecting electrodes to the volunteer participant's wrists of both arms and the elbow of right arm (ground) which were cleaned with alcohol-based wipe, ECG signal was monitored on the battery-powered oscilloscope and by the flashing LED. The sensitivity level was adjusted to ensure that the flashing LED corresponds to the pulse rate.

ECG synchronised retinal camera can be triggered at any time delay after the detected R-wave following operator commands from the computer. After testing, the eight divisions of R-R interval (RR) were chosen to balance the discomfort to subjects and the proper presence in the cardiac cycle. This was also comparable with previous studies.

A time of 0.125*RR was calculated as the base time delay. Numerical commands were sent from the computer interface to the microcontroller for operating retinal camera. The number '0' was used to test R-R interval. For the camera triggering point n, the image was photographed at time delay of (n-1)*0.125*RR after R-wave. For example, the number '1' was to trigger the retinal camera at R-wave and '2' was to trigger at 0.125*RR time delays after R-wave. ECG signal and triggering pulse were monitored by the examiner on the oscilloscope to ensure accurate trigging. The examples are shown in Figure 3.4 and Figure 3.5. The retinal photos were transferred

to the computer automatically and electrically. ECG R-R interval and trigger information were recorded electrically in the same folder as the captured retinal photos.

Each participant was asked to keep seated and relaxed during the experiment of taking nine photographs. No drink or food was allowed during the experiment. Only left eyes were photographed according to the previous study that high correlation was found between left and right eyes (Leung et al., 2003a).

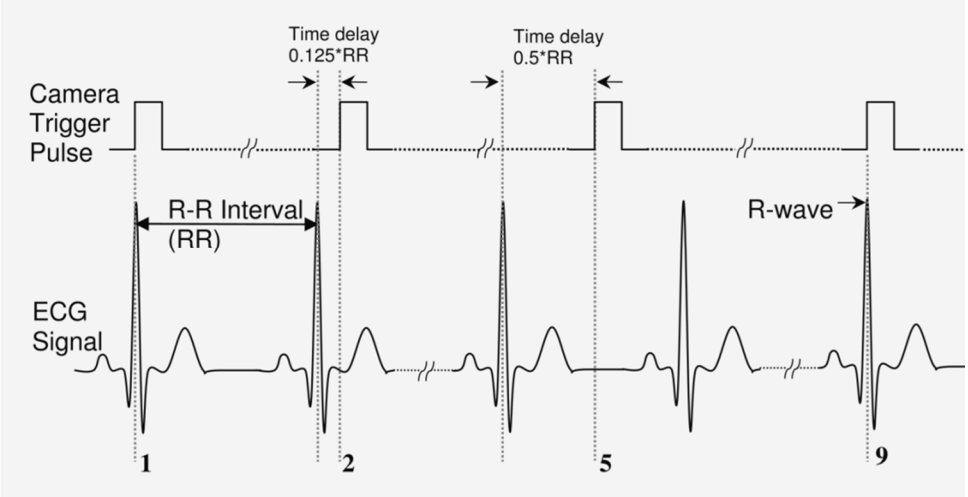

Figure 3.4 Time delay calculation and cardiac cycle points when retinal image are captured. The 1st and 9th points are corresponding to R-wave and other seven points are equally distributed during the cardiac cycle. Figure illustrates the outputs of ECG signal and trigger pulse at 1st, 2nd, 5th and 9th point.

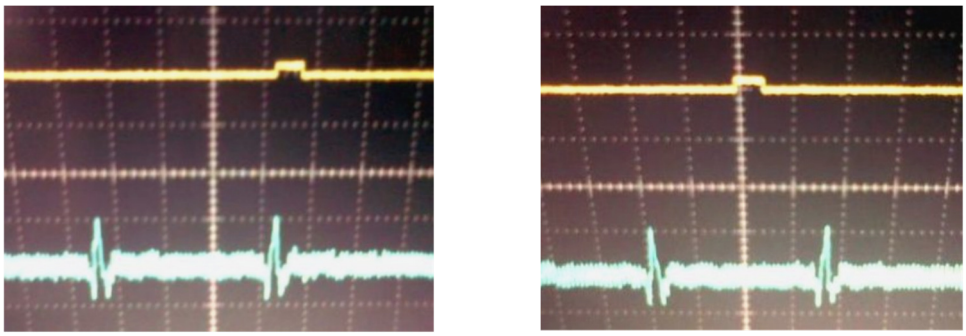

(a) (b)

Figure 3.5 Oscilloscope display of ECG and camera triggering pulse (a) at 1st point (R wave); and (b) at 5th point (half R-R interval time delay).

3.4 Retinal Vascular Parameter Measurement

In this thesis, retinal vascular parameters were measured using several standard and customised computer assisted systems. Blinded grading was performed with each of these systems for all measurements. The grading was performed on one image at a time following a standardised protocol, and during the grading, the other images were masked to avoid any bias. In addition, the image frames (01 to 09) for grading were randomised to eliminate potential systematic error. Images were considered as 'poor quality' if they were blurred or had incomplete representation of the measured zones, and marked as 'ungradable' if there were fewer than 4 gradable large arterioles or venules.

3.4.1 Measurement of Retinal Vascular Geometry using SIVA

SIVA (Singapore 'I' Vessel Assessment version 3.0, Singapore) measurement technique has been described previously (Cheung et al., 2011a, Sasongko et al., 2010). Briefly, SIVA automatically detects the centre of the optic disc and divides the region into 3 concentric subzones surrounding the optic disc. Each zone corresponds to the area between optic disc margin to 0.5 optic disc diameter (Zone A), 0.5 to 1.0 disc diameter (Zone B) and 0.5 to 2.0 optic disc diameters (Zone C) away from the optic disc margin. SIVA measures retinal microvascular geometric parameters in Zone B and Zone C respectively. The grader confirms the correct detection of the optic disc and the three concentric subzones by the program, and then the grader executes the program to generate a line tracking of the retinal vessels. This software also has an automated function to identify arterioles and venules, indicated by two different colours generated by the program, red for arterioles and blue for venules. The grader subsequently checks whether all arterioles and venules are correctly identified and the software allows the grader to make any corrections if required (Figure 3.6). Measurements using SIVA are based on the summary of the arterioles and venules separately. The software combines the individual measures into summary diameters, tortuosity, branching angles,

LDR and optimality deviation separately. The technical details of these parameters have been introduced in Chapter 2.

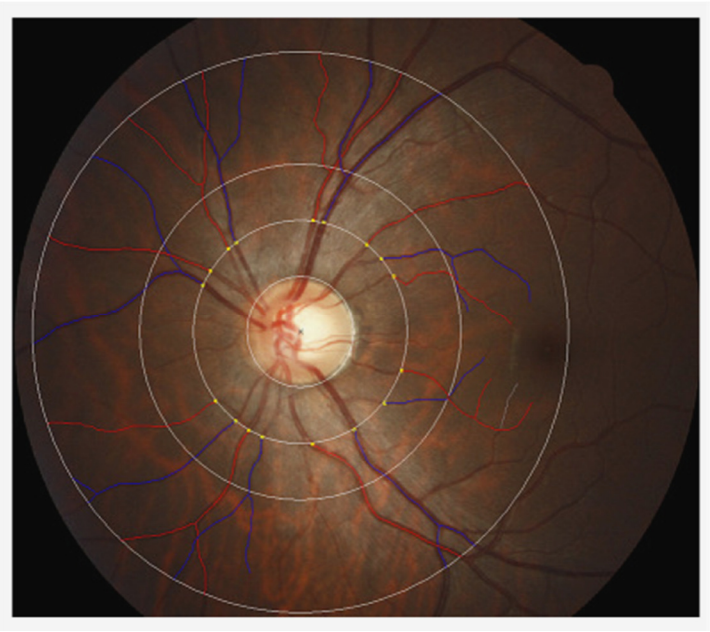

Figure 3.6: Retinal image is measured using SIVA.

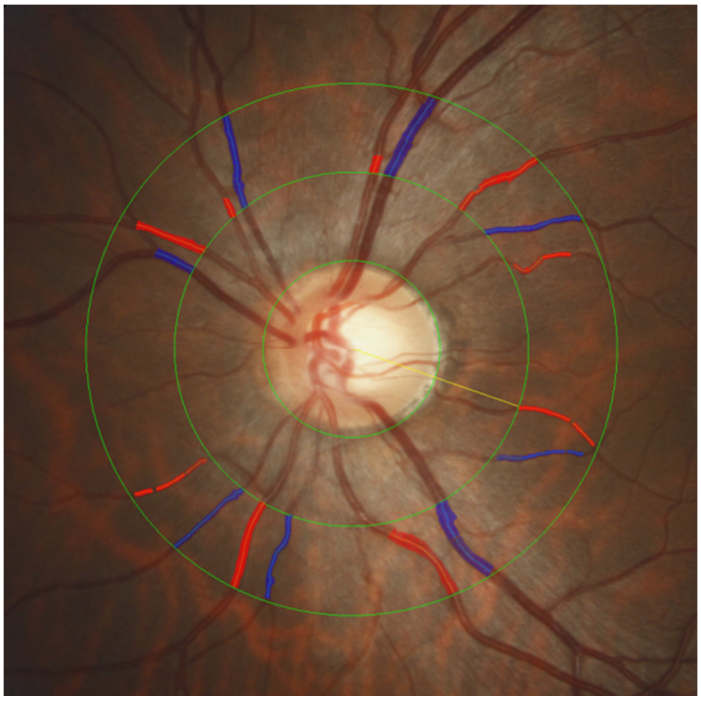

Figure 3.7 Retinal image is measured using IVAN.

3.4.2 Measurement of Retinal Vascular Geometry using IVAN

Another semi-automated retinal image analysis software (IVAN, Department of Ophthalmology Visual Science, University of Wisconsin, Madison, WI) is compared in this thesis. The IVAN measurement procedure has been previously described (Wong et al., 2004c, Sherry et al., 2002) and is similar to SIVA. An example of IVAN measurement is shown in Figure 3.7. Apart from the different approaches of image processing techniques, the major differences between IVAN and SIVA measurements are that (i) IVAN performs the measurement only in zone B while SIVA is able to measure the vessels in Zone B and Zone C; (ii) IVAN only measures retinal vessel diameter related parameters (CRAE, CRVE and AVR) while SIVA is also able to measure other retinal vascular parameters, such as tortuosity and branching angle.

3.4.3 Measurement of Retinal Individual Vessel Diameter

To study the variations of a single retinal vessel, the diameter of the individual vessel at a single cross-section is measured using specially developed software, which is programmed on the platform MATLAB (The MathWorks Inc., USA). The vessel is manually located in the first frame approximately 1.0 to 2.0 disk diameters from the optic disk (Figure 3.8). Twenty cross-sectional profiles of the vessel are obtained and modeled using a combination of Gaussian and Twin Gaussian functions (Gao et al., 2000) where the diameter of the vessel is estimated as the maximum distance between a pair of two peaks of the second order derivatives of the Gaussian model. Although ECG synchronised retinal photographs were captured during a short period and the participants were asked to sit still during photography, there are displacement and motion artifacts in the captured time series images. Commercial retinal registration software (i2k Retina®, DualAlignTM) based on previous detailed algorithm (Stewart et al., 2003) is used to register all images of same participant to ensure the sampling of the cross-sections at the same spatial location.

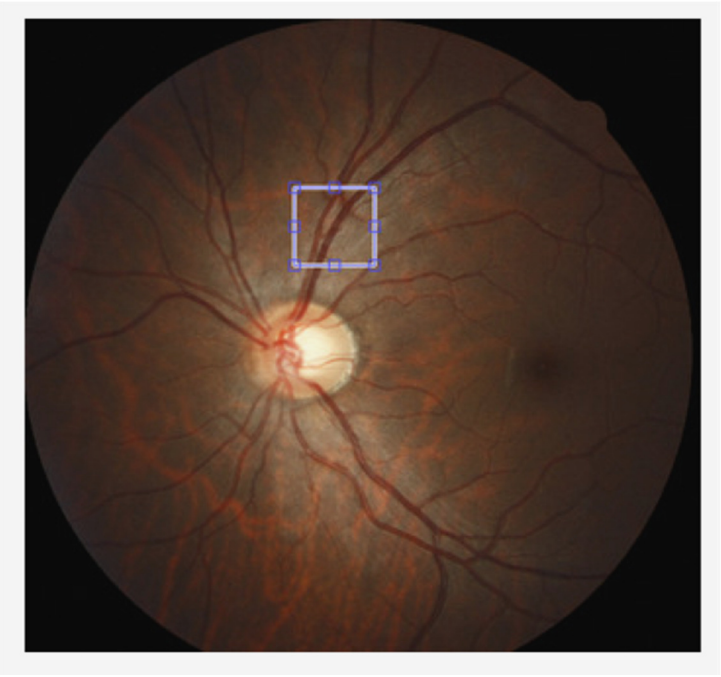

Figure 3.8 Blue box indicates the location of individual vessel diameter measurement. Individual vessel diameter measurements are calculated from 20 cross-sections from arteriole and venule segments.

3.4.4 Measurement of Continuous Retinal Vessel Diameter Change

A Matlab based software program is developed to assess the continuous change of retinal vessel over time. The technique is presented below.

3.4.4.1 Image Pre-Processing

ECG synchronised retinal photographs are down-sampled and registered to the first frame using i2k Retina®. All images in our database are disk-centred and have higher intensity value of OD compared to background. Automatic OD detection is based on labeling of the brightest segments after Gaussian blurring and calculating Euclidean distances between the segments. After the approximate OD centre is identified and then nearby segments are grouped, a circle is drawn automatically to form the grouped segments into OD. The circle centre and circle diameter are automatically calculated as OD centre and OD diameter (R).

Three concentric circles are drawn from the OD centre automatically on the image to outline the optic disk (0.5*R), area with R diameter and area with 2*R diameter from the OD centre (Figure 3.9). The area between 0.5*R and 2*R diameter overlaps Zone B and covers three quarters of Zone C. The reason for using 2*R circle instead of 2.5*R circle (Zone C) is that some images do not fully cover Zone C. This ensures that the vessels are comparable in the standardised area. The concentric circles are automatically drawn across the registered images.

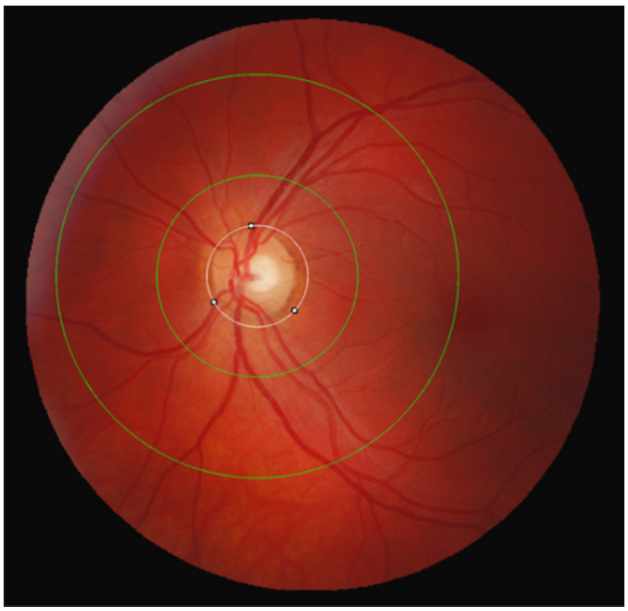

Figure 3.9 Retinal image with optic disk (white circle) and the concentric circles.

3.4.4.2 Vessel Edge Detection

The traditional edge detection algorithms are often inefficient in the edge extraction of retinal vessels due to the artifacts, such as light reflection and central reflex. The gradient-based edge detection (Oram et al., 2008) is used by convolving the image with the second order derivative of Gaussian filter. In second order derivative of Gaussian, the gradient of the image I is given by the vector $\nabla^2 I = \left[\frac{\partial^2 I}{\partial x^2}, \frac{\partial^2 I}{\partial y^2}\right]$. The image is smoothed with Gaussian mask G to remove the artifacts. Gaussian mask and

convolving the image with this mask are combined as $\nabla^2(G \otimes I) = \nabla^2 G \otimes I$

The direction gradient is given by $\tan^{-1}(\frac{\partial^2 I}{\partial y^2} / \frac{\partial^2 I}{\partial x^2})$.

The gradient-based edge detection was reported as having the problems of missing corners and generating closed contours (Umbaugh, 2011). However, the proposed software benefits from these for producing the continuous and smooth edges, shown in Figure 3.10.

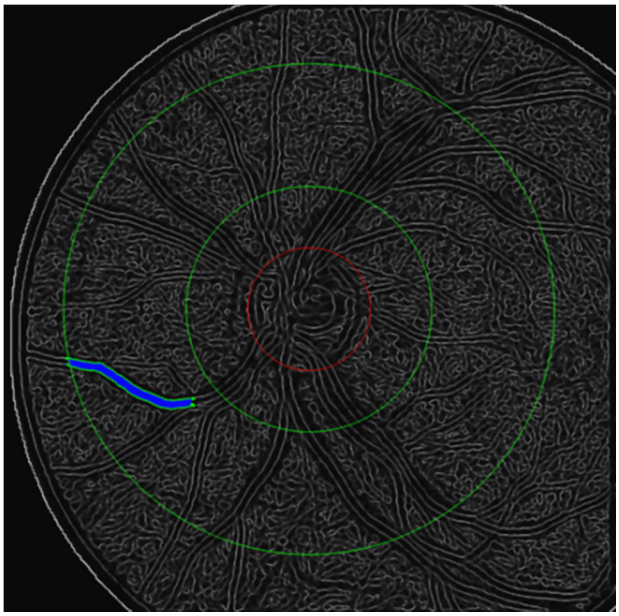

Figure 3.10 Retinal vessels are enhanced with the continuous binary contours using gradient-based edge extraction. Vessel tracking is performed using neighbourhood searching.

3.4.4.3 Vessel tracking

Semi-automated vessel-tracking algorithm is used to ensure correct vessel tracking. The algorithm requires manual selection of two starting points and a third point for indicating the direction of tracking. The automatic tracking process is monitored by the grader and reselection is encouraged when tracking error occurs.

The automatic tracking process searches 5x5 pixels neighborhood to find the linked pixels close to the starting points. Then the mask is reduced to 3x3 neighborhood to track linked pixels. The detector traces the 8 connected neighbourhood pixels in

binary image. Nonzero pixels link to original point and 0 pixels constitute the background. If the linked pixels are more than one, the tracking follows these pixels until the maximum distance is decided. Tracking continues to the longest distance in the designated area. In Figure 3.11, the tracked vessel edges and the centreline that is the average value between two edges are shown.

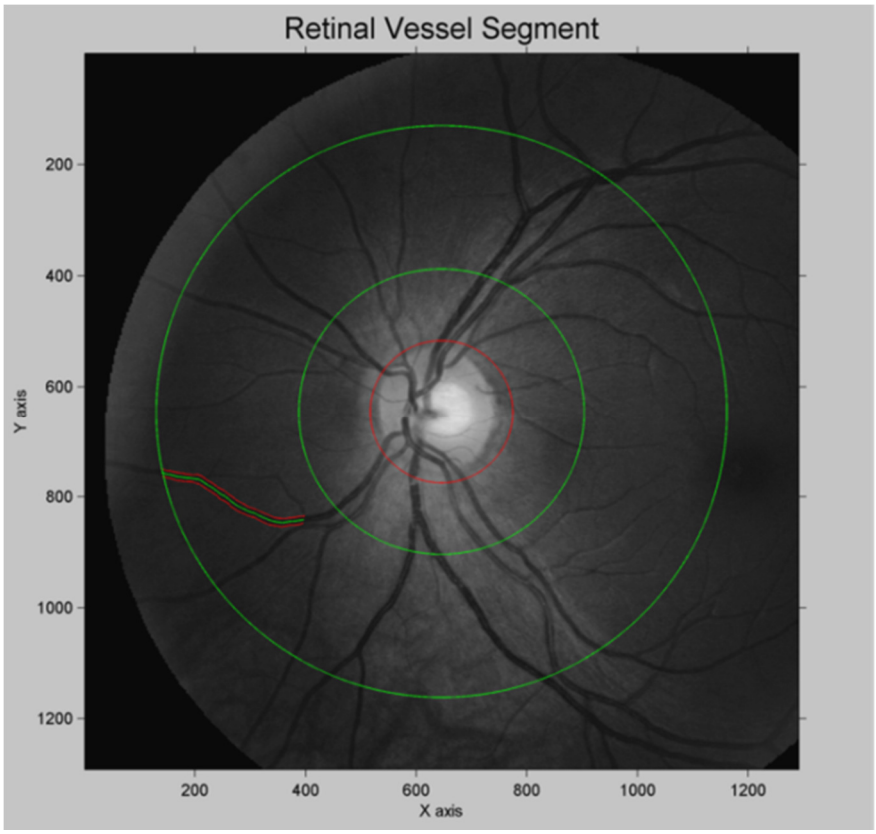

Figure 3.11 Tracked vessel edges (red) and the centreline (green) on a grayscale image.

The edge extraction and tracking are processed automatically on nine registered images. If the tracking fails in one of the images, a warning message is displayed and another trial is encouraged by selecting a different starting point or direction. In Figure 3.12, the edge tracking result of a vessel segment across multiple registered images is shown.

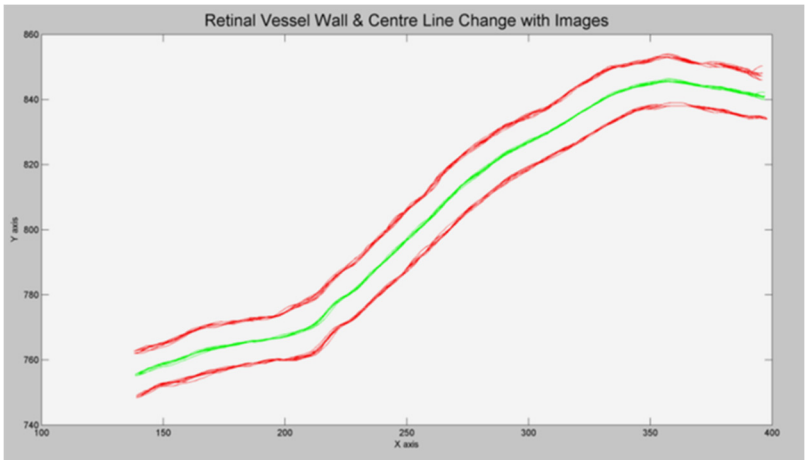

Figure 3.12 Same vessel is tracked across multiple registered images. Red curves denote vessel edges. Green curves denote the centrelines.

3.4.4.4 Vessel Cross-section Diameter Measurement

Vessel width (diameter) is often defined as the distance between two edges of the vessel and through a point perpendicular to the vessel direction vector (Al-Diri et al., 2010). Based on this definition, this thesis proposes a method to measure multiple cross-section diameters of a vessel. These cross-section diameters are through evenly distributed points on centreline and perpendicular to centreline, therefore, called centreline perpendicular diameter. The measurement of centreline perpendicular diameters (CPDM) includes the following steps: 1) calculate the centreline; 2) calculate the direction vector of centreline by the differentiation of dy/dx; 3) create a perpendicular line which has crossing points with both edges; 4) calculate the distance between two crossing points and 5) move to the next points on the centreline and repeat the process until the second last point. An example is shown in Figure 3.13.

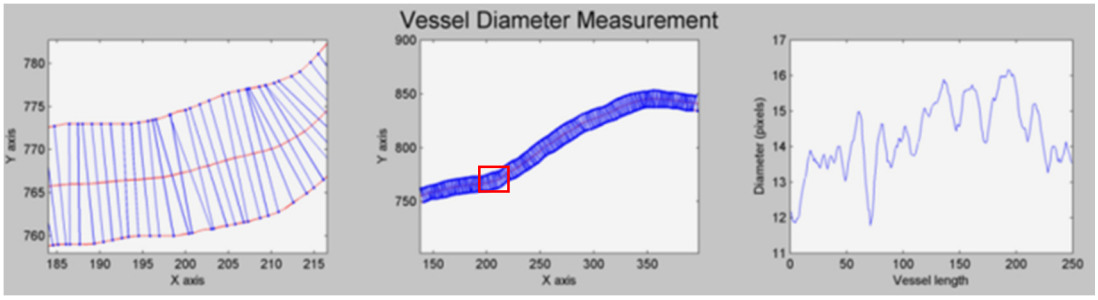

Figure 3.13 A vessel segment is measured using CPDM. Left figure is the zoom-in section of red box in middle figure. Right figure illustrates the measured vessel cross-section diameter.

3.4.5 Summary

This chapter detailed an ECG synchronised retinal photography method that captured time series retinal images electronically and automatically during the cardiac cycle. Several standard and customised computer assisted systems were introduced to measure retinal vascular parameters. These measurement methods will be used for the studies of the cardiac variation (Chapter 4), the grader and software variations (Chapter 5), the summary method and protocol impact (Chapter 6) and measurement of the retinal dynamic (Chapter 7).

Chapter Four

Cardiac Variation and Retinal Vascular Measurement

4.1 Introduction

Since the past decade, advances in retinal imaging technique have allowed direct, in-vivo observations of the human circulation system. In Chapter 2, the quantitative measurement of retinal vascular geometric parameters from retinal photographs was presented, including diameter, tortuosity, and length-diameter ratio (LDR), which are strongly associated with blood pressure (Wong et al., 2004b, Cheung et al., 2011a), major systemic vascular diseases (Wong et al., 2002b, Witt et al., 2006), and diabetes mellitus (Wong et al., 2002c). Consistent with these, it has been suggested that such geometric parameters reflect the optimality state of the retinal circulation (Zamir et al., 1976) and therefore hemodynamic changes associated with pathophysiological processes (i.e., blood pressure, diabetes, inflammation, and other mechanisms) may alter the geometrical organization (e.g., dilated vessels, more tortuous, wider branching angle, low LDR, fractal dimension) of the retinal vasculature (Wong et al., 2002a, Cheung et al., 2011a, Witt et al., 2006, Sasongko et al., 2010, Kawasaki et al., 2011).

Physiologically, spontaneous increase in blood volumetric flow entering the ophthalmic vascular system is expected during the peak-systolic phase of cardiac cycle, and lower flow may occur during the diastolic phase (Riva and Schmetterer, 2008). Furthermore, blood flow changes would correspond to variations in intravascular pressure that may induce vasomotor responses to adjust vessel diameter size (Riva and Schmetterer, 2008). While previous studies have shown that static measures of retinal vessel diameter varied at different points during the cardiac cycle (Dumskyj et al., 1996, Chen et al., 1994, Knudtson et al., 2004), variations in other retinal vascular geometric parameters (tortuosity, branching angle, LDR, optimality deviation and fractal dimension) during the cardiac cycle have never been investigated.

Considering the potential variations of retinal vascular geometry resulting from the ambient hemodynamic during the cardiac cycle, understanding temporal changes during normal cardiac rhythm is important to ensure that observed changes in retinal vascular geometry in relation to several diseases are due to specific pathological

conditions, but not physiological variations. Therefore, these parameters can be warranted as sub-clinical markers for systemic vascular diseases. It is also important to determine the inherent variations in the current static retinal imaging technique, where the image is obtained without considering the temporal location of the sample with respect to the cardiac cycle. In this study, the variations of retinal vascular geometric parameters (individual vessel diameter, summary diameter, tortuosity, branching angle, LDR, optimality deviation and fractal dimension), quantitatively measured from ECG synchronised retinal photographs, during normal cardiac cycle in generally healthy participants is investigated.

4.1 Materials and Methods

Fifteen volunteers, aged 25 – 45 years (mean 33 years, 11 male and 4 female), were recruited to participate in this study. The exclusion criteria were subjects having the following conditions: (i) prescribed or other medication on the day of the experiment, (ii) hypertension, (iii) history of cardiovascular disease, (iv) diabetes, (v) current smoker, (vi) eye disease, and (vii) eye surgery. The participants were chosen to be young and healthy, with the aim to minimise the impacts of ageing and diseases.

Retinal photography and vascular measurement have been detailed in Chapter 3, Briefly, nine disc-centred retinal images of the non-dilated left eye of each participant (a total of 135 disc-centred retinal images) were captured using the ECG synchronised retinal photography method. The individual vessel diameter, Higuchi and box-counting fractal dimension were measured using the customised software. The retinal vessel summary diameter, tortuosity, branching angle, LDR and optimality deviation were measured in Zone C using the software SIVA.

Statistical analysis was performed using STATA 10.1 for Windows (StataCorp LP, College Station, Texas, USA). The variance measuring the difference between each image and the reference image (first image) was used for the analysis because it

eliminates the inter-individual difference of retinal vascular geometric measures. Log-transformation was applied to LDR. All parameters were analysed using repeated measures ANOVA with post-hoc multiple comparison tests to compare the mean value of each parameter from different frames during the cardiac cycle and to estimate the P-value for variation of a particular parameter across different points in the cycle. Fractional polynomial regression was also performed to test for any non-linear trends in each parameter during the cardiac cycle (Greenland, 1995).

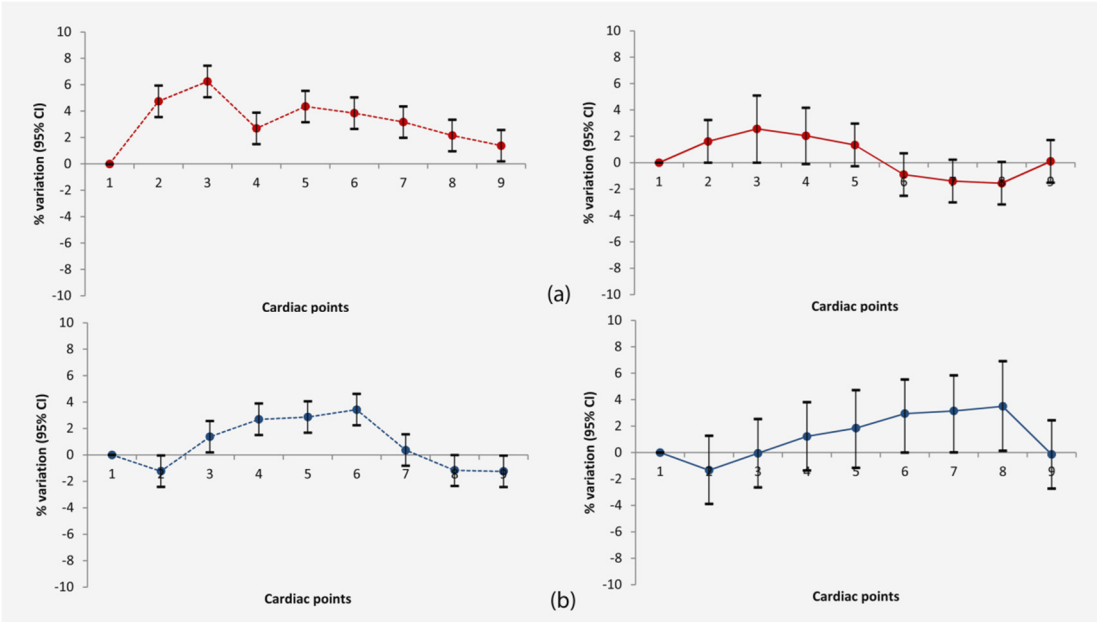

Figure 4.1 Variations of summary of individual vessel diameter (dashed line) and vessel summary diameter (CRAE and CRVE) (solid line) at different cardiac points. a) Arteriole diameter (red) change across cardiac cycle. b) Venule diameter (blue) change across cardiac cycle.

4.2 Results

In Figure 4.1, the trend of the variations of vessel diameter during the cardiac cycle is shown. At each point of the cardiac cycle (shown on X-axis), the measures are averaged from fifteen subjects and plotted with Mean value and 95% confidence interval. Changes at each point of the cardiac cycle form a pattern that are similar in

both individual vessel diameter and summary diameter measures (CRAE and CRVE). The pattern shows arterioles peak before venules. Furthermore, CRAE becomes narrowest when the CRVE peaks. While variations in individual arteriolar and venular diameters are statistically significant ($P<0.001$), both CRAE and CRVE do not show significant variation over the multiple images recorded during the cardiac cycle (all $P>0.05$). Other retinal vascular geometry parameters do not show the observable trend.

In Table 4.1, the mean value and the absolute variation (in percent) of each parameter from images recoded at different points in the cardiac cycle are shown. Overall, there is no significant variation found for arteriolar or venular parameters across different cardiac points (all P-values for variations>0.1; P for non-linear trends>0.8) except when the vessel diameter is measured individually ($P<0.001$). The variation of the arteriolar and venular tortuosity between different images recorded at different points in the cardiac is the smallest (variations range 0 – 1.5%), compared to diameter (0 – 4.1%), branching angle (0 – 3.5%), LDR (0 – 2%), and optimality deviation (0 – 37%). Optimality deviation of both arterioles and venules shows the most variation compared to other parameters. The variations of region based Higuchi and Box-counting fractal dimension have been calculated by my colleague (Aliahmad et al., 2013). The result shows a statistically significant difference between the mean Higuchi fractal dimensions of 1st and 4th cardiac points measured in zone B ($P=0.048$, $\alpha=0.05$). No statistical significance is found for other fractal measures (all P-values >0.05).

4.3 Discussion

This study has demonstrated that there is a significant variation in the diameter of individual retinal vessels over a cardiac cycle in generally healthy volunteers and both the arterioles and venules are affected. The diameter variation follows a trend, where the diameter of the arterioles peaks close to the R-wave, while the peak of the

venules diameter occurs midway between the systolic and diastolic. The vessel summary diameter (CRAE and CRVE) and other geometric parameters (vessel tortuosity, branching angle, LDR, and optimality deviation) of the retinal vasculature measured from retinal photographs using software SIVA have none to little, non-significant variations across different time points during the cardiac cycle. This suggests that these geometric parameters are unlikely to be influenced by physiological changes during the normal cardiac rhythm.

The retinal vasculature is a unique site where there is lack of autonomic nerve supply and scarce muscular components, unlike other vascular beds elsewhere in the body (Maenhaut et al., 2007). It has been suggested that the geometric organization of the retinal vasculature is controlled by local autoregulation system, to adjust to concurrent hemodynamic setting (Riva and Schmetterer, 2008). Any fluctuations in retinal blood flow may therefore geometrically alter the retinal vasculature to maintain local blood circulation in an optimal manner (maximum blood supply and diffusion with least amount of energy) (Murray, 1926).

During the cardiac cycle, there are variations in blood velocity entering the eyeball. The blood velocity in the main supplying vessels of the retina, ophthalmic artery and central retinal artery, at the peak-systolic are 3 – 4 fold higher than at the end-diastolic phase (Riva and Schmetterer, 2008). This difference may explain some variations in vessel diameter as observed in this study and demonstrated in earlier studies (Knudtson et al., 2004, Chen et al., 1994), which shows a specific pattern following systolic and diastolic phase for individual vessels. However, these are not significant when the revised formula is used to summarise measures from six biggest arterioles and venules into an index of each vessel type; therefore, the index appears to be robust against the variability occurring in each individual vessel (Hubbard et al., 1999, Knudtson et al., 2003). Sizeable variation in optimality deviation is plausible since optimality deviation was determined by the diameters of two branches relative to the diameter of parent vessel, from which a combination of errors is magnified by the

power of 3 (Patton et al., 2005, Zamir et al., 1979, Zamir et al., 1976). On the other hand, recent evidence (Moret et al., 2011) suggests that spontaneous pulsation in retinal vasculature does exist in some individuals, which could be another explanation to the findings, but requires further study.

During the cardiac cycle, both the individual vessels and their summary measures (CRAE or CRVE) show specific pattern of variations, although the summary measures are not statistically significant. However, in contrast, tortuosity, branching angle, LDR and fractal dimension do not demonstrate any pattern. The reason for the differential pattern of variations in diameter than in other parameters during the cardiac cycle is yet to be determined. It has been suggested that changes in diameter size are the earliest form of vascular responses to blood flow changes (Pries and Secomb, 2008). This study speculates that changes in vessel tortuosity, branching angle, LDR and fractal dimension may represent further stages of vascular adaptation subsequent to changes in diameter size. Previous evidence proposed that increased vessel tortuosity is observed when the intravascular pressure increases beyond the elasticity limit of the vessel after vessel dilatation, as a compensatory mechanism to prevent exceeding capillary resistance (Kylstra et al., 1986) which supports the current findings. Additionally, animal experiments also showed that fluctuating blood flow might trigger branching remodeling, appear as increased/decreased angle, to maintain a steady and optimal flow to target tissue (Djonov et al., 2002). Therefore, these parameters (tortuosity, branching, LDR or fractal dimension) might be less sensitive to subtle hemodynamic changes than diameter, but possibly more specific to adverse changes associated with some diseases (e.g., diabetes, cardiovascular diseases). This is an area needing further studies.

The post hoc power analysis shows that this study should have over 80% study power to detect as little as 0.7% variations during the cardiac cycle in diameter or other vessel parameters. However, limitation is also noted. There may be subtle changes in single vessel or local region of the retinal vasculature of these parameters associated

with the cardiac cycle that are masked by the summary measures. Therefore, further studies to compare these summary measures with individual vessel measures are needed.

4.4 Summary

This chapter has shown while there is a significant change in the individual vessel diameter during the cardiac cycle, the vessel summary diameters (CRAE and CRVE) and static retinal vascular geometric measures (tortuosity, branching angle, LDR and optimality deviation) quantitatively measured from retinal images in Zone C using software SIVA, are relatively consistent across different cardiac points. Importantly, this study supports previous findings that there are significant changes to the diameter of individual vessels over the cardiac cycle; however, these changes are not significant when the summary of the vascular diameters using a summary method, tortuosity, branching angle, LDR and fractal dimension are considered. These summary measurements are associated with several diseases and are likely due to pathophysiological processes than normal physiological variations during the cardiac cycle. Future studies exploring the clinical performance (e.g., sensitivity, specificity) of these parameters as sub-clinical markers for systemic vascular diseases (e.g. cardiovascular diseases, diabetes) are warranted.

While variations in the summary diameters are non-significant during the cardiac cycle, there are large variations present in the repeated measures. Further study on these variations regarding the measurement method and grader will be presented in Chapter 5. The speculation of summary method against variation will be verified in Chapter 6.

Table 4.1 Variation of retinal vascular parameters at different cardiac cycle points compared to baseline (the measures from the image captured at cardiac cycle reference point 1).

Vascular parameters (unit)	Cycle point	Arterioles		Venules	
		Mean (SD)	% variation*	Mean (SD)	% variation*
Individual vessel diameter (microns)		P-value†<0.001		P-value†<0.001	
	1	67.6 (8.00)	reference	88.0 (14.7)	reference
	2	70.7 (11.0)	4.7	86.8 (14.5)	1.2
	3	71.5 (12.8)	6.3	89.1 (15.6)	1.4
	4	69.3 (9.30)	2.7	90.3 (15.7)	2.7
	5	70.6 (11.3)	4.4	90.7 (17.4)	2.9
	6	70.1 (9.70)	3.8	91.0 (16.0)	3.4
	7	69.6 (9.80)	3.2	88.1 (14.4)	0.4
	8	69.0 (9.50)	2.2	86.9 (15.0)	1.2
	9	68.7 (10.3)	1.4	86.9 (16.1)	1.2
Summary diameter		P-value†=0.52		P-value†=0.12	
	1	151.1 (13.3)	reference	216.4 (17.5)	reference
	2	153.5 (13.3)	1.6	214.6 (15.9)	0.8
	3	154.9 (13.6)	2.5	217.4 (16.9)	0.5
	4	154.1 (13.4)	2.0	220.2 (17.3)	1.8
	5	153.1 (14.8)	1.3	221.6 (17.3)	2.4
	6	149.7 (14.0)	0.9	223.9 (17.1)	3.5
	7	148.9 (13.9)	1.4	224.5 (18.2)	3.8
	8	148.8 (15.5)	1.5	225.1 (18.0)	4.1
	9	151.2 (13.0)	0.0	217.3 (17.9)	0.4
S. tortuosity (index)		P-value†=0.93		P-value†=0.92	
	1	1.09 (0.02)	reference	1.10 (0.01)	reference
	2	1.09 (0.02)	0.0	1.10 (0.02)	0.2
	3	1.09 (0.02)	0.0	1.10 (0.02)	0.0
	4	1.09 (0.02)	0.0	1.10 (0.01)	0.1
	5	1.09 (0.02)	0.0	1.10 (0.01)	0.0
	6	1.09 (0.02)	0.0	1.10 (0.02)	0.0
	7	1.09 (0.02)	0.0	1.10 (0.02)	0.0
	8	1.09 (0.02)	0.0	1.10 (0.02)	0.0
	9	1.09 (0.02)	0.0	1.10 (0.02)	0.1
C. tortuosity ($x10^5$)		P-value†=0.97		P-value†=0.91	
	1	5.93 (1.15)	reference	6.52 (0.60)	reference
	2	5.93 (1.20)	0.0	6.59 (0.79)	1.1
	3	5.86 (1.17)	0.9	6.47 (0.64)	0.7
	4	5.89 (1.08)	0.3	6.57 (0.69)	0.6
	5	5.92 (1.22)	0.2	6.50 (0.68)	0.1
	6	5.88 (1.11)	0.4	6.32 (0.72)	1.1
	7	6.00 (1.16)	1.5	6.59 (0.70)	1.3
	8	5.83 (1.04)	1.1	6.52 (0.64)	0.0
	9	5.88 (1.07)	0.3	6.52 (0.64)	0.0
Branching angle (degree)		P-value†=0.88		P-value†=0.19	
	1	76.9 (22.7)	reference	82.2 (7.25)	reference
	2	76.0 (21.9)	0.7	80.3 (13.3)	2.3
	3	75.5 (21.9)	1.3	80.9 (13.4)	1.5
	4	76.7 (23.1)	0.0	81.2 (11.2)	1.2
	5	76.4 (23.1)	0.0	79.2 (11.6)	3.4

	6	75.4 (21.5)	0.2	84.5 (8.81)	2.9
	7	77.3 (23.5)	0.8	82.4 (13.2)	0.8
	8	77.5 (22.6)	1.2	81.4 (7.44)	1.0
	9	75.3 (25.5)	0.4	82.4 (13.1)	0.1
LDR		P-value†=0.84		P-value†=0.90	
	1	2.52 (0.89)	reference	2.88 (0.11)	reference
	2	2.47 (0.89)	1.9	2.90 (0.25)	0.6
	3	2.56 (0.85)	1.5	2.84 (0.11)	1.3
	4	2.52 (0.67)	0.0	2.89 (0.10)	0.3
	5	2.57 (0.84)	1.9	2.91 (0.11)	1.0
	6	2.56 (0.84)	1.5	2.89 (0.09)	0.3
	7	2.56 (0.90)	1.5	2.87 (0.11)	0.3
	8	2.52 (0.81)	0.0	2.89 (0.11)	0.3
	9	2.52 (0.89)	0.0	2.89 (0.12)	0.3
Optimality deviation		P-value†=0.84		P-value†=0.15	
	1	-0.47 (0.34)	reference	-0.41 (0.35)	reference
	2	-0.45 (0.30)	4.2	-0.38 (0.30)	7.3
	3	-0.50 (0.35)	6.4	-0.38 (0.30)	7.3
	4	-0.46 (0.37)	2.1	-0.38 (0.39)	7.3
	5	-0.32 (0.38)	32.0	-0.33 (0.29)	19.5
	6	-0.36 (0.32)	23.4	-0.29 (0.31)	29.2
	7	-0.38 (0.36)	19.1	-0.26 (0.37)	36.6
	8	-0.40 (0.41)	14.9	-0.33 (0.32)	19.5
	9	-0.47 (0.36)	0.0	-0.41 (0.32)	0.0

Chapter Five

Grader, Software and Other Variability in Retinal Vascular Diameter Assessment

5.1 Introduction

Retinal vascular diameter measurement has been widely used in disease assessment (Wong et al., 2006a, Lindley et al., 2009, Ding et al., 2014, McGeechan et al., 2009). Computer-assisted measurement techniques have been developed to reduce variability and improve the reliability (Newsom et al., 1992). However, the presence of noise and other artefacts due to the lighting condition and the physical condition of the eye result in uneven background and central reflex in retinal images. Furthermore, methods that summarise the individual vessel diameters in disc-centred retinal images have been developed to quantitatively measure the vessel size and reduce the variability in the measurements (Parr and Spears, 1974, Hubbard et al., 1999, Knudtson et al., 2003). Commonly used summary measurement methods require a grader to confirm or correct the error in the process of optic disc identification, arteriole and venule classification, vessel selection and tracking. Manual intervention is essential in current retinal vascular diameter assessment and this leads to the dependency of the measurements on the expertise of the graders (Couper et al., 2002, Sherry et al., 2002).

Variability in retinal vessel diameter measurement has been studied previously. A wide homeostatic range between the summary measures were observed from the retinal images taken on different days at different locations (Kofoed et al., 2009); however, no changes were found in another study (McCanna et al., 2013). Cardiac cycle has been identified as one of the factors responsible for the variability between the repeated photographs of same person (Sasongko et al., 2012, Knudtson et al., 2004). Newsom et al (1992) speculated that changes in retinal vessel diameter were due to changes in retinal perfusion pressure during the cardiac cycle. However, these variations were not found to be significant in the summary measures at different points of the cardiac cycle, as presented in Chapter 4. Furthermore, different measurement software has shown distinct results and demonstrated the varied strength in the pathological assessment (Yip et al., 2012).

Previous research has studied individual sources of variation such as difference between graders (Sherry et al., 2002), different software programs (Yip et al., 2012), difference between the repeated retinal images of the same eye (McCanna et al., 2013, Sasongko et al., 2012), and variation over the cardiac cycle (Knudtson et al., 2004). However, none of these studies has comprehensively measured all of these factors. This chapter simultaneously considers various sources of variation by taking multiple retinal images of multiple matched subjects over the cardiac cycle, measured in different regions by multiple graders using different software programs. This aims to develop a better understanding of the variability in retinal vessel diameter measurement.

Identifying the sources and the extent of variability in measuring retinal vessels diameter is essential for validating the epidemiology findings (Benbassat and Polak, 2009). It will lead to new techniques and methodology to reduce the variation. It will also assist in improving the comparisons between different studies, and in developing the necessary reporting procedures. This study has experimentally measured and statistically analysed the variations in retinal vessel summary diameter measurement due to the factors of repeated recordings over the cardiac cycle, graders, software programs and region of interest differences.

5.2 Materials and Methods

Eighteen volunteers (15 male and 3 female), aged 21 to 42 years (mean 27 years), participated in this study. The exclusion criteria for the subjects were (i) cardiovascular diseases, (ii) diabetes and (iii) current smoker. This selection minimised the differences between the volunteers.

Nine disc-centred retinal images of the non-dilated left eye of each participant were captured using the ECG-synchronised retinal photography module over a period of approximately 30 minutes, already described in Chapter 3. These nine images corresponded to repetition over similar physiological and ambient conditions.

Three trained and experienced graders (A, B and C) from the Centre for Eye Research Australia (CERA) independently assessed the images using two semi-automated computer software packages, IVAN (University of Wisconsin-Madison, Madison, WI) and SIVA (Singapore 'I' Vessel Assessment, Singapore) (Cheung et al., 2011b, Sasongko et al., 2010, Wong et al., 2006b). The measurements using these two software programs were detailed in Chapter 3. The measurement was conducted in Zone B (the area between 0.5 to 1.0 disc diameter away from the optic disc margin) and Zone C (the area between 0.5 to 2.0 optic disc diameters away from the optic disc margin). Each image was graded individually. The graders were blind to the metadata associated with the images. There were four sets of measures corresponding to same data set, including the measures conducted by Grader A in Zone B using IVAN (Grading 1), the measures conducted by Grader B in Zone B using IVAN (Grading 2), the measures conducted by Grader C in Zone B using SIVA (Grading 3) and the measures conducted by Grader C in Zone C using SIVA (Grading 4).

Statistical analysis was performed using STATA 10.1 for Windows (StataCorp LP, College Station, USA) and Matlab (R2012a, The MathWorks, Inc. USA). Repeated measures mixed model was used to analyse the mixed effects of 'grader', 'repeat', 'ROI' and 'subject'. Intra-class correlation with two-way mixed effect analysis of variance model ICC(2,1) was used to assess the degree of consistency among measurements (McGraw and Wong, 1996). The difference between each set of measures was computed as the percentage, for example difference between two graders A and B was calculated by $100*|A-B|/(A+B)/2$.

5.3 Definition of Variation

There are inherent variations in every measurement method. For the purpose of this study, the variations in retinal vessel diameter measurement are defined as follows:

i. Within-subject variation is the difference among the repeated measures of nine images of the same subject, measured by one grader using one software.

ii. Inter-grader variation is the difference between the measurements of the same set of images by two graders using the same software (IVAN).

iii. Inter-software variation is the difference between the measurements obtained using different software (SIVA and IVAN) on the same set of images measured in Zone B region.

iv. Region of interest (ROI) variation is the difference between the measurements from the regions of Zone B and Zone C, conducted by one grader using same software (SIVA).

5.4 Normality Test of Measurement Data

A data set with normal distribution tends to a single mean value. Because of wider existence of normal distribution and the support of central limit theorem, random variables with unknown distributions are often assumed to be normally distributed, although this assumption can be dangerous in situations where it may not be applicable (Weisstein, Whittaker and Robinson, 1967). The probability distribution of a continuous data set is determined uniquely by the cumulative distribution function (CDF), probability density function (PDF) or possibly a transform of one of these (Hajek, 2013).

Furthermore, the normal distribution of a data set is important in statistical analysis. In descriptive statistics, continuous data can be described and analysed using parametric statistics, such as the mean and standard deviation, only when the data approximates to normal distribution. In the baseline comparisons, many popular statistical tests require data with normal distribution, such as z-test, t-test and ANOVA (Walker and Almond, 2010). Using statistical tests and descriptive statistics with an unknown distribution may lead to a false result.

The randomness of retinal photography leads to the assumption of normal distribution in the measurement data. This needs to be verified to assure the correct descriptive statistics and statistical analysis. Multiple measurements in this thesis have provided an opportunity to study the distribution of data under different conditions, such as different graders and software. In Figures 5.1 and 5.2, the box plot and probability plot of CRAE and CRVE in four sets of grading are shown. Box plot graphically describes the measures of each subject with mean value and 95% confidence interval (95% CI). In the probability plot, the reference line forms an estimate of the CDF from the data. If measures are close to their reference lines in the probability plot, it indicates the normal distribution of the measures. Anderson-Darling normality test has also been used to determine the distribution of the measures.

From the box plots in Figures 5.1 and 5.2, individual differences of retinal vessel diameter are noticed in all measures regardless of the factors of grader and software. The measures are close to their reference line in probability plots, and thus demonstrate the normal distribution of the measures. Anderson-Darling normality tests on each measurement confirmed all measures are normally distributed and all P values are less than 0.05, except CRVE measures in grading 1 and 2 (P-values < 0.1).

In conclusion, the probability plots and Anderson-Darling normality tests have proven that the measures of retinal vessel summary diameters in this thesis are normally distributed regardless of the measurement methods and graders. This provides the evidence for a future study using descriptive statistics and statistical tests where normal distribution of data set is required.

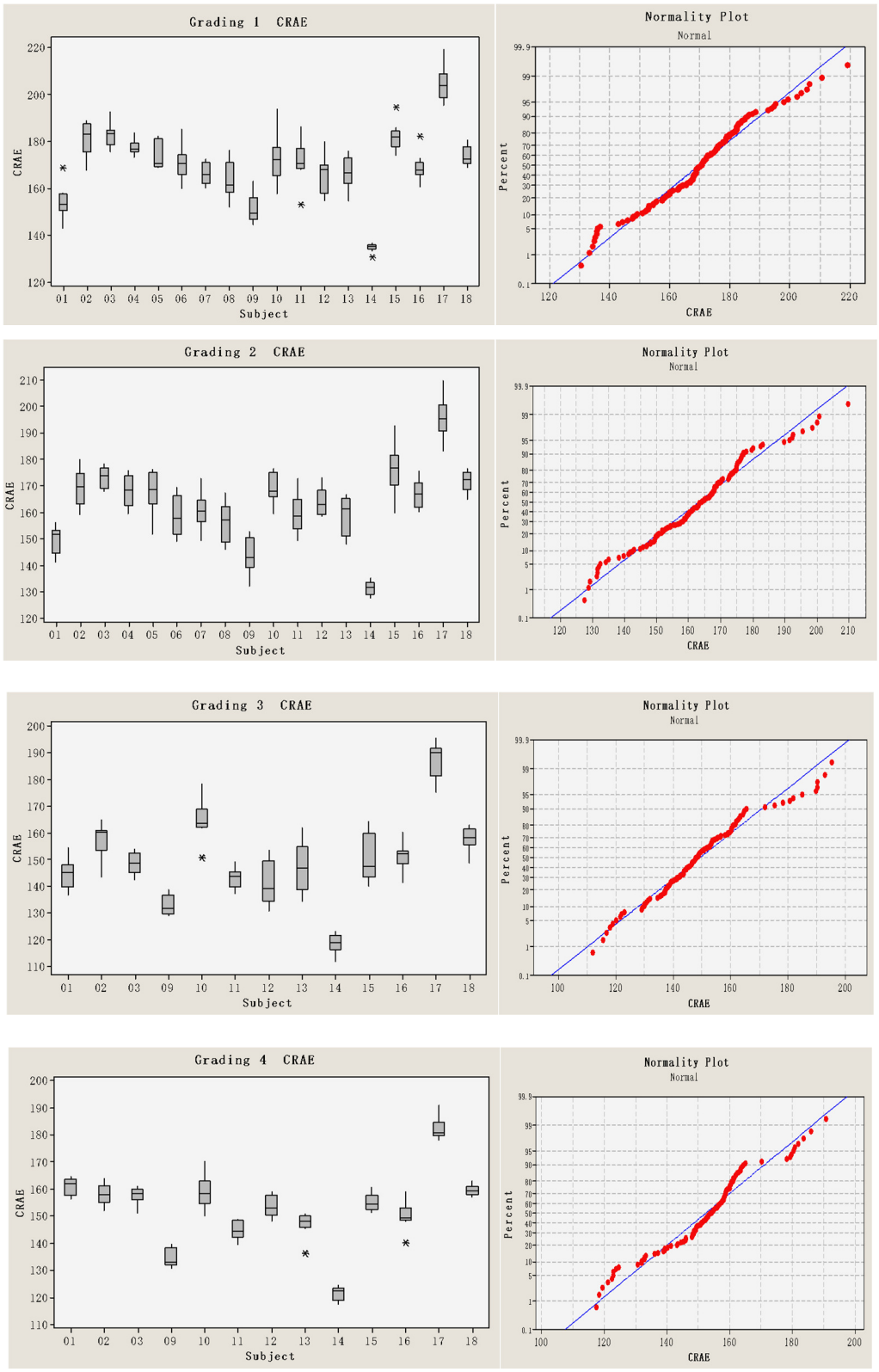

Figure 5.1 Box plot and normality plot of four sets of CRAE measures

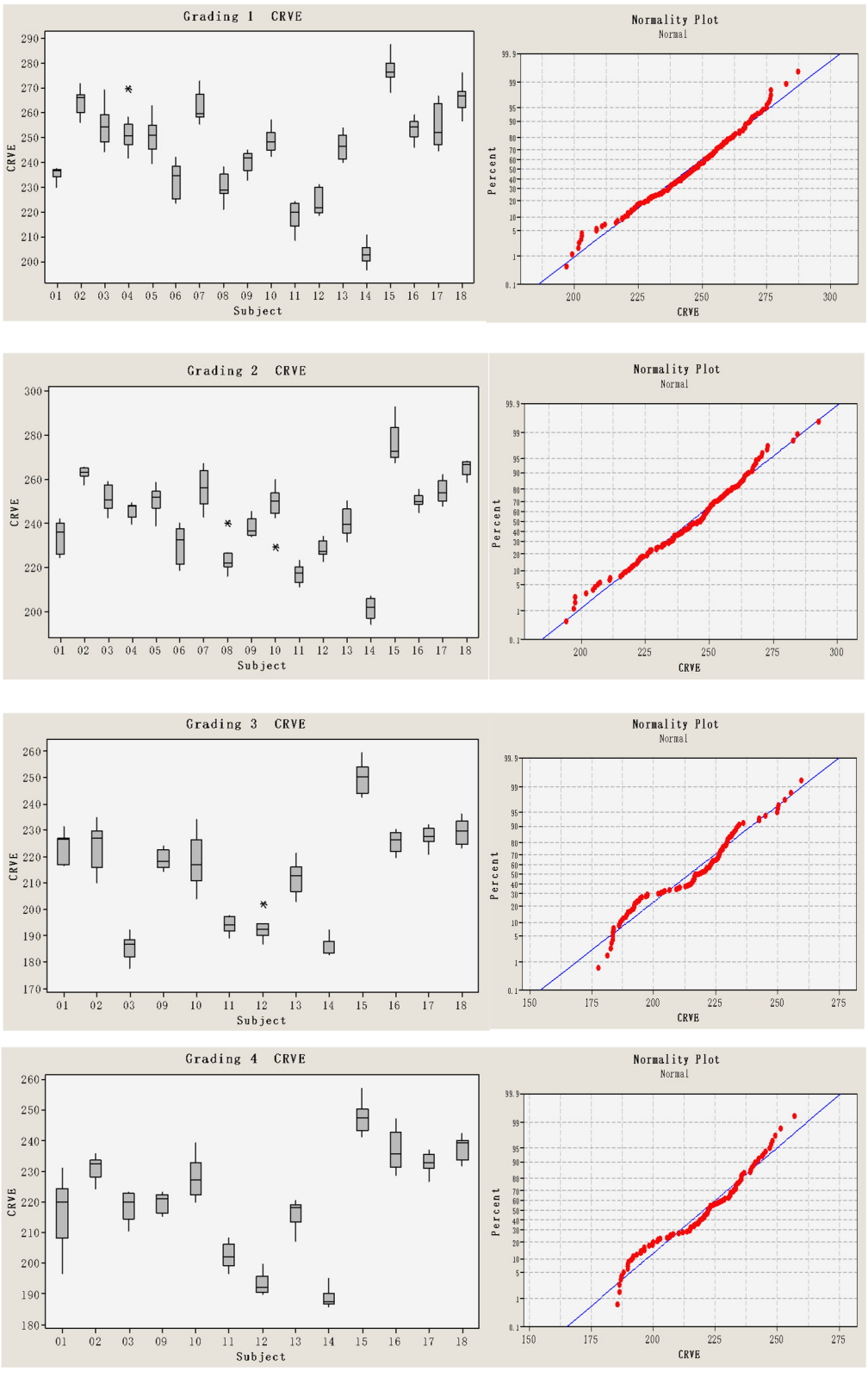

Figure 5.2 Box plot and normality plot of four sets of CRVE measures

5.5 Within-subject Variation in Repeated Photographs

The within-subject variation was assessed from the nine images of each subject. These images were captured during a short duration and considered to be same in current retinal vascular assessment.

In Tables 5.1 and 5.2, the mean values and standard deviations of CRAE and CRVE obtained from nine images of each subject are shown, measured by different graders using software SIVA and IVAN. Grading 1, 2 and 3 were the vessel measurements conducted in Zone B, while grading 4 measured the vessels in Zone C. The validation and consistency of each grading were assessed using ICC(2,1) based on Matlab function. Results show good correlation within the subject in all measures regardless of the grader and software (ICC=0.86 ~ 0.98). This confirms the high reproducibility of each measurement method.

In CRAE measures, three measurements conducted in Zone B have similar amounts of SD, 6.38μm, 6.28μm and 6.20μm respectively, while measurement in Zone C has less variation (SD=3.67μm). However, differences are not obvious in CRVE, with SD in four sets of measures between 4.73 and 5.64μm. Though these measures are statistically non-significant at different points during the cardiac cycle, as presented in Chapter 4, the size of variation is comparable to the difference between case and control groups in other studies (Smith et al., 2004, Leung et al., 2003b). In a population based study of aging (Leung et al., 2003b), CRAE and CRVE were reported to decrease 4.8 μm and 4.1μm respectively per decade increase in age. Small retinal arteriolar and venular changes were also found in a diabetes study (Ronald et al., 2006). Many studies found less than 10μm pathological change in retinal vessel diameter assessment between the case and control groups. The impact of large within-subject variation on disease assessment is further discussed using an example.

Table 5.1 Mean and SD in four sets of CRAE measures

Subject	No. of Images	Grading 1		Grading 2		Grading 3		Grading 4	
		Mean	SD	Mean	SD	Mean	SD	Mean	SD
1	9	154.32	7.11	149.15	5.17	144.60	5.57	161.08	2.96
2	9	180.29	7.43	168.64	7.12	223.00	5.81	157.65	4.08
3	9	182.68	5.31	172.90	3.91	224.14	8.58	157.64	3.21
4	9	177.48	3.08	167.91	5.70	-	-	-	-
5	9	174.26	5.99	167.70	8.83	-	-	-	-
6	9	170.73	7.29	158.80	7.45	-	-	-	-
7	9	166.22	4.47	160.55	6.62	-	-	-	-
8	9	163.52	8.12	156.04	7.52	-	-	-	-
9	9	151.12	6.17	143.60	6.63	133.01	3.82	134.31	3.26
10	9	172.45	10.44	169.50	5.63	164.67	7.52	159.14	6.01
11	9	171.27	9.36	159.74	7.54	143.03	3.72	144.76	3.32
12	9	165.89	8.05	163.62	5.05	141.02	8.12	153.68	3.89
13	9	166.62	6.81	158.06	7.34	147.43	9.10	146.84	4.50
14	9	134.71	1.87	131.24	2.50	118.54	3.54	121.40	2.48
15	9	181.58	6.06	176.14	9.11	150.24	8.74	154.95	3.14
16	9	168.65	6.05	166.82	5.39	150.89	5.13	149.99	5.03
17	9	204.45	7.21	195.68	7.69	186.80	6.52	182.30	3.96
18	9	173.80	4.01	171.59	3.79	157.59	4.36	159.54	1.92
Average		170.00	6.38	163.21	6.28	160.38	6.20	152.56	3.67

Note: SIVA measures are conducted on 13 subjects that are among 18 subjects of IVAN measures

Table 5.2 Mean and SD in four sets of CRVE measures

Subject	No. of Images	Grading 1		Grading 2		Grading 3		Grading 4	
		Mean	SD	Mean	SD	Mean	SD	Mean	SD
1	9	235.46	2.49	233.54	6.99	223.00	5.81	216.39	11.09
2	9	263.94	5.15	262.31	2.74	224.14	8.58	231.12	3.83
3	9	254.45	7.84	251.44	5.83	185.47	4.57	218.66	4.81
4	9	251.83	7.97	245.88	3.31	-	-	-	-
5	9	251.19	7.37	250.12	6.20	-	-	-	-
6	9	232.19	6.83	230.48	8.22	-	-	-	-
7	9	262.17	5.95	255.59	8.08	-	-	-	-
8	9	230.09	5.43	224.25	7.23	-	-	-	-
9	9	240.16	4.18	238.21	4.10	218.89	3.55	219.93	3.00
10	9	248.48	4.84	248.39	8.72	218.29	9.77	228.01	6.40
11	9	218.55	5.61	217.21	4.17	194.06	2.84	202.21	3.89
12	9	223.83	5.03	228.61	3.80	192.70	4.29	193.16	3.32
13	9	245.92	5.19	240.56	6.27	211.77	5.84	215.99	4.29
14	9	202.94	4.31	201.27	4.85	185.22	3.31	188.49	2.89
15	9	276.77	5.46	275.87	8.63	249.79	5.76	247.40	4.86
16	9	253.29	4.19	250.08	3.15	225.57	3.80	236.68	6.37
17	9	254.27	8.28	254.66	5.17	227.65	3.50	232.73	3.01
18	9	265.63	5.42	264.93	3.46	229.41	4.61	237.31	3.74
Average		245.06	5.64	242.97	5.61	214.31	5.10	220.62	4.73

Note: SIVA measures are conducted on 13 subjects that are among 18 subjects of IVAN measures

An hypertension study (Smith et al., 2004) differentiated the hypertension group and non-hypertensive group, illustrated in Figure 5.3. The two groups were well separated, based on the data provided in the paper. However, the result becomes unfounded when extra within-subject variation, 6μm according to the previous result, is considered, as shown in Figure 5.4. The 95% confidence interval areas of two distribution curves are overlapped. The extent of overlapping depends on the parameters of the subjects (mean value and within-subject variation) and measurement accuracy (standard deviation and 95% confidence interval).

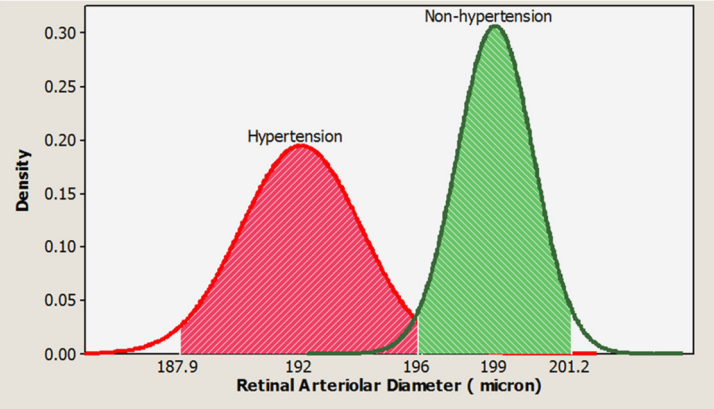

Figure 5.3 An example of hypertension study (Smith et al., 2004). Red colour denotes hypertension group. Green colour denotes non-hypertension group. Shaded area denotes 95% of given population (mean±2 SD). The hypertension and non-hypertension group are well separated.

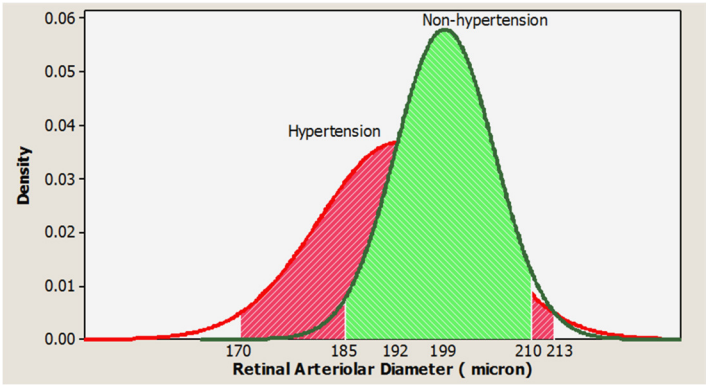

Figure 5.4 Same hypertension study as above. The figure shows the distribution plot of retinal arteriole diameters after extra within-subject variation is added. The distribution of the two groups now overlap. The hypertension and non-hypertension groups cannot be separated.

Current retinal vascular assessments do not consider variations in repeated photographs. Large population based studies and proper statistical analysis might correctly interpret the results and the related pathological causes. Those studies had a large sample size, sufficient to validate the assumption that group average of retinal vessel diameters without consideration of variation in the repeated photographs might not have major impact on their findings of disease association. However, those assumptions may not held in the assessments.

5.6 Inter-grader Variation

Inter-grader variation was assessed from grading 1 and 2, with measurements conducted by two graders using software IVAN. In Tables 5.3 and 5.4, the CRAE and CRVE measures with mean value, standard deviation and 95% confidence interval are shown. The mean value difference of two measures (Grader A and B) is defined by 100*|A-B|/(A+B)/2, shown in absolute percentage.

Table 5.3 CRAE measured by two graders using software IVAN

Subject	No. of Images	Grader A			Grader B			Difference in Mean %
		Mean	SD	95%CI	Mean	SD	95%CI	
1	9	154.32	7.11	(148.85, 159.78)	149.15	5.17	(145.17, 153.13)	3.41
2	9	180.29	7.43	(173.42, 187.17)	168.64	7.12	(162.06, 175.23)	6.68
3	9	182.68	5.31	(178.24, 187.12)	172.90	3.91	(169.64, 176.17)	5.50
4	9	177.48	3.08	(175.12, 179.85)	167.91	5.70	(163.53, 172.30)	5.54
5	9	174.26	5.99	(168.72, 179.80)	167.70	8.83	(159.54, 175.87)	3.83
6	9	170.73	7.29	(165.13, 176.34)	158.80	7.45	(153.08, 164.53)	7.24
7	9	166.22	4.47	(162.78, 169.65)	160.55	6.62	(155.46, 165.64)	3.47
8	9	163.52	8.12	(156.74, 170.31)	156.04	7.52	(149.75, 162.32)	4.68
9	9	151.12	6.17	(146.38, 155.86)	143.60	6.63	(138.51, 148.70)	5.10
10	9	172.45	10.44	(164.43, 180.47)	169.50	5.63	(165.17, 173.83)	1.73
11	9	171.27	9.36	(164.08, 178.47)	159.74	7.54	(153.95, 165.53)	6.97
12	9	165.89	8.05	(159.71, 172.07)	163.62	5.05	(159.74, 167.50)	1.38
13	9	166.62	6.81	(161.39, 171.86)	158.06	7.34	(152.42, 163.70)	5.27
14	9	134.71	1.87	(133.27, 136.14)	131.24	2.50	(129.32, 133.15)	2.61
15	9	181.58	6.06	(176.92, 186.23)	176.14	9.11	(169.13, 183.14)	3.04
16	9	168.65	6.05	(164.00, 173.30)	166.82	5.39	(162.68, 170.96)	1.09
17	9	204.45	7.21	(198.90, 209.99)	195.68	7.69	(189.77, 201.59)	4.38
18	9	173.80	4.01	(170.72, 176.89)	171.59	3.79	(168.68, 174.51)	1.28
Average		170.00	6.38		163.21	6.28		4.07

Table 5.4 CRVE measured by two graders using software IVAN

Subject	No. of Images	Grader1			Grader2			Difference in Mean%
		Mean	SD	95%CI	Mean	SD	95%CI	
1	9	235.46	2.49	(233.54, 237.37)	233.54	6.99	(228.16, 238.91)	0.82
2	9	263.94	5.15	(259.18, 268.70)	262.31	2.74	(259.78, 264.84)	0.62
3	9	254.45	7.84	(247.89, 261.00)	251.44	5.83	(246.56, 256.31)	1.19
4	9	251.83	7.97	(245.71, 257.95)	245.88	3.31	(243.34, 248.42)	2.39
5	9	251.19	7.37	(244.38, 258.00)	250.12	6.20	(244.38, 255.86)	0.43
6	9	232.19	6.83	(226.94, 237.44)	230.48	8.22	(224.16, 236.80)	0.74
7	9	262.17	5.95	(257.60, 266.74)	255.59	8.08	(249.37, 261.80)	2.54
8	9	230.09	5.43	(225.55, 234.63)	224.25	7.23	(218.21, 230.30)	2.57
9	9	240.16	4.18	(236.95, 243.38)	238.21	4.10	(235.06, 241.36)	0.82
10	9	248.48	4.84	(244.76, 252.20)	248.39	8.72	(241.68, 255.09)	0.04
11	9	218.55	5.61	(214.24, 222.86)	217.21	4.17	(214.00, 220.41)	0.62
12	9	223.83	5.03	(219.97, 227.70)	228.61	3.80	(225.69, 231.53)	2.11
13	9	245.92	5.19	(241.93, 249.91)	240.56	6.27	(235.74, 245.38)	2.20
14	9	202.94	4.31	(199.63, 206.26)	201.27	4.85	(197.55, 204.99)	0.83
15	9	276.77	5.46	(272.58, 280.97)	275.87	8.63	(269.23, 282.51)	0.33
16	9	253.29	4.19	(250.07, 256.51)	250.08	3.15	(247.66, 252.50)	1.28
17	9	254.27	8.28	(247.90, 260.64)	254.66	5.17	(250.68, 258.63)	0.15
18	9	265.63	5.42	(261.46, 269.79)	264.93	3.46	(262.27, 267.59)	0.26
Average		245.06	5.64		242.97	5.61		1.11

From Table 5.3, difference is observed between the graders A and B. The average difference between the graders A and B for CRAE is 4.07% (range 1.09-7.24%). The results show that for all measures, grader A estimates are consistently higher than of grader B and indicate a grader bias. From Table 5.4, it is observed that the average difference between the graders A and B for CRVE is 1.11% (range 0.15 – 2.57 %). There is no noticeable bias between the graders in CRVE measures. The lower difference in the measurement of the retinal venules compared with the arterioles may be attributed to the venules having higher contrast compared to the arterioles, leading to lower measurement error.

Statistical analysis of repeated measures mixed model with fixed effect of ‘grader’ and random effect of ‘repeat’ and ‘subject’ is conducted to analyse the mixed effects. Results show the significant inter-grader difference in retinal arteriolar and venular summary measures (P=0.016 in CRAE measures and P=0.048 in CRVE measures). These significant inter-grader variations raise the issue of the comparability of results measured by different graders. Future studies should be aware of these inter-grader variations.

5.7 Inter-software Variation

Inter-software variation was assessed with a similar process described in inter-grader variation assessment. Both grading 1 and 2 were measured in Zone B using software IVAN. The measures from grading 1 and 2 were averaged to minimise grader effect and then compared with grading 3 that was measured in Zone B using SIVA.

Table 5.5 Result of inter-software variation

Subject	No. of Images	CRAE					CRVE				
		IVAN		SIVA		Difference in Mean%	IVAN		SIVA		Difference in Mean%
		Mean	SD	Mean	SD		Mean	SD	Mean	SD	
1	9	151.66	5.42	144.60	5.57	1.19	234.17	4.06	223.00	5.81	1.22
2	9	174.47	6.26	223.00	5.81	6.11	263.13	3.48	224.14	8.58	4.00
3	9	177.79	3.38	224.14	8.58	5.77	252.94	5.47	185.47	4.57	7.69
9	9	146.97	6.37	133.01	3.82	2.49	239.22	4.03	218.89	3.55	2.22
10	9	171.87	7.38	164.67	7.52	1.07	248.42	6.32	218.29	9.77	3.23
11	9	164.40	7.45	143.03	3.72	3.48	217.15	3.42	194.06	2.84	2.81
12	9	164.63	5.65	141.02	8.12	3.86	226.49	3.90	192.70	4.29	4.03
13	9	163.64	5.67	147.43	9.10	2.61	243.89	5.36	211.77	5.84	3.52
14	9	132.78	1.73	118.54	3.54	2.83	202.47	4.25	185.22	3.31	2.22
15	9	179.72	6.93	150.24	8.74	4.47	276.74	6.48	249.79	5.76	2.56
16	9	168.26	4.64	150.89	5.13	2.72	251.67	3.16	225.57	3.80	2.73
17	9	200.12	5.98	186.80	6.52	1.72	254.36	6.29	227.65	3.50	2.77
18	9	173.13	3.49	157.59	4.36	2.35	266.23	2.88	229.41	4.61	3.71
Average		166.88	5.41	160.38	6.20	3.13	244.37	4.55	214.31	5.10	3.29

In Table 5.5, the result of inter-software variation shows differences between the mean values as 3.13% and 3.29% for CRAE and CRVE respectively. The sizes of inter-software variations in CRAE and CRVE are similar regardless of vessel type, while inter-grader variation discussed previously was larger in the arteriolar measures compared to the venular measures.

Statistical analysis of repeated measures mixed model with fixed effect of 'software' and random effect of 'repeat' and 'subject' is conducted to analyse the mixed effects. Results show the significant inter-software difference in retinal arteriolar and venular summary measures (both $P<0.001$). However, these significant variations might be due to one or both of the effects of grader and measurement software, which cannot be determined in this work. The grader effect is difficult to differentiate in this case due to the distinguishable measurement protocols of different software programs.

However, the significant difference between the measures using different software programs indicates that these measures were not comparable and the results are not interchangeable.

5.8 ROI Difference

In Table 5.6, the measures in Zone B and Zone C conducted by the same grader using software SIVA are compared. Results show the ROI caused differences are 2.01% and 0.90% for CRAE and CRVE measures respectively. The differences are less than those caused by grader and software, but have some dependency on the vessel type.

Table 5.6 ROI difference in the measures by single grader using software SIVA

		CRAE					CRVE				
Subject	No. of Images	Zone B		Zone C		Difference in Mean%	Zone B		Zone C		Difference in Mean%
		Mean	SD	Mean	SD		Mean	SD	Mean	SD	
1	9	144.60	5.57	161.08	2.96	2.70	223.00	5.81	216.39	11.09	0.75
2	9	223.00	5.81	157.65	4.08	8.58	224.14	8.58	231.12	3.83	0.77
3	9	224.14	8.58	157.64	3.21	8.71	185.47	4.57	218.66	4.81	4.11
9	9	133.01	3.82	134.31	3.26	0.24	218.89	3.55	219.93	3.00	0.12
10	9	164.67	7.52	159.14	6.01	0.85	218.29	9.77	228.01	6.40	1.09
11	9	143.03	3.72	144.76	3.32	0.30	194.06	2.84	202.21	3.89	1.03
12	9	141.02	8.12	153.68	3.89	2.15	192.70	4.29	193.16	3.32	0.06
13	9	147.43	9.10	146.84	4.50	0.10	211.77	5.84	215.99	4.29	0.49
14	9	118.54	3.54	121.40	2.48	0.60	185.22	3.31	188.49	2.89	0.44
15	9	150.24	8.74	154.95	3.14	0.77	249.79	5.76	247.40	4.86	0.24
16	9	150.89	5.13	149.99	5.03	0.15	225.57	3.80	236.68	6.37	1.20
17	9	186.80	6.52	182.30	3.96	0.61	227.65	3.50	232.73	3.01	0.55
18	9	157.59	4.36	159.54	1.92	0.31	229.41	4.61	237.31	3.74	0.85
Average		160.38	6.20	152.56	3.67	2.01	214.31	5.10	220.62	4.73	0.90

Statistical analysis of repeated measures mixed model with fixed effect of 'ROI' and random effect of 'repeat' and 'subject' is conducted to analyse the mixed effects. Results show the difference is non-significant in CRAE measures (P=0.314), but significant in CRVE measures (P=0.027). However, significant differences are obtained in both CRAE and CRVE measures when the measures are compared between two graders using IVAN in Zone B and SIVA in Zone C (all P<0.001). This result shows the mixed effect of grader and ROI. It provides explanation for the varied association with

disease using IVAN and SIVA measures in the previous studies (Kotliar and Lanzl, 2011, Yip et al., 2012).

5.9 Can ECG Synchronised Retinal Images Reduce Cardiac Variation?

Previous studies have suggested that cardiac cycle synchronised retinal images should be used to achieve accurate measurement and to avoid an unrecognized source of variation in the measurements of retinal vessel diameters between individuals or over time in the same individual (Chen et al., 1994, Knudtson et al., 2004). However, results were conflicting in Reshef's experiment (Reshef, 1999) in which the ECG synchronised images taken at the same point in the cardiac cycle also incurred the similar amount of variation as non-synchronised images.

The question has been raised again if ECG synchronised retinal images are able to reduce the variation during the cardiac cycle.

Reshef's experiment used an ECG synchronisation method, though the details of synchronisation were not described. Captured images were measured using software IVAN which is also used in this thesis. To assess repeated photographs at the same point of the cardiac cycle, this work obtained nine retinal images captured over the cardiac cycle, of which the 1st and 9th images were both captured at the peak of ECG R-wave. This ensured accurate synchronisation regardless of the varied R-R intervals caused by heart rate variability.

The previous analysis in this chapter showed that variations in retinal vessel summary diameters were affected by the factors of cardiac cycle, grader, assessment software, ROI and the repeated photographs. These factors should be considered simultaneously to determine if ECG synchronisation could reduce the variation. In Figures 5.5 and 5.6, the changes of retinal vessel summary diameter during the cardiac cycle in four sets of CRAE and CRVE measures are visualised.

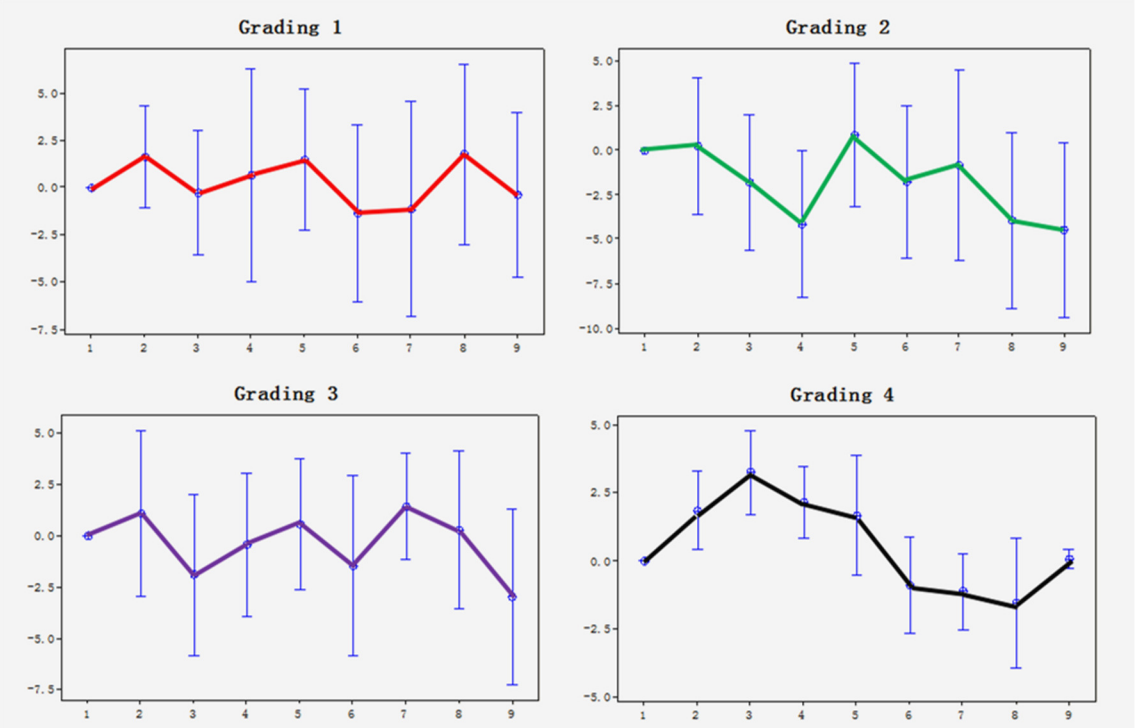

Figure 5.5 Variation at different points of cardiac cycle in CRAE measures. X-axis is cardiac points. Y-axis is the variation compared to first frame of nine images. Grading 1 (red) and grading 2 (green) are measured in Zone B using software IVAN by two graders. Grading 3 (purple) and grading 4 (black) are measured by same grader using software SIVA in Zone B and Zone C respectively. Blue circles and vertical lines denote the mean value and 95% CI of variance. The bold solid lines indicate the change of the mean value during the cardiac cycle.

The comparison in CRAE measures is in Figure 5.5. The measures in Zone B (grading 1 to grading 3) have larger within-subject variation regardless of the grader or software used. The measures conducted in Zone C using SIVA have less within-subject variation and the change follows the rhythm of the cardiac cycle. This is speculated to be due to the difference in measurement protocols and the measured vessel lengths, which will be discussed in Chapter 6. A similar result for CRVE measures is shown in Figure 5.6. Only CRVE measures using SIVA in Zone C show the trend of following the rhythm of the cardiac cycle.

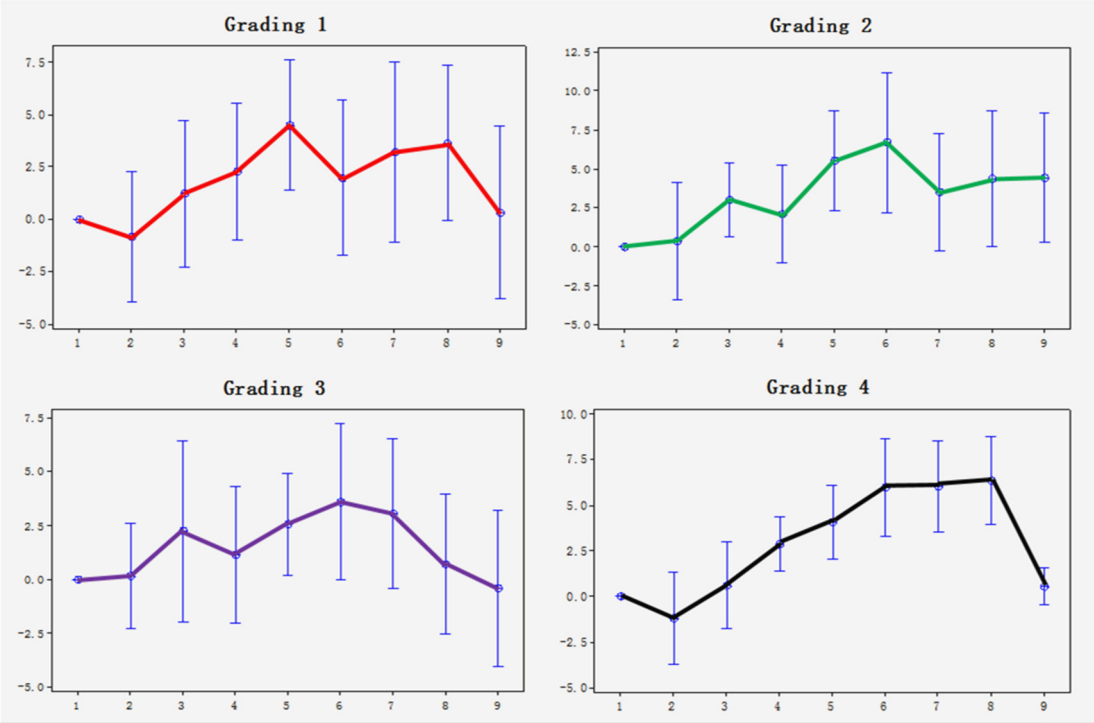

Figure 5.6 Variation at different points of cardiac cycle in CRVE measures. X-axis is cardiac points. Y-axis is the variation compared to first frame of nine images. Grading 1 (red) and grading 2 (green) are measured in Zone B using software IVAN by two graders. Grading 3 (purple) and grading 4 (black) are measured by same grader using software SIVA in Zone B and Zone C respectively. Blue circles and vertical lines denote the mean value and 95% CI of variance. The bold solid lines indicate the change of the mean value during the cardiac cycle.

To quantitatively assess the variations in the measures with or without ECG synchronisation, the variances are calculated as the absolute value of mean and SD among the measures of 1st to 8th images, where time intervals were equally distributed during the cardiac cycle, and between the measures of 1st and 9th images for those synchronised with ECG R-wave. The results are listed in Table 5.7 and Table 5.8 for CRAE and CRVE measures respectively.

Table 5.7 Variation (μm) in CRAE measures with and without ECG synchronisation

	Grading1		Grading2		Grading3		Grading4	
	Mean	SD	Mean	SD	Mean	SD	Mean	SD
Image 1-8	5.87	5.07	6.21	4.98	4.22	3.42	2.40	1.98
Image 1&9	3.40	4.81	4.71	6.66	2.68	3.79	0.24	0.34

Table 5.8 Variation (μm) in CRVE measures with and without ECG synchronisation

	Grading1		Grading2		Grading3		Grading4	
	Mean	SD	Mean	SD	Mean	SD	Mean	SD
Image 1-8	5.29	4.33	5.81	4.63	3.99	3.02	3.96	2.74
Image 1&9	3.12	4.42	3.77	5.33	2.36	3.34	0.65	0.92

From Table 5.7, it is observed that the mean variation between 1st and 9th images is consistently smaller than the mean variation among 1st to 8th images in all measures. This indicates that the measures using ECG synchronised retinal photographs have less variation compared to the measures without ECG synchronisation. However, the grading 1, 2 and 3 conducted in Zone B have large standard deviations which affect the significance in variation reduction using ECG synchronisation. This explains the previous results (Reshef, 1999) why ECG synchronised retinal photographs failed to minimise the cardiac variation. There is efficient variation reduction in grading 4, where the vessels were measured in Zone C using software SIVA. The variation and standard deviation between 1st and 9th images are significantly less than those among 1st to 8th images. This shows that ECG synchronised retinal images are able to minimise photography and measurement variation during the cardiac cycle.

5.10 Summary

The multiple studies conducted in this chapter have comprehensively assessed the variations in retinal vascular summary diameter measurement, which are affected by the repeated photographs, graders, software programs and ROI. Results have shown the presence of grader bias and highlighted the importance of reporting the software that has been used for the analysis. Due to the inherent variability in the measures affected by various factors, there is need for caution when interpreting retinal vascular summary diameters in assessments and comparing the results between the studies.

The reduction of the cardiac variation in retinal vascular summary diameter can be achieved using ECG synchronised photographs, even if with some dependence on the measurement method. Accurate ECG synchronisation, proper measurement method and the grader expertise are essential in this case. The synchronisation at ECG R-wave is recommended to avoid the effect of heart rate variability.

Chapter Six

Summary Method and Measurement Protocol Associated Variation

6.1 Introduction

Previous chapters have studied the impact of the cardiac cycle, grader and software on retinal vascular parameter measurements. A few questions have been raised.

As stated in Chapter 4, non-significant cardiac variation was found in the retinal vessel summary diameters, while the individual vessel diameters showed significant difference. It was speculated that the summary method using the revised formula was robust against variation. A question was also raised that the subtle changes of the individual vessel may be masked by the summary method. A simulation study is used in this chapter to investigate the impact of the summary method.

Two retinal vascular measurement programs were compared in Chapter 5. The results showed that inter-software variation was statistically significant, which meant the same set of retinal images might be interpreted differently due to software differences. One of the differences is the region of interest where vessels are measured. This leads to the speculation that the measured vessel length affected the result though the summary method was applied. This chapter investigates the impact of measured vessel length and the concept of the minimum length of measured vessel is suggested to minimise measurement variation.

The measurement protocol defines the region where the vessels should be measured and guides the grader to perform the measurement. The manual intervention induced in this process results in inter-grader and inter-software variations. In the final part of this chapter, issues related to the measurement protocol are discussed.

6.2 Summary Method

The summary method used in retinal vacular diameter measurement was developed to measure the vessel diameters quantitatively. The summary formulas, such as the Parr-Hubbard formulas (Parr and Spears, 1974, Hubbard et al., 1999) and the

revised formulas (Knudtson et al., 2003), pair the biggest arterioles and venules and summarise them into CRAE and CRVE, as detailed in Chapter 2. The summary formulas are estimations based on the experimental data and are non-linear. For example, the summary diameter of two arterioles of the same size using the revised formula is 1.24 times larger. In this part, a simulation study is used to investigate the impact of the summary method with varied sample size and additive error. The advantages and limitations of the summary method are discussed.

6.2.1 Materials and Methods

Matlab (Mathworks, USA) based model is built to perform the tasks. The model adjusts the inputs with varied sample size, branching coefficients and additive errors. A measurement protocol has suggested that all vessels over 80μm should be measured (Knudtson et al., 2003). Therefore, the six vessels are chosen as 80, 100, 120, 140, 160 and 180μm. After calculation using the revised formulas, CRAE=234.86 μm and CRVE=287.25μm are considered as the baseline.

A data set with random numbers of the mean values and standard deviations based on normal distribution is generated using Matlab function 'normrnd'. An example data set with 1000 samples is shown in Table 6.1.

Table 6.1 An example data set generated by MATLAB

Sample	Vessel1	Vessel2	Vessel3	Vessel4	Vessel5	Vessel6
1	182.84	161.47	137.86	117.57	97.65	75.29
2	175.38	162.32	141.53	118.42	98.90	79.30
3	180.79	155.19	142.68	122.18	96.94	73.74
4	183.52	158.84	136.92	120.60	103.76	78.93
5	186.50	164.05	139.50	124.44	98.30	83.93
...	…	…	…	…	…	…
1000	182.64	160.38	139.74	119.19	98.00	79.50

6.2.2 The Impact of Standard Deviation

Corresponding to each standard deviation value from 1μm to 100μm (standard deviation more than 20μm is unlikely to happen in a real measurement, but simulation shows the trend), a data set with 1000 samples are generated. MATLAB program calculates these 1000 samples into CRAE and CRVE using the revised formulas (detailed in Chapter 2) and averages them into the mean values.

The calculations of CRAE and CRVE are close to the baseline value in Figure 6.1 when standard deviation is less than 10 μm. The trend of CRAE and CRVE calculations are similar because the summary formulas of CRAE and CRVE have similar equations only with different branching coefficients. Therefore, only the CRAE formula will be studied later.

Various reasons may produce a larger standard deviation, such as human error, poor quality image and blurred vessel edge, which will be discussed later in this chapter. The summary formulas seem to be able to correct for the standard deviation error up to 10μm.

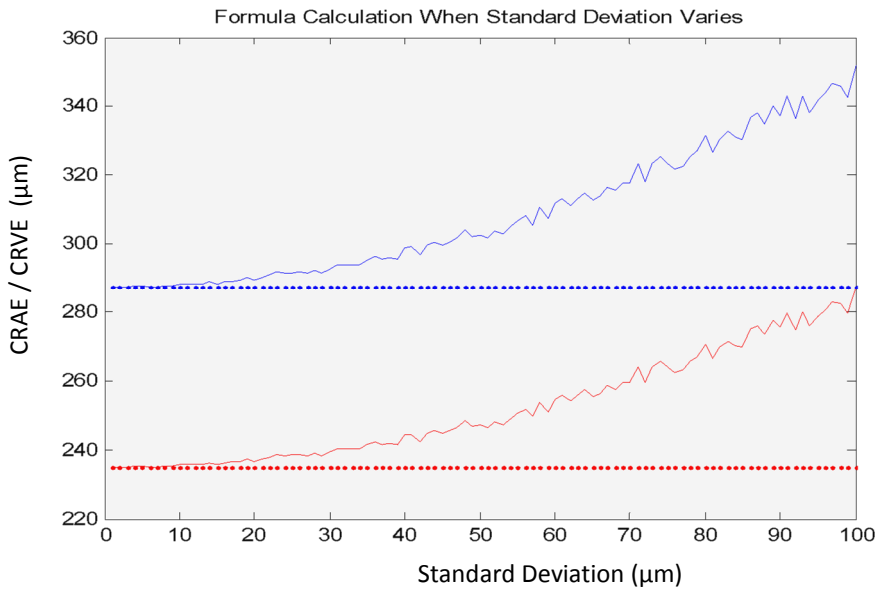

Figure 6.1 CRAE/CRVE calculations using the revised formulas when standard deviation varies. Red curve denotes CRAE and dash line is baseline. Blue colour denotes CRVE and its baseline.

6.2.3 The Impact of Sample Size

A total of 1000 data sets are generated and processed corresponding to each sample size that is chosen from 1 to 1000. The multiple data sets aim to remove random effect. The mean CRAE values corresponding to each sample size are calculated and plotted in Figure 6.2.

Result shows the CRAE calculations using the revised formula have the larger variation when the sample size is small. With the increase in sample size, the summary calculations are close to the baseline value. This implies that population based study with a large sample size provides a more reliable result and the summary formula is unable to minimise the larger variation that occurs in the data sets with a small sample size.

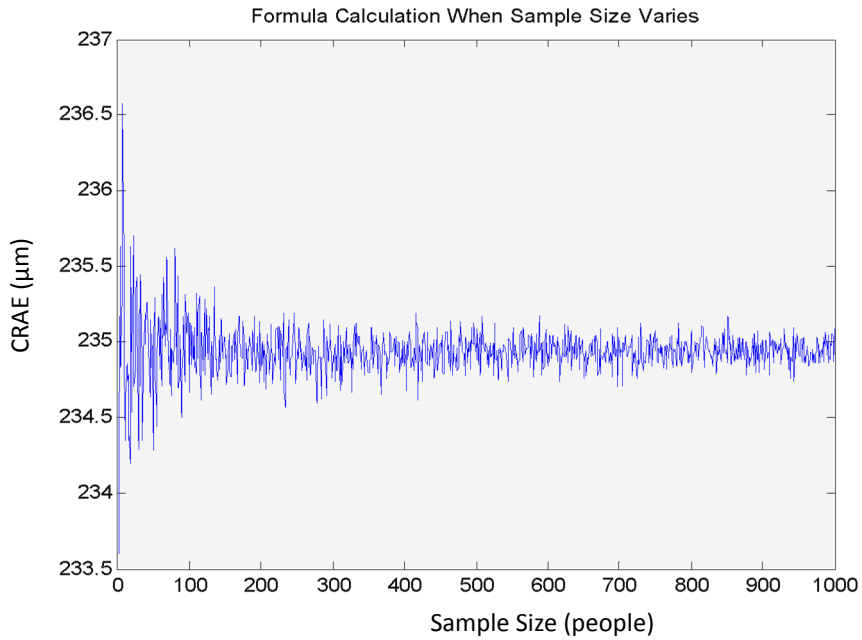

Figure 6.2 Calculations using CRAE summary formula when sample size varies.

6.2.4 The Impact of Measurement Error in Retinal Vessels

Different graders may have different judgments on the optic disk location and size, the retinal vessel edges and the vessel selection. Assuming the graders measure the same set of retinal images with high consistency and minimum error, the measures

from a grader are consistently larger or smaller than those from another grader, which indicates grader bias. To assess this impact, additive errors of 1, 3, 5, 10 and 20 are respectively added to all six vessels.

In Figure 6.3, the simulation result shows that the differences between each group measures are significant (paired t-test, all $P<0.05$). This demonstrates that the measures from multiple graders are significantly different if grader bias exists. This explains the inter-grader variation found in Chapter 5.

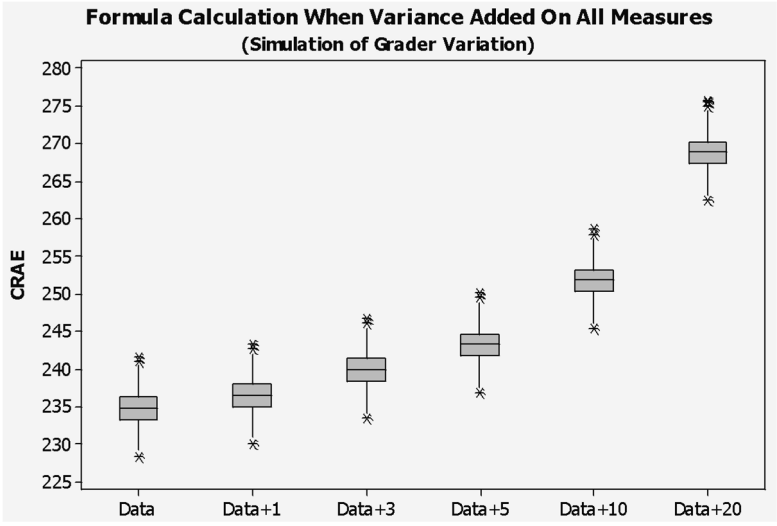

Figure 6.3 Calculations using CRAE summary formula when different additive errors are added to all measures ('Data' denotes orignal measures, 'Data+1' denotes 1µm is added to all vessel measures, 'Data+3' denotes 3µm is added to all vessel measures, and so on). The boxplot shows 95% confidence intervals and mean values.

Figure 6.3 also shows that if the variances on all vessels are similar in amount, the calculations using the summary formula amplify the variation by 1.6 to 1.8 times. For example, if each one of the largest six vessels is measured to be 10µm larger, the CRAE value is around 252µm, which is 17µm larger than the baseline 234.85µm. The 17µm variation in CRAE is about 1.7 times larger compared to 10µm variation in each individual vessel. If a grader bias is 20µm larger than another grader consistently, the calculated CRAE value results in 33µm difference, which is 1.65 times larger than 20 µm. The summary formulas were developed to reduce the variations and quantify the

individual measures. However, the summary formulas are inefficient to reduce the variation caused by grader bias and systemic errors that are constant in one direction.

An experienced grader may have less chance to make human error on overall measurement; however, the measurement error on a single vessel often happens. To simulate this situation, additive errors of 1, 3, 5, 10 and 20 are added respectively to one of the six vessels. The preliminary test has shown the results are not affected by which vessel the additive error is added.

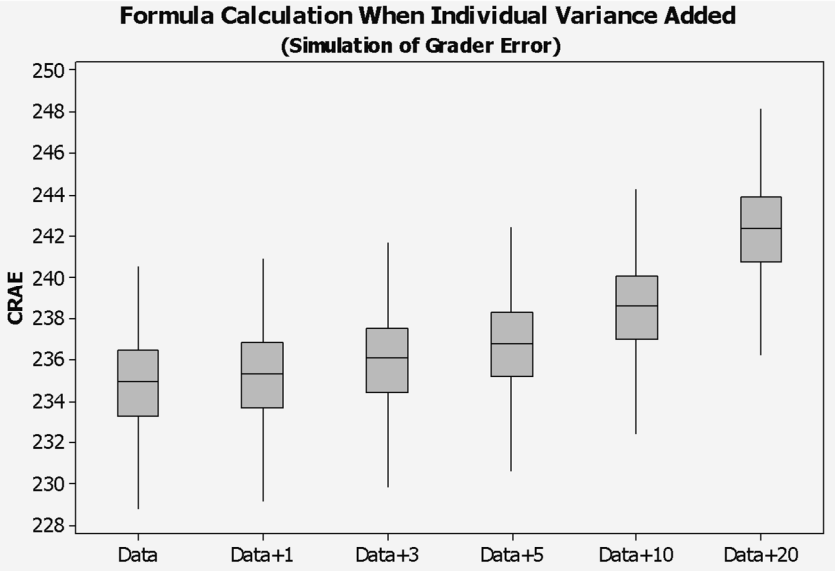

Figure 6.4 Calculations using CRAE summary formula when different additive errors are added to one measure ('Data' denotes orignal measures, 'Data+1' denote 1μm is added to one of the vessel measures, 'Data+3' denotes 3μm is added to one of the vessel measures, and so on). The boxplot shows 95% confidence intervals and mean values.

In Figure 6.4, the simulation result also shows that every unit of additive error has approximately one-third impact on the summary result and reduces two thirds of the variation. Therefore, the variation occurring on a single vessel has less impact on the summary measures. This confirms the speculation in Chapter 4 that the summary formulas are robust against variation. On the other hand, if there is subtle change on a single vessel, this change may not be detected when the summary formulas are used.

Another study (Moret et al., 2011) has confirmed that retinal pulsation does not exist for all people and for all vessels within the same person. This leads to the conclusion that the summary measures using the revised formulas may not be suitable for detecting subtle changes from an individual vessel, such as retinal pulsation.

6.3 Length of the Measured Vessel

Systemic diseases have impacts on the retinal vessel diameters that are quantitatively measured in a designated region (zone) (Wong et al., 2006a, Kifley et al., 2007, Sasongko et al., 2010). The optic disc centred retinal image analysis often defines the region-of-interest (ROI) into three concentric subzones surrounding the optic disc, described in Chapter 2. Briefly, each zone corresponds to the area between optic disc margin to 0.5 optic disc diameter (Zone A), 0.5 to 1 disc diameter (Zone B) and 0.5 to 2 optic disc diameters (Zone C) away from the optic disc margin. Currently Zone B and Zone C are the popular ROIs where most measurements are conducted.

The lengths of measured vessels vary in these zones. Though the individual vessel diameters are averaged from multiple cross-section diameters in a segment and then summarised into the summary diameter using the revised formulas, the analysis in Chapter 5 showed that there was significant difference in the summary diameters of the same vessels measured in different zones. Furthermore, the natural structure of retinal vessels often have branching and crossing which causes a difference in the measured vessel length defined by measurement protocols. For example, retinal vascular assessment software IVAN defines that the vessel trunk should be measured before the branching regardless of the length of the measured segment (RETVIC, 2008). However, it also warns that the measures may not be reliable if the trunk length is short.

The measured lengths of retinal vessels affect the measurement results. This impact needs to be investigated if the minimum measured length is required to achieve a reliable result. This will be useful for the future development of assessment protocol.

6.3.1 Materials and Methods

Thirty-four healthy volunteers, aged 20 – 39 years (18 male and 16 female), were recruited to participate in this study. The selected participants were considered young and in a narrow age band which minimised the possible impact of age. The exclusion criteria for the participants were: (i) any previous or current medical conditions; (ii) being on any medication and (iii) current smoker. Nine disc-centred retinal images of the non-dilated left eye of each participant were captured using ECG synchronised retinal photography method, described in Chapter 3. There were a total of 306 disc-centred retinal images.

The image processing and the vessel measurement using CPDM were previously detailed in Chapter 3. A total of 1161 retinal arteries and 1224 retinal veins were extracted and tracked. The diameters were calculated and all measured diameters were adjusted to follow the direction outbound of OD. The measured vessel diameters were averaged with each length unit, using the formula:

$$D(n) = \frac{\sum_{k=1}^{n} d(k)}{n} \quad (n > 0)$$

where *d* is the measured cross-section diameter along the vessel wall and *D* is the mean diameter. For example, a vessel segment has 1000 tracked points on the centreline and the diameters are measured perpendicular to the centreline and through these points. *D(1)* is the diameter through the 1st point. *D(2)* is the mean value of the first two diameters. *D(1000)* is the mean value of the measured 1000 cross-section diameters. The intervals between nearby two points are fixed. The mean diameters in the varied lengths are normalized by subtracting each value from its overall mean value.

6.3.2 Results and Discussion

In Figure 6.5, the mean diameters in the varied lengths of retinal venules are plotted. The maximum variation can reach 20μm for some vessels, particularly when the measured lengths are short. The absolute values calculated from the averaged

variations indicate the trend, shown in Figure 6.6. The trend shows that there is less variation when the measured lengths of retinal venules are longer. The variation has dropped to below 2µm when the measured lengths are longer than around 350 µm. The measurements of the retinal arterioles have similar results, shown in Figure 6.7. The averaged variation becomes less than 2µm when the length of the measured retinal arteriole is longer than around 400µm.

There is a knee point in the figure of variation versus the measured vessel length regardless of the vessel type. The knee point is corresponding to the measured length around 400µm. If the measured vessel length is longer than 400µm which is around a quarter of optic disc diameter, the variation in the mean value is stable and less than 2µm.

This study has demonstrated that the longer length of measured vessel has less variation and provides the more reliable results. The popular retinal assessment software often measures vessels in Zone B and Zone C. Zone C measures have the longer measured vessel length compared to Zone B measures. The results of this study indicate that the measures have less variation if the vessels are measured in Zone C compared to those measured in Zone B. This can explain why only the measures of Zone C in four sets of grading have smaller standard deviations, presented in Chapter 5. An earlier study (Yip et al., 2012) reported that the retinal vascular diameters measured in Zone C using SIVA had stronger associations with systemic variables compared to Zone B IVAN measures. This study provides an explanation for their finding.

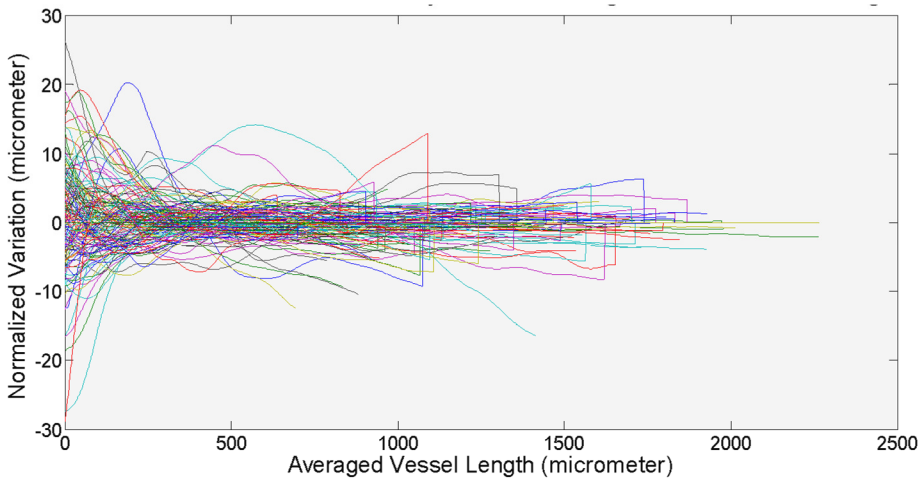

Figure 6.5 Mean diameters of retinal venules vary with the measured lengths.

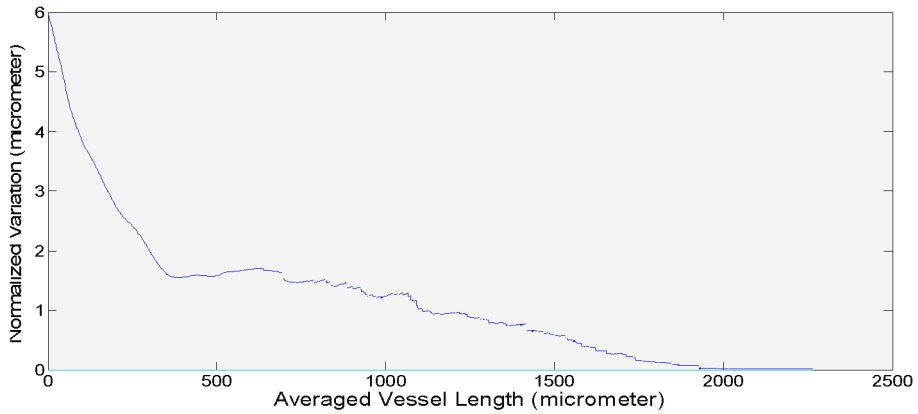

Figure 6.6 The trend of variation in varied lengths of measured retinal venules.

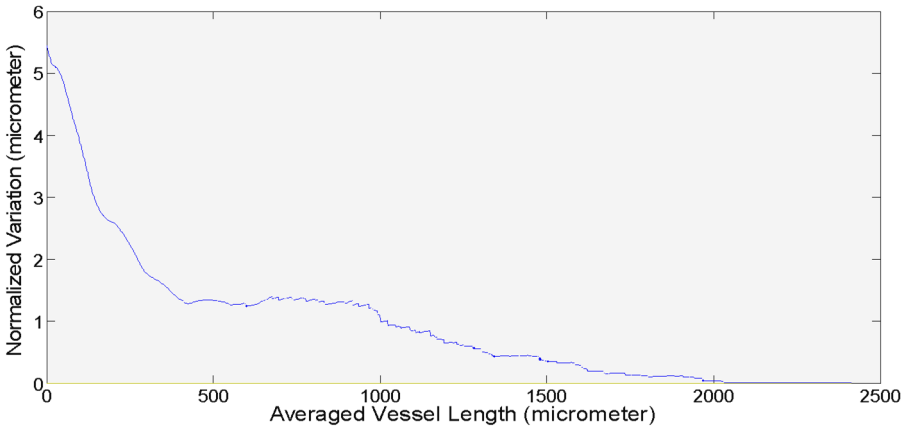

Figure 6.7 The trend of variation in varied lengths of measured retinal arterioles.

6.4 Measurement Protocol

Semi-automated retinal vascular assessments require manual intervention and a well-defined measurement protocol is important for a standardised procedure. A measurement protocol defines the measurement rules, such as region of interest, vessel selection, grader operation and image quality assessment. Semi-automated assessment software is able to roughly identify the optic disk, classify and track arterioles and venules. These processes require confirmation from a grader. If there is error on OD identification or vessel tracking, the grader needs to correct and re-track the vessel manually. The grader may also need to shorten or extend the measured vessel length, especially when a vessel has branching or two vessels are crossing. In Figure 6.8, two examples of IVAN measurement are shown. The grading protocol (RETVIC, 2008) defines the measurement of the trunk close to the optic disk rather than the branches even though the trunk is much shorter than the branches. The short measured vessel length may induce large variation in the measurement as discussed earlier and the minimum measured vessel length should be considered in the measurement protocol.

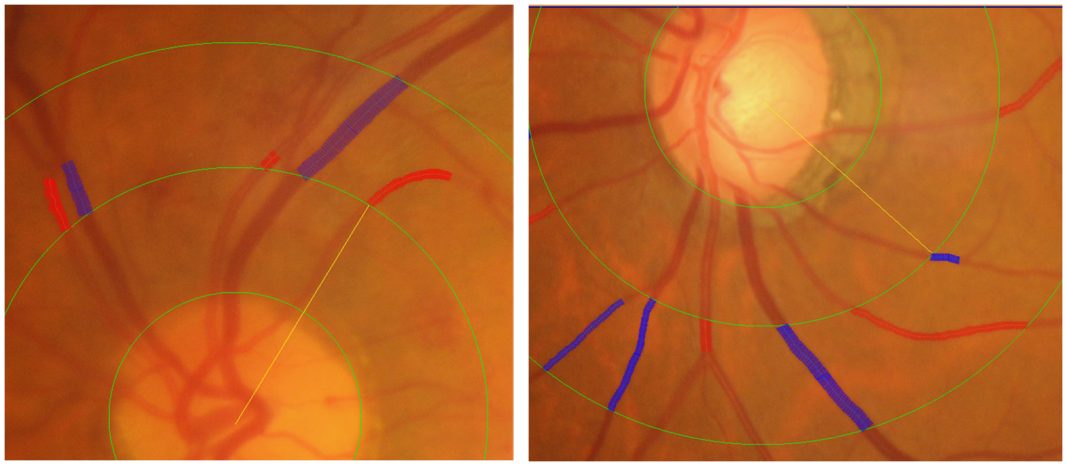

(a) (b)

Figure 6.8 Two examples of IVAN measurement. The vessel measurements are generated automatically by the software. According to the grading protocol, (a) the vessel is measured before the crossings and (b) the trunk is measured rather than branches regardless of the length.

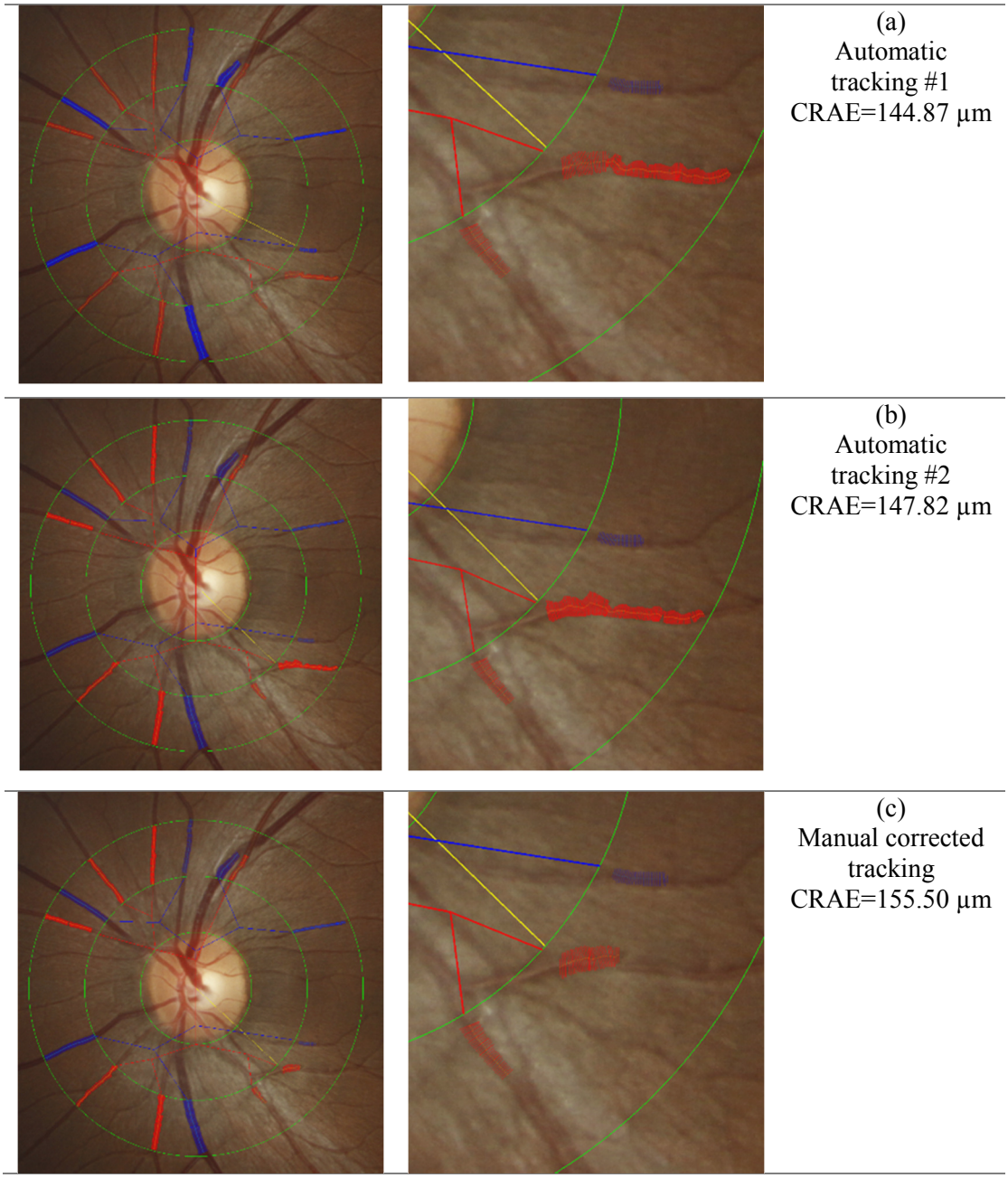

Figure 6.9 Calculated CRAE summary diameter when an arteriole is re-tracked automatically and manually. (a) and (b) automatic vessel tracking. (c) the tracking error is manually corrected by the grader according to the grading protocol.

.

In Figure 6.9, the CRAE measures are compared when an arteriole is re-tracked multiple times. Small difference is shown in CRAE measures between two automatic tracking processes, though both tracked edges do not reflect the vessel correctly, shown in Figure 6.9 (a) and (b). The repeated measurements of a vessel diameter can be

different and this has been noticed in both SIVA and IVAN measurements. The automatic tracking starts from a point on or close to the identified optic disk edge or the calculated zone edge. Different starting points result in different tracking paths of vessel edge. Thus, the diameter measured between the tracked edges may be different in each automatic tracking process. Figure 6.9(c) shows that the CRAE difference becomes larger when the tracking is manually corrected according to the protocol. This demonstrates that manual intervention in the vessel edge tracking process induces variations. Well-defined protocol and strict measurement rules can limit these variations. However, errors in automatic vessel tracking may be overlooked. Possible elimination of these errors can only be assumed when study population is large.

6.5 Summary

The summary method provides a solution to quantitatively measure retinal vessels by summarising the individual measures using the summary formulas. The simulation study has investigated the effects of the summary method using the revised formulas on the aspects of sample size, grader bias and systemic error, and random measurement error. The results have proven that these summary formulas are robust against variation and show promise in the population based studies.

However, the simulation study also found that: (i) the summary formulas were inefficient to reduce the systemic errors and inter-grader variations if they were consistent in one direction; (ii) the subtle change on a single vessel can be masked by the summary formulas and thus difficult to be detected. Therefore, the summary method may not be suitable for monitoring the change of an individual vessel. Methods need to be developed for the future studies such as individual longitudinal study and retinal pulsation study.

The study of the measured vessel length experimentally proved that the mean value of individual vessel diameters varies with the measured vessel lengths. Retinal

vessel diameter assessments often report that the changes associated with the systemic diseases are small (Leung et al., 2003b, Smith et al., 2004). Therefore, the variations in the measurement are crucial for measurement reliability and assessment credibility. Minimising the variations in the individual vessel measurement can reduce the variation in the summary measures, and improve the reliability of assessment. The concept of the minimum measured vessel length of 400μm is suggested for this purpose.

This chapter has also demonstrated the importance of a measurement protocol in the cause of variation. A proper measurement method with well-defined protocol is essential to eliminate measurement variation. A grader must follow strict rules defined in the protocol to achieve a reliable measurement result.

Chapter Seven

Visualisation and Measurement of Retinal Vessel Dynamic Change

7.1 Introduction

There is a technical distinction between the terms ‘variation’ and ‘variability’. Gerald Van Belle described ‘variability’ as one category of variation and ‘refers to natural variation in some quantity’, whereas ‘uncertainty refers to the degree of precision with which a quantity is measured’ (Van Belle, 2008). The term ‘variation’ used in this thesis refers to the various sources of variability and uncertainty, either one or the other.

In Chapter 3 and 4, the cardiac ‘variability’ in the retinal vascular parameters was studied. In Chapter 5 and 6, the ‘uncertainty’ (measurement error) induced by the measurement protocol, graders and software was discussed. This chapter is to study the natural variability in the retinal vessels, and the visualisation and measurement of retinal vessel dynamic change are the focus. Dynamic changes among time series retinal images provide the information associated with the natural states of retinal vessels and retinal pathology (Morgan et al., 2004). ECG synchronised retinal photography introduced in Chapter 3 has established a platform for this study.

7.2 Visualisation of Retinal Vessel Dynamic Change

7.2.1 Flash-less Retinal Photography

Retinal photography requires retina illumination through the pupil. Pupil dilation is often used in clinical settings to overcome pupil contraction (Morgan et al., 2004). This requires operation by an ophthalmic professional. Continuous retinal illumination makes patients feel uncomfortable. Furthermore, the retina illumination induces noise in the captured image. Light reflections from the background and vessel surface cause artifacts in the measurements, often known as uneven background and centre reflex (Kumar et al., 2012). In Figure 7.1, flash noise on a retinal image is shown and its impact on retinal vessel intensity profile. In Figure 7.1(b), the centre reflex often causes

false identification of vessel edges during automatic processing. The uneven edges in intensity profile induce the variation on diameter estimation. In Figure 7.1(c), the background light reflection noise that distorts the vessel edges is shown. This often causes difficulty and error in vessel extraction and tracking (Sofka et al, 2006).

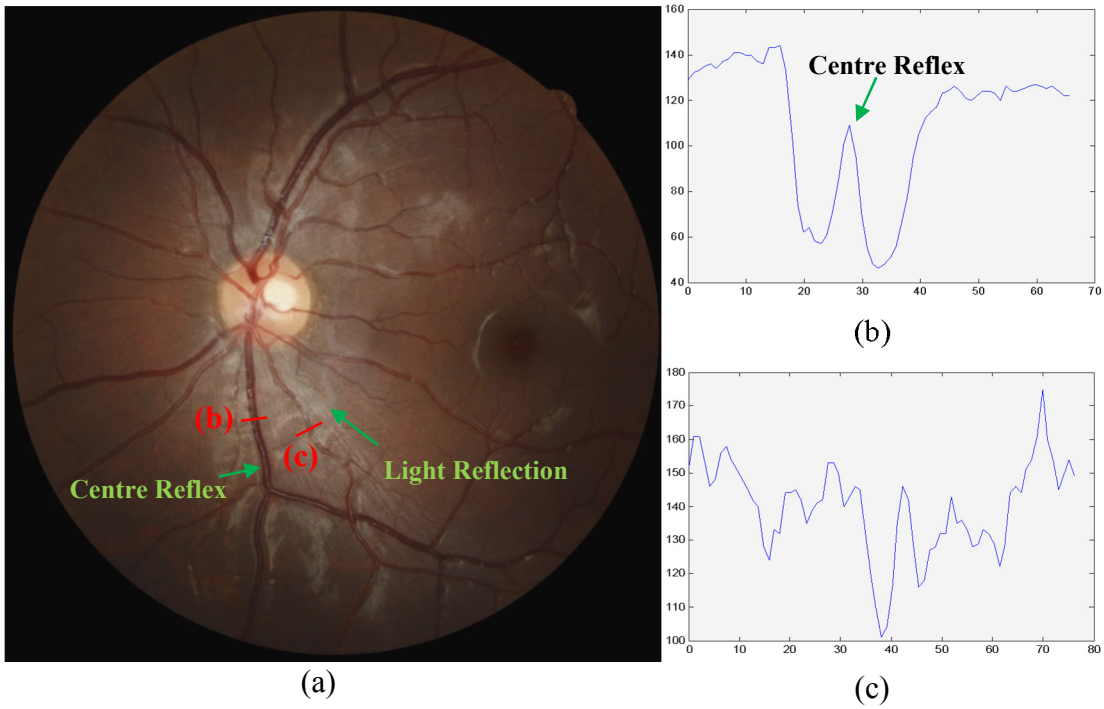

Figure 7.1 Light noise in a retinal image. (a) Retinal image with flash noise, centre reflex on a vessel and light reflection on background. (b) Grayscale intensity profile of a retinal venule with centre reflex. The location is marked on the image. (c) Grayscale intensity profile of a retinal arteriole with distorted edges due to background light reflection.

Flash-less retinal photography using Infrared (IR) technology has been considered to overcome these problems (Elsner et al., 1996). IR light has longer wavelength than visible light and is invisible to human eyes. In Figure 7.2, the electromagnetic spectrum is shown. IR is used in daily lives, such as remote control and night vision surveillance, and safety can be assured. Near infrared wavelength range is employed in retinal imaging (Charbel et al., 2009, Neider, 2004), such as Spectralis® cSLO using 820 nm IR reflectance. Infrared photography technique was evaluated for the purpose of flash-less retinal imaging in this thesis.

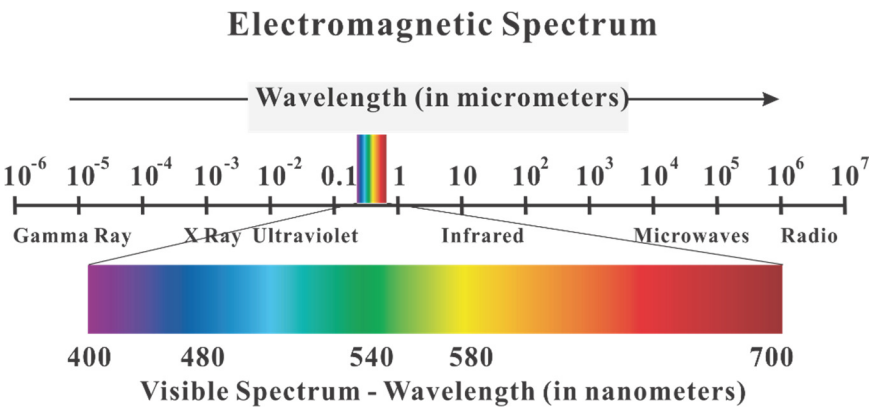

Figure 7.2 Electromagnetic spectrum and visible spectrum

In Chapter 2, the mechanism of the retinal camera was introduced. The retinal camera captures an image with an attached digital camera body through a shared optical path, illuminating the retina with a built-in flash. The purpose-built flash-less retinal photography includes (i) near infrared light with peak wavelength 940nm and photon energy 1.2 eV that is invisible to human eyes; (2) camera body where built-in filter is removed to sensor full band of lights. The modification of the retinal camera was supervised by a military night vision company to ensure safety. The camera body modification and parameter adjustment were done professionally by a third party.

The flash-less retinal camera is able to capture a retinal image successfully, shown in Figure 7.3. Compared to retinal image captured using a normal digital camera (Figure 7.4), flash-less retinal image does not have full colour and looks different. For example, the retinal major vessels are nearly ‘filtered’ and the choroidal vasculature is visible. This is due to longer wavelengths that allows better penetration through blood and retinal pigment epithelium (Neider, 2004).

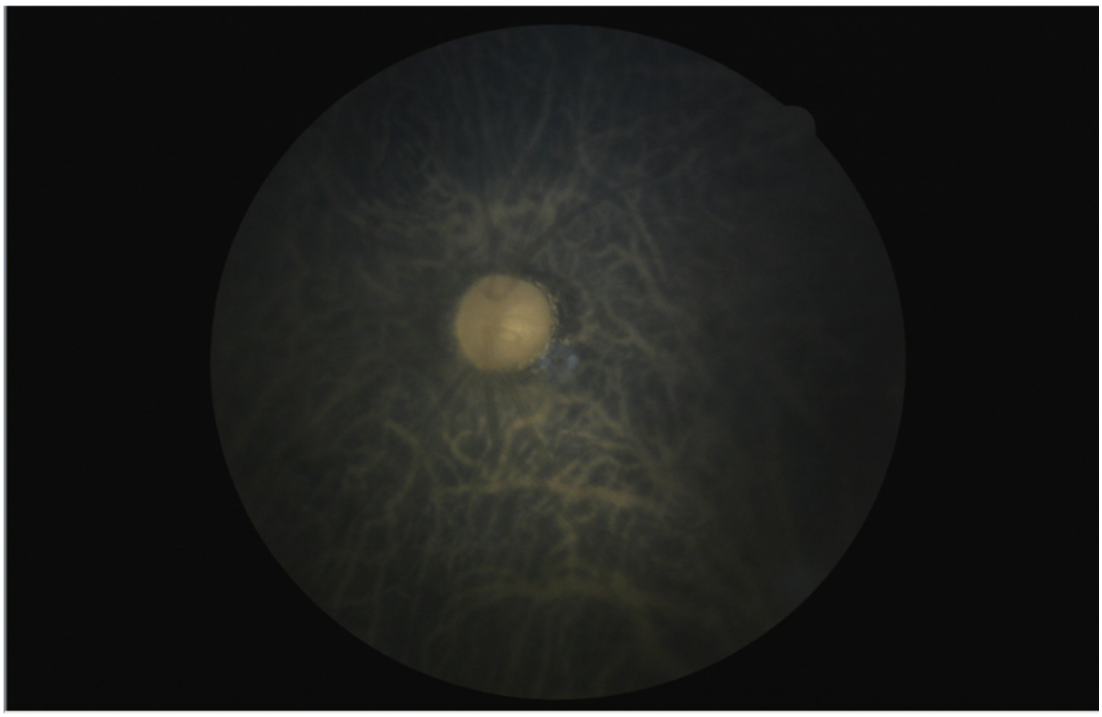

Figure 7.3 Flash-less infrared retinal photograph

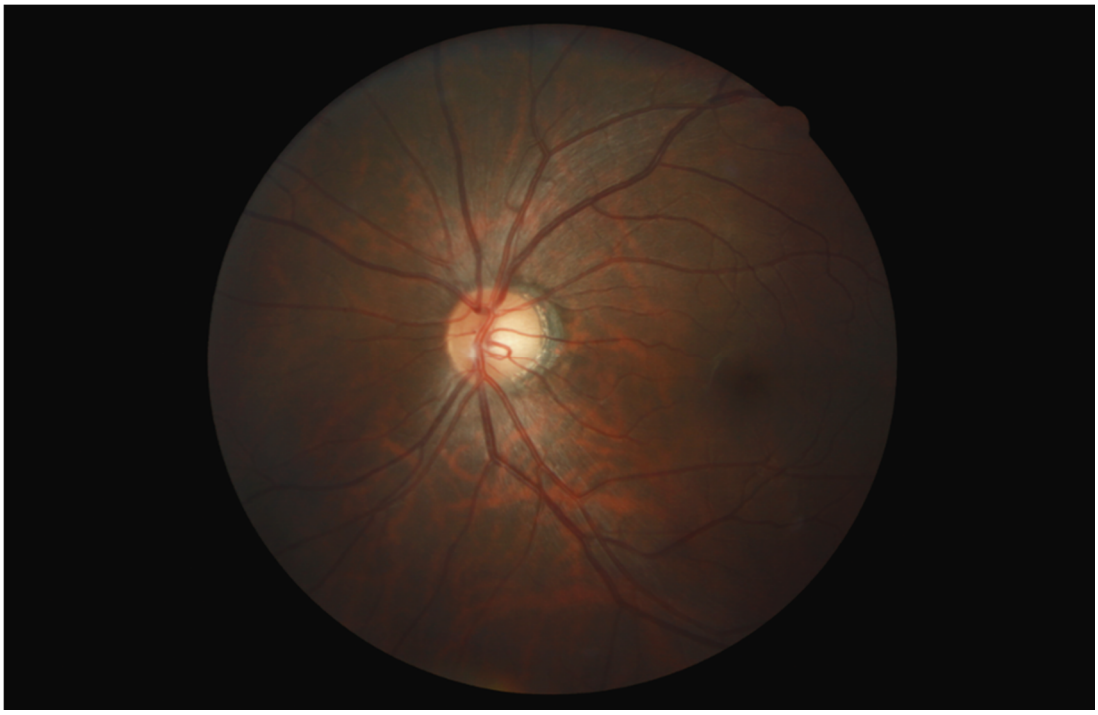

Figure 7.4 Normal retinal photograph of the same eye shown in Figure 7.3

The retinal images using the flash-less retinal photography are not suitable for current retinal vascular assessment where retinal vessels are study objects. The images captured using flash-less retinal camera contain similar features as indocyanine green angiography (Elsner et al., 1994) without invasive dye injection and the unique background pattern can be extracted as features for biometrics. Further study may improve image quality and discover other applications.

7.2.2 Smartphone Based Retinal Imaging and Video Recording

Welch Allyn iExaminer system (Allyn, 2014) is a recent retinal imaging method using smart phone and PanOptic™ Ophthalmoscope. This system was replicated in this thesis and evaluated for capturing continuous retinal images. Welch Allyn iExaminer system is only designed for Apple® iphone. This thesis redesigned the system to be usable with any smartphone. In Figure 7.5, the design of the PanOptic™ Ophthalmoscope with a customised removable mount is shown.

Figure 7.5 Ophthalmoscope and adjustable mount to smart phone (latter not displayed).

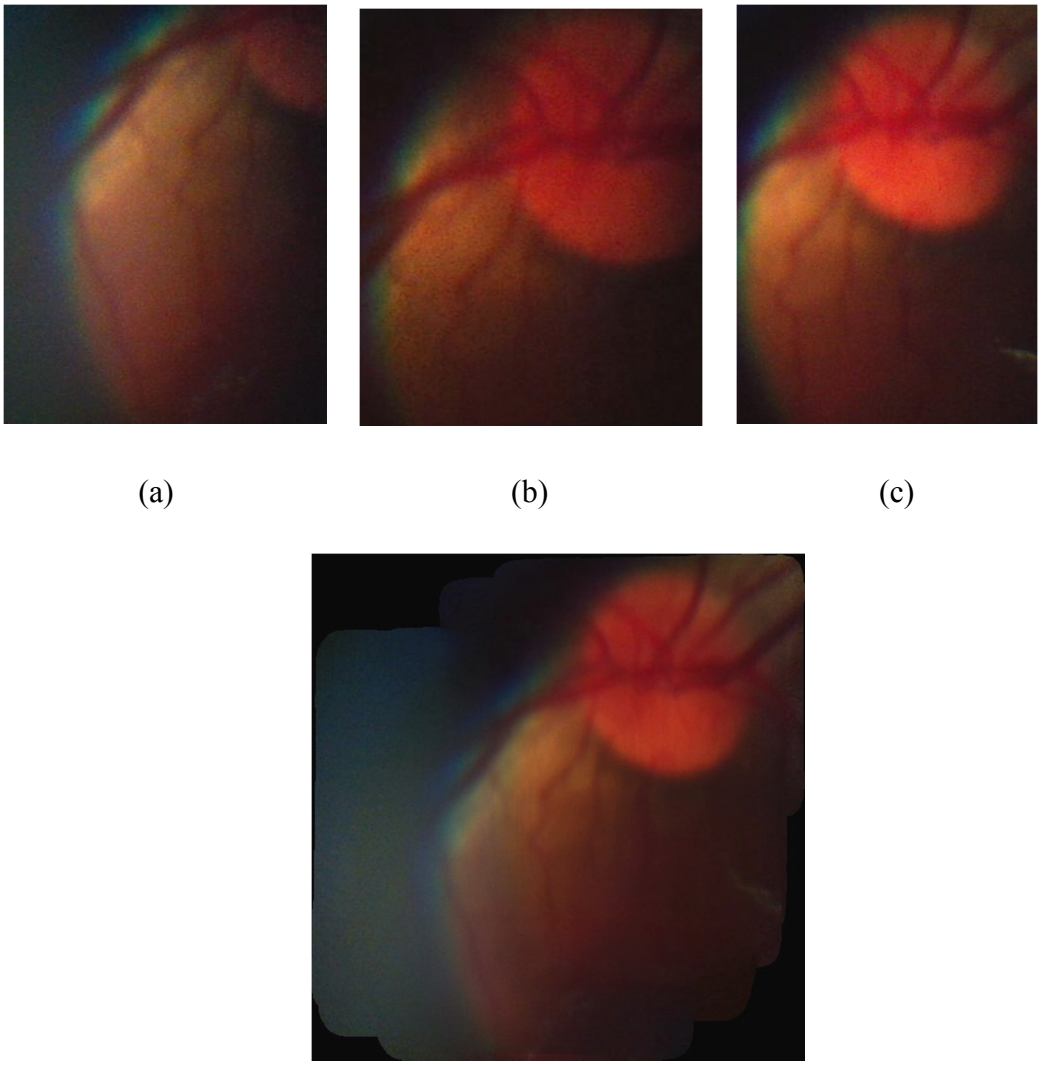

Figure 7.6 Image montaging. Three images (a, b, c) were automatically selected from the image sequence (video) and formed into a larger view image (d).

Though the integration of PanOptic™ Ophthalmoscope and smart phone has shown advantages of low cost and portability, the limitations are noted. Compared to the digital camera used in this thesis (Canon EOS 50D digital SLR camera with 18 Megapixel image resolution), the smart phone can only capture up to 12 Megapixel resolution images using most current smart phone. The extracted images from the recorded video have lower resolution. Moreover, PanOptic™ Ophthalmoscope can only capture 15 degrees of view, which is approximately one third of the image captured

using 45 degree of view retinal cameras. This can be compensated using a montaging technique to form multiple images of 15 degree of view into a larger view and Figure 7.6 shows an example of montaging multiple images using Retinal registration software (i2k Retina®, DualAlignTM). Furthermore, PanOptic™ Ophthalmoscope is held by the operator's hand and photography is difficult due to movements of the hand, the patient's head and eyeball.

7.2.3 Visualisation of Time Series Retinal Photographs

ECG synchronised retinal photography captures time series retinal images with time reference of the human cardiac cycle. These images can be formed into an image sequence. As the retinal vascular changes are considered to alter periodically with the cardiac cycle (Levine, 1998), the repeat of image sequence shows retina dynamic and provides direct information of the retinal vascular dynamic change.

Image registration is required to form the ECG synchronised retinal photographs correctly into an image sequence with the same spatial reference. The commercial retina registration software (i2k Retina®, DualAlignTM) is used to register all images to the first frame for each subject. Freeware AnimateGif (Version 1.1, Xylem Studios) is chosen to create GIF format animation. GIF format is considered as an image format that is small and easy for distribution. The examples can be downloaded from thesis CD or online (Appendix 1).

7.3 Measurement of Retinal Vessel Dynamic Change

The visualisation of retinal dynamic change can provide direct information to the optometrist or ophthalmologist for visual assessment of the eye. The dynamic change in time series retinal images needs to be quantitatively measured to ensure accurate assessment.

Current retinal image analysis is based on the captured single image where all vessels are considered to be still over time. However, this does not reflect the reality of the dynamic change of retinal vessels. The cause of the dynamic change includes the retinal pulsation and other unknown factors, previously discussed in chapter 2. Studies have previously reported that the retinal vessel dynamic change (retinal pulsation) differs between both the individuals and the vessels (Kumar et al., 2013, Moret et al., 2011). Significant differences have been found on individual retinal vessel diameters across time series retinal images during the cardiac cycle, presented in Chapter 4.

There is no established method to measure the change of retinal vessel across time series retinal images. In this part, methods are proposed to monitor these dynamic changes in retinal vessels. This will benefit a future study of retinal pulsation and longitudinal assessment in individuals.

7.3.1 Materials and Methods

Eighteen male volunteers aged 20 to 39 years were recruited. The selected participants were considered young and healthy. The exclusion criterion for the subjects was (i) any previous and current medical conditions, (ii) being on any medication and (iii) current smoker. Nine disc-centred retinal images of the non-dilated left eye of each participant (a total of 162 images) were captured using ECG synchronised retinal photography described previously in Chapter 3.

The image processing and centreline perpendicular diameter measurement (CPDM) have been introduced in Chapter 3. The ideal vessel edges with a smooth change of the vessel direction provide good results using CPDM. However, when the retinal vessel edges are asymmetric or the changes of direction are irregular, the estimated diameters may not correspond with the same spatial location in time series images, shown in Figure 7.7 (top figure). Therefore, this thesis proposed fixed-point cross-section measurement (FPCM). FPCM sets fixed points equally on both edges

between the identified starting and ending points and monitors the distance change between the paired points located on two edges. When comparing the same vessel in time series images, FPCM results seem more related to the spatial change, with the estimated diameters close together or overlapped, as shown in the bottom figure of Figure 7.7. The diameters measured using FPCM are not traditionally defined retinal vessel diameters because the cross-section of paired fixed points are not always perpendicular to vessel direction. FPCM is proposed to measure the change of vessel in the same spatial location. Compution of the vessel direction vector and the centrelines are not required, thus the implementation of FPCM is simple and fast.

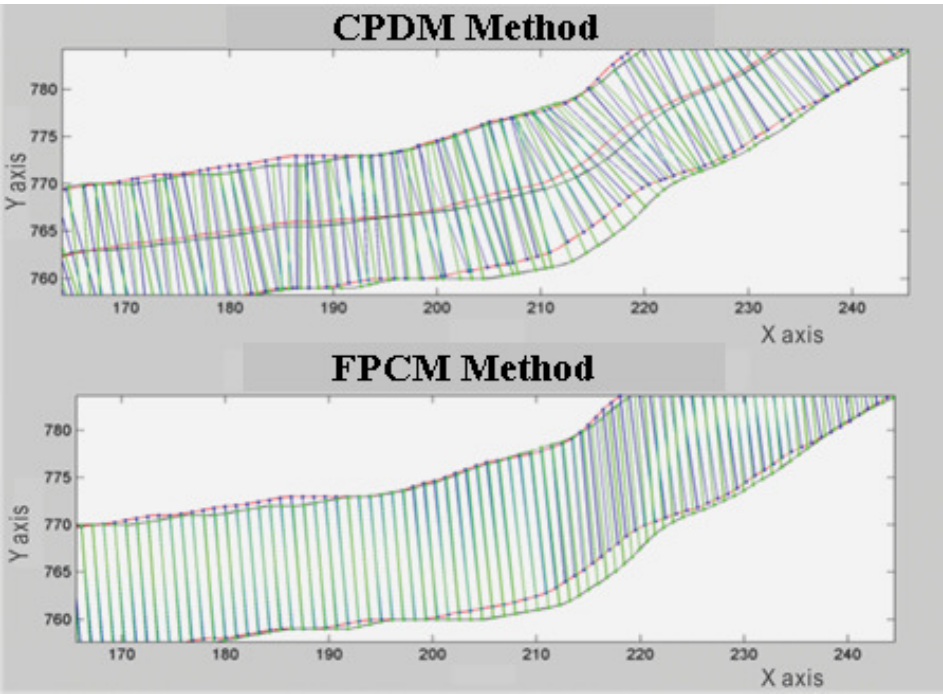

Figure 7.7 A vessel segment measured in two of time series images. Top figure shows CPDM result. The measured points are not corresponding to same spatial location due to centreline displacement. Bottom figure using FPCM shows a reasonable result.

The cross-section diameter measurement using FPCM includes the following steps: 1) start with the first point on one edge and identify the shortest distance to the other edge in the first frame of image sequence; 2) start with the first point on the other

edge and identify the shortest distance to another edge; 3) compare the distances from step 1 and 2. The shorter one is selected as the starting line and extended; 4) check if this extended line has two edge crossing points in all registered time series images. If failed, move to next point and repeat step 1 to 3 until the starting line has crossing points on both edges in all time series images; 5) use the same process to find the ending line; 6) set the fixed points equally on both edges between starting and ending lines in registered time series images; and 7) calculate the cross-section diameter between the paired points located on two edges.

In Figure 7.8, the measurements of the continuous vessel edge changes in time series retinal images using CPDM and FPCM methods are compared. Nine curves in the top figure show the diameter measures of the same vessel change along the vessel length in time series images using CPDM method. These curves have similar shapes that indicate high correlation (Pearson correlation coefficients are calculated in the result). This correlation can be also observed in the measures using FPCM method, shown in bottom figure.

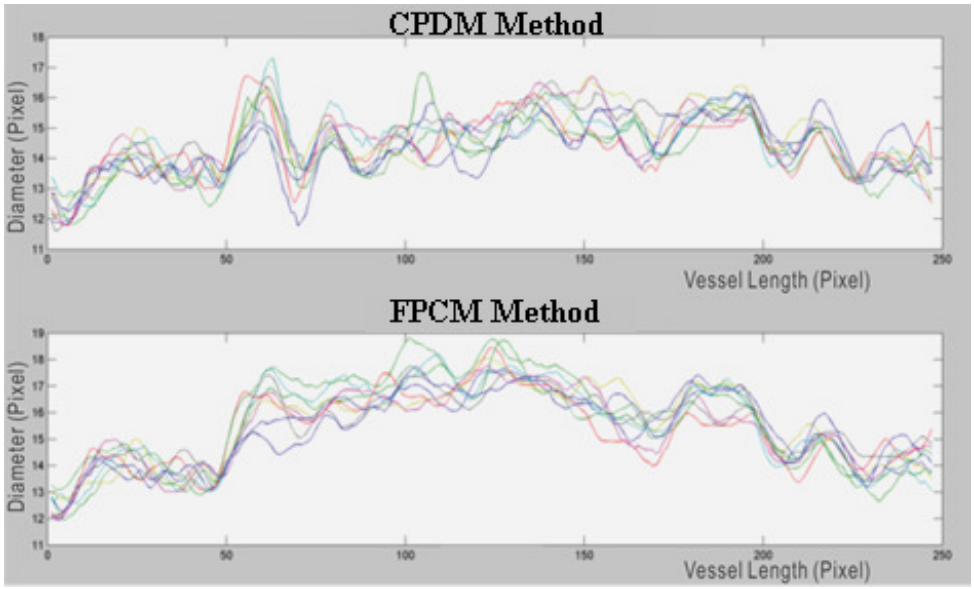

Figure 7.8 The estimated change of same vessel from time series images (nine images) are measured using CPDM (top figure) and FPCM (bottom figure).

7.3.2 Results and Discussion

A total of 621 retinal arterioles and 693 venules were tracked and measured from time series retinal images of 18 subjects. The mean value and standard deviation are calculated from each arteriole and venule and averaged, shown in Table 7.1. Paired t-test shows no significant difference between the measures using CPDM and FPCM methods ($P<0.001$).

Table 7.1 Continuous diameter measurement using CPDM and FPCM methods

Diameter (pixel)	Arterioles		Venules	
	Mean	SD	Mean	SD
CPDM	13.67	1.38	15.51	2.02
FPCM	14.10	1.45	16.08	2.11

Pearson correlation coefficient is used to assess the correlation between CPDM and FPCM methods, which are 0.59 for retinal arterioles and 0.62 for retinal venules. This indicates moderate correlation between the two methods. The average correlation coefficients among time series images are 0.68 for arterioles and 0.72 for venules using CPDM, while 0.71 for arterioles and 0.71 for venules using FPCM.

When estimating the dynamic change of a single vessel, three parameters, the mean ratio, standard deviation ratio (SD ratio) and correlation, are proposed to measure the change quantitatively. The mean value represents the size of the vessel, which is similar to retinal vessel diameter in other retinal vascular assessment. The mean ratio, which is defined as the mean value of vessel diameters at different cardiac points divided by the mean value in the first frame of time series images, is proposed to normalize the individual differences. Therefore, the mean ratio in the first frame is fixed to 1. Similarly, SD ratio is proposed to standardise the SD values. The changes of SD ratio at different cardiac cycle points shows the perpendicular change of vessel edges. The correlation is calculated between the vessel diameter matrix at each cardiac cycle point and those of first frame. Higher correlation value indicates higher similarity of the edge shapes.

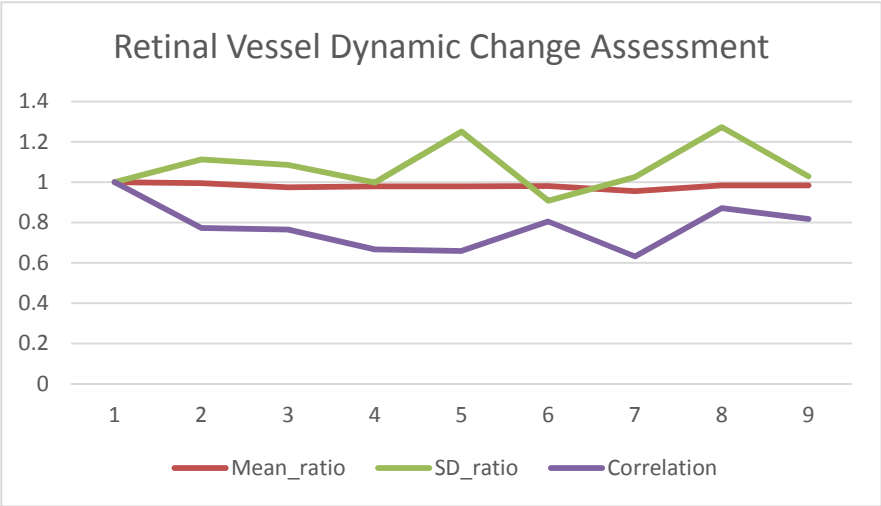

Figure 7.9 Proposed retinal vessel dynamic change measurement using CPDM. The change can be represented with the mean ratio, SD ratio and correlation.

In Figure 7.9, an example of the changes in a retinal arteriole over the cardiac cycle is shown. The mean ratios are close to one, which indicates minor changes in vessel size over the time. Both mean ratio and SD ratio are smaller between the cardiac cycle point 6 and 7, which indicates vessel size and change become smaller. The dynamic change of vessel size appears larger at point 5 and 8. The vessel shape change is large during the middle points of cardiac cycle. In Figure 7.10, similar results are shown when same vessel is measured using FPCM.

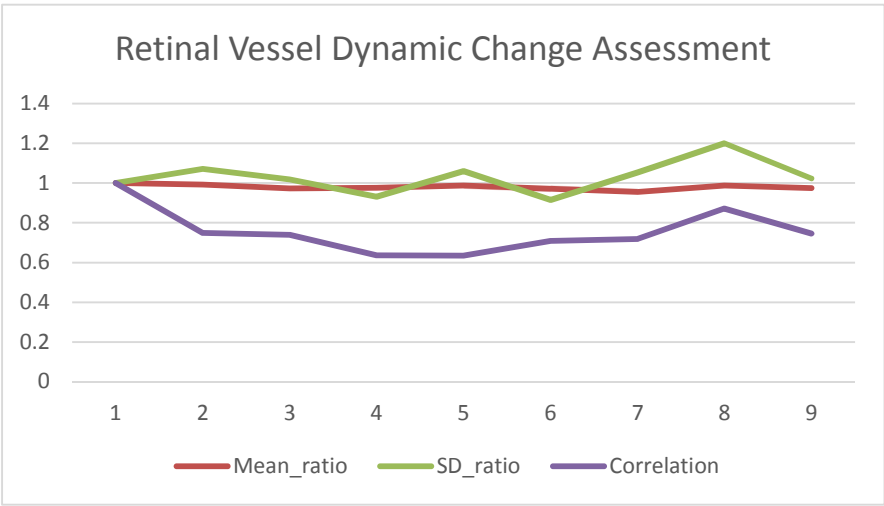

Figure 7.10 Retinal vessel dynamic change measurement using FPCM.

Both CPDM and FPCM methods have advantages and limitations. CPDM follows the vessel direction vector and the estimate is approximate to the definition of retinal vessel diameter. The drawback of CPDM is that the centreline perpendicular diameter does not reflect corresponding changes in the same spatial location where the centrelines have displacement across time series images. If the direction vector has a sudden change of direction, measurement error will occur. The concept of FPCM is to monitor distance changes between fixed points located on both vessel edges. It is simple and easy to implement. The computation time depends on the tracked vessel length but FPCM is faster than CPDM. Though FPCM reflects changes of retinal vessel edges over time, estimates using FPCM may be misread when the measured vessel has a large curve. When the appearance of a vessel is close to a straight line, the measures using CPDM and FPCM methods illustrate high similarity, shown in Figure 7.11.

7.4 Summary

This chapter focused on methodology development for the visualisation and measurement of retinal dynamics. It studied and verified several methods for the purposes of capturing time series retinal images and visualising retinal vessel change. ECG synchronised retinal photography creates a platform for capturing multiple retinal images synchronized with the cardiac cycle. Visualisation of the retinal image sequence using ECG synchronised photographs provided direct view of retinal vascular dynamics.

New methods have been developed to measure the retinal dynamics quantitatively based on consideration of three aspects of retinal vessel changes: (i) the change on vessel size; (ii) the edge change perpendicular to vessel direction; and (iii) the change on edge shape. Both CPDM and FPCM methods have demonstrated the ability of quantitatively measuring and monitoring the vessel changes across time series

retinal images. This preliminary study has built a framework for future methodology development, and clinical study is needed to verify this method.

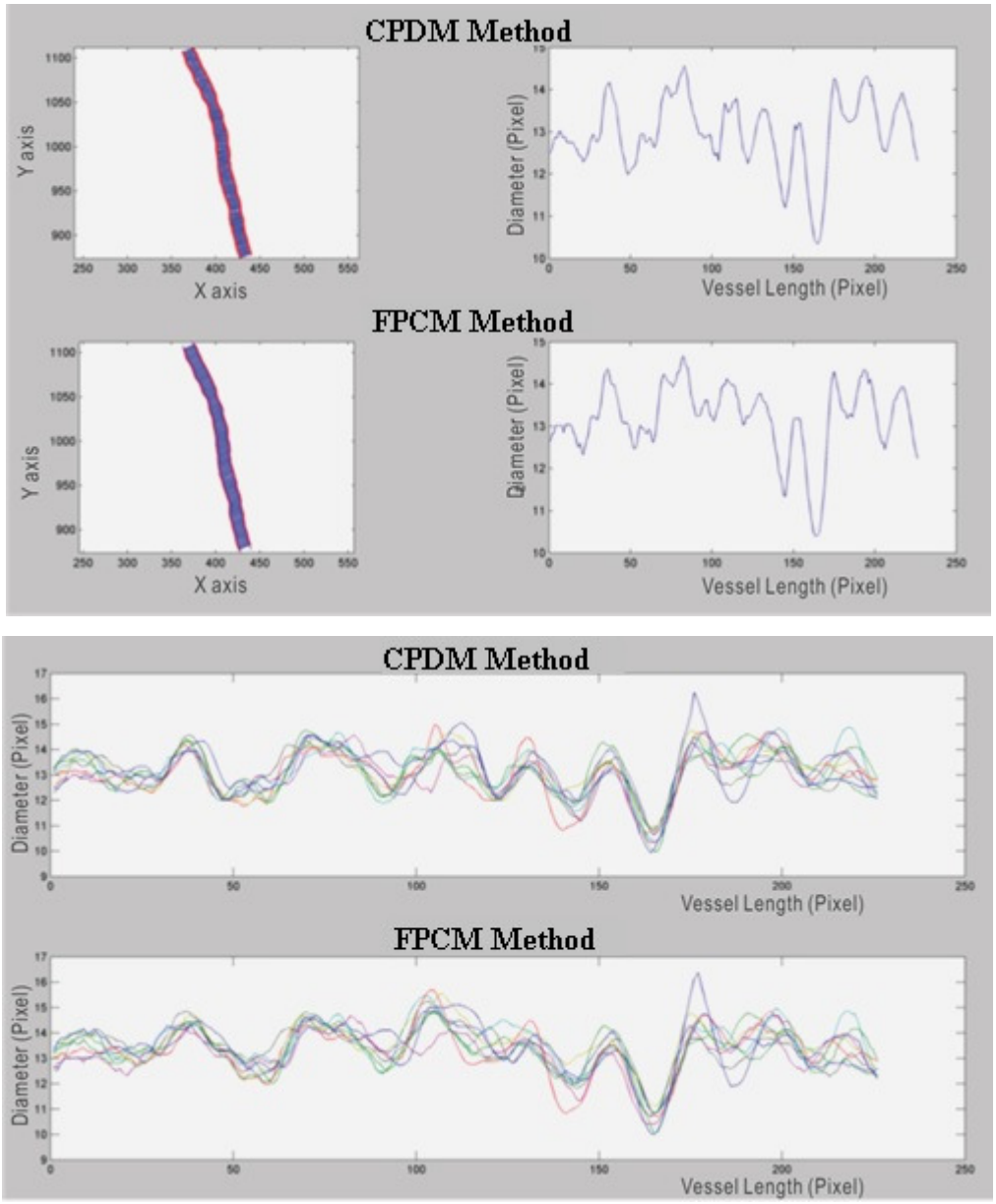

Figure 7.11 Dynamic measures of a vessel using CPDM and FPCM show similar results

Chapter Eight

Conclusion and Future Work

8.1 Conclusion

Retinal vascular parameters have been shown to have association with a number of disease conditions. However, outcomes have not yet demonstrated an improvement in risk assessment (Sun et al., 2009). Earlier studies have suggested that poor specificity of the retinal vascular assessment against disease is because of variations in the measurements. However, this has not been comprehensively studied, nor methods to mitigate these variations identified.

This thesis has comprehensively studied the variations and their sources in retinal vascular assessment. It has concluded that there are significant variations due to a range of factors and has identified some methods to reduce the variability. The findings of this thesis can be summarised as follows:

i. It has been confirmed that random retinal photography without consideration of the cardiac cycle leads to large variations in measurement. There is significant difference in the individual vessel diameter of retinal arterioles and venules during the cardiac cycle.

ii. The summary diameters, which are summarised from the individual diameters using the revised formulas, have non-significant variation during the cardiac cycle.

iii. Other retinal vascular parameters, such as tortuosity, branching angle, LDR and fractal dimension, have none to little variation during the cardiac cycle.

iv. ECG synchronised retinal photography is able to reduce the variations in retinal vascular diameter measurements.

v. Significant inter-grader variability was found when commercially available semi-automated retinal vascular measurement software was used. This raises the need for caution in interpreting assessment results and comparing between different studies. The significant variations between graders also suggest that there is need for a more well-defined measurement protocol.

vi. Measurement software and protocols induce variations in the aspects of vessel selection and the regions where vessels are measured. There are significant differences in the measures using different software programs or conducted at different regions. This indicates that the results measured using different software programs or at different regions are not comparable.

vii. The study of the summary method has confirmed that the summary method is robust against variation in retinal vascular diameter measurement. However, the work also shows that small changes such as due to the cardiac cycle are not captured when the summary measures are taken, and indicates that subtle changes are masked by the summary method.

viii. Simulation study demonstrates that the summary method is suitable for comparing different groups in population-based studies but not for monitoring small changes of an individual. The summary method used in current retinal vascular assessment shows the limitation in the assessment of individual vessel or individual person.

8.2 Methodology Improvement

This thesis has concluded based on statistically significant experimental results that there are various sources of variation in retinal vascular assessment, which are due to a range of causes such as the timing of the photograph, and methods of measuring the parameters. Following are some suggestions to reduce the variation and thus improve the relevance of retinal image analysis.

i. The study of measurement software and ROI has found that the variation in retinal vessel summary diameter is less if a longer length of vessel is measured. The results suggest that the minimum length of measured vessel should be over 400μm to minimise possible variation.

ii. The measurements conducted in Zone C shows less variation compared to Zone B measures. Therefore, software and methods conducted in Zone C are suggested for reliable retinal vascular assessment.

iii. To minimise uncertain variations induced in retinal vascular measurement, ECG synchronised retinal photography is suggested to synchronise the photographs at ECG R-waves. The novel methodology described in the thesis has demonstrated the ability to minimise cardiac variations.

iv. ECG synchronised retinal photographs provide the opportunity to study retinal vessel dynamic changes using high-resolution images that are essential for detecting minor changes. Several methods to visualise and quantitatively measure retinal vessel dynamic changes have been proposed in this thesis.

8.3 Future Work

This thesis has comprehensively investigated the process of current retinal vascular assessment. The findings have assured current assessment methodology but also demonstrated the limitations and need for improvement. Based on the findings of this thesis, the future work is suggested.

Current semi-automated measurement methods require significant manual intervention from a trained grader. This has not only restricted the modality to be accessed by patients who are not located close to major medical facilities, but it also leads to significant variations. An automated retinal vascular assessment is essential for minimising the variations and for wider access of retinal image analysis.

There are potential applications of vasculature pulsation for diagnostic purposes. However, this requires clinical studies that may use the technological developments reported in this thesis to validate and test for disease associations.

References

AHAMMER, H. 2011. Higuchi Dimension of Digital Images. *PLoS ONE,* 6**,** e24796.

AL-DIRI, B., HUNTER, A. & STEEL, D. 2010. Accurate methods for manually marking retinal vessel widths. *7th European Symposium on Biomedical Engineering.*

ALIAHMAD, B., KUMAR, D. K., HAO, H. & KAWASAKI, R. Does fractal properties of retinal vasculature vary with cardiac cycle? Biosignals and Biorobotics Conference (BRC), 2013 ISSNIP, 18-20 Feb. 2013 2013. 1-4.

ALLEN, L. 1964. Stereoscopic fundus photography with the new instant positive print films. *American Journal of Ophthalmology* 539-43.

ALLYN, W. 2014. *The Welch Allyn iExaminer System* [Online]. Available: http://www.welchallyn.com/promotions/iExaminer/index.html 2014].

AMERASINGHE, N., AUNG, T., CHEUNG, N., FONG, C. W., WANG, J. J., MITCHELL, P., SAW, S.-M. & WONG, T. Y. 2008. Evidence of Retinal Vascular Narrowing in Glaucomatous Eyes in an Asian Population. *Investigative Ophthalmology & Visual Science,* 49**,** 5397-5402.

BAILLIART, P. 1918. La circulation veineuse rétinienne. *Ann. Ocul.***,** 453-472.

BAKER, M. L., HAND, P. J., WANG, J. J. & WONG, T. Y. 2008. Retinal Signs and Stroke. *Stroke,* 39**,** 1371-1379.

BENBASSAT, J. & POLAK, B. C. P. 2009. Reliability of screening methods for diabetic retinopathy. *Diabetic Medicine,* 26**,** 783-790.

CHARBEL ISSA, P., FINGER, R. P., HOLZ, F. G. & SCHOLL, H. P. N. 2009. Multimodal Imaging Including Spectral Domain OCT and Confocal Near Infrared Reflectance for Characterization of Outer Retinal Pathology in Pseudoxanthoma Elasticum. *Investigative Ophthalmology & Visual Science,* 50**,** 5913-5918.

CHE AZEMIN, M. Z. 2012. *Greyscale analysis of retina scans.* PhD Thesis, RMIT University.

CHEN, H., PATEL, V., WIEK, J., RASSAM, S. & KOHNER, E. 1994. Vessel diameter changes during the cardiac cycle. *Eye (London, England),* 8**,** 97.

CHEUNG, C. Y.-L., ZHENG, Y., HSU, W., LEE, M. L., LAU, Q. P., MITCHELL, P., WANG, J. J., KLEIN, R. & WONG, T. Y. 2011a. Retinal Vascular Tortuosity, Blood Pressure, and Cardiovascular Risk Factors. *Ophthalmology,* 118**,** 812-818.

CHEUNG, C. Y., TAY, W. T., MITCHELL, P., WANG, J. J., HSU, W., LEE, M. L., LAU, Q. P., ZHU, A. L., KLEIN, R., SAW, S. M. & WONG, T. Y. 2011b. Quantitative and qualitative retinal microvascular characteristics and blood pressure. *Journal of Hypertension,* 29**,** 1380-1391.

CHEUNG, N., ISLAM, F. M. A., SAW, S. M., SHANKAR, A., DE HASETH, K., MITCHELL, P. & WONG, T. Y. 2007. Distribution and Associations of Retinal Vascular Caliber with Ethnicity, Gender, and Birth Parameters in Young Children. *Investigative Ophthalmology & Visual Science,* 48**,** 1018-1024.

CHEUNG, N., LIEW, G., LINDLEY, R. I., LIU, E. Y., WANG, J. J., HAND, P., BAKER, M., MITCHELL, P. & WONG, T. Y. 2010. Retinal fractals and acute lacunar stroke. *Annals of Neurology,* 68**,** 107-111.

CLARK, T. 2002. *Scanning laser ophthalmoscopes, In: Saine PJ, Tyler ME, eds. Ophthalmic Photography: Retinal Photography, Angiography and Electronic Imaging. 2nd ed.* , Butterworth-Heinemann Medical.

COUPER, D. J., KLEIN, R., HUBBARD, L. D., WONG, T. Y., SORLIE, P. D., COOPER, L. S., BROTHERS, R. J. & NIETO, F. J. 2002. Reliability of retinal photography in the assessment of retinal microvascular characteristics: the atherosclerosis risk in communities study. *American Journal of Ophthalmology,* 133**,** 78-88.

DE MENDONCA, M. B., DE AMORIM GARCIA, C. A., NOGUEIRA RDE, A., GOMES, M. A., VALENCA, M. M. & OREFICE, F. 2007. Fractal analysis of retinal vascular tree: segmentation and estimation methods. *Arq Bras Oftalmol,* 70**,** 413-22.

DING, J., WAI, K. L., MCGEECHAN, K., IKRAM, M. K., KAWASAKI, R., XIE, J., KLEIN, R., KLEIN, B. B. K., COTCH, M. F., WANG, J. J., MITCHELL, P., SHAW, J. E., TAKAMASA, K., SHARRETT, A. R., WONG, T. Y. & GROUP, F. T. M.-E. S. 2014. Retinal vascular caliber and the development of hypertension: a meta-analysis of individual participant data. *Journal of Hypertension,* 32**,** 207-215.

DJONOV, V. G., KURZ, H. & BURRI, P. H. 2002. Optimality in the developing vascular system: branching remodeling by means of intussusception as an efficient adaptation mechanism. *Dev Dyn,* 224**,** 391-402.

DOUBAL, F. N., MACGILLIVRAY, T. J., PATTON, N., DHILLON, B., DENNIS, M. S. & WARDLAW, J. M. 2010. Fractal analysis of retinal vessels suggests that a distinct vasculopathy causes lacunar stroke. *Neurology,* 74**,** 1102-1107.

DUMSKYJ, M., ALDINGTON, S. & DORE, C., ET AL. 1996. The accurate assessment of changes in retinal vessel diameter using multiple frame electrocardiograph synchronised fundus photography. *Curr Eye Res,* 15**,** 625-32.

EDS 2008. 100 Years of Infrared. *The RPS Journal (Royal Photographic Society)* 148 571.

ELSNER, AE.; BURNS, S.A; WEITER, J.J.; HARTNETT, M. E., "Diagnostic applications of near infrared solid-state lasers in the eye," *Lasers and Electro-Optics Society Annual Meeting, 1994. LEOS '94 Conference Proceedings. IEEE* , vol.1, no., pp.14,15 vol.1, 31 Oct-3 Nov 1994

ENCYCLOPAEDIA 1987. Sensory Reception: Human Vision: Structure and function of the Human Eye. *Encyclopaedia Britannica.*

FRAZ, M. M., REMAGNINO, P., HOPPE, A., UYYANONVARA, B., RUDNICKA, A. R., OWEN, C. G. & BARMAN, S. A. 2012. Blood vessel segmentation methodologies in retinal images – A survey. *Computer Methods and Programs in Biomedicine,* 108**,** 407-433.

GAO, X. W., BHARATH, A., STANTON, A., HUGHES, A., CHAPMAN, N. & THOM, S. 2000. Quantification and characterisation of arteries in retinal images. *Computer Methods and Programs in Biomedicine,* 63**,** 133-146.

GARHOFER, G., BEK, T., BOEHM, A. G., GHERGHEL, D., GRUNWALD, J., JEPPESEN, P., KERGOAT, H., KOTLIAR, K., LANZL, I., LOVASIK, J. V., NAGEL, E., VILSER, W., ORGUL, S. & SCHMETTERER, L. 2010. Use of the retinal vessel analyzer in ocular blood flow research. *Acta Ophthalmologica,* 88**,** 717-722.

GRAUSLUND, J., GREEN, A., KAWASAKI, R., HODGSON, L., SJ LIE, A. K. & WONG, T. Y. 2010. Retinal Vascular Fractals and Microvascular and Macrovascular Complications in Type 1 Diabetes. *Ophthalmology,* 117**,** 1400-1405.

GREENLAND, S. 1995. Dose-response and trend analysis in epidemiology: alternatives to categorical analysis. *Epidemiology,* 6**,** 356-365.

Grisan E., Foracchia M., Ruggeri A. (2008). A novel method for the automatic grading of retinal vessel tortuosity. IEEE Trans. Med. Imaging 27, 310–319. 10.1109/TMI.2007.904657

GUGLETA, K., KOCHKOROV, A., KATAMAY, R., ZAWINKA, C., FLAMMER, J. & ORGUL, S. 2006a. On Pulse-Wave Propagation in the Ocular Circulation. *Investigative Ophthalmology & Visual Science,* 47**,** 4019-4025.

GUGLETA, K., ZAWINKA, C., RICKENBACHER, I., KOCHKOROV, A., KATAMAY, R., FLAMMER, J. & ORGUL, S. 2006b. Analysis of Retinal Vasodilation after Flicker Light Stimulation in Relation to Vasospastic Propensity. *Investigative Ophthalmology & Visual Science,* 47**,** 4034-4041.

GULLSTRAND, A. 1910. Neue methoden der reflexlosen ophthalmoskopie. *Berichte Deutsche Ophthalmologische Gesellschaft,* 36.

HAJEK, B. 2013. *An Exploration of Random Processes for Engineers* [Online]. Available: http://www.ifp.illinois.edu/~hajek/Papers/randomprocJan09.pdf 2013].

HANI, A. F. M. & NUGROHO, H. A. Model-based retinal vasculature enhancement in digital fundus image using independent component analysis. Industrial Electronics & Applications, 2009. ISIEA 2009. IEEE Symposium on, 4-6 Oct. 2009 2009. 160-164.

HAO, H., SASONGKO, M. B., WONG, T. Y., AZEMIN, M. Z. C., ALIAHMAD, B., HODGSON, L., KAWASAKI, R., CHEUNG, C. Y., WANG, J. J. & KUMAR, D. K. 2012. Does Retinal Vascular Geometry Vary with Cardiac Cycle? *Investigative Ophthalmology & Visual Science,* 53**,** 5799-5805.

HART, W. E., GOLDBAUM, M., COTE, B., KUBE, P. & NELSON, M. R. 1999. Measurement and classification of retinal vascular tortuosity. *Int J Med Inform,* 53**,** 239-52.

HECKE, M. V. V., DEKKER, J. M., NIJPELS, G., STOLK, R. P., HENRY, R. M. A., HEINE, R. J., BOUTER, L. M., STEHOUWER, C. D. A. & P, P. B. C. 2006. Are retinal microvascular abnormalities associated with large artery endothelial dysfunction and intima-media thickness? The Hoorn Study. *Clin. Sci. ,* 110**,** 597-604.

HEITMAR, R., BLANN, A. D., CUBBIDGE, R. P., LIP, G. Y. H. & GHERGHEL, D. 2010. Continuous Retinal Vessel Diameter Measurements: The Future in Retinal Vessel Assessment? *Investigative Ophthalmology & Visual Science,* 51**,** 5833-5839.

HIGUCHI, T. 1988. Approach to an irregular time series on the basis of the fractal theory. *Physica D: Nonlinear Phenomena,* 31**,** 277-283.

HUBBARD, L. D., BROTHERS, R. J., KING, W. N., CLEGG, L. X., KLEIN, R., COOPER, L. S., SHARRETT, A. R., DAVIS, M. D. & CAI, J. 1999. Methods for evaluation of retinal microvascular abnormalities associated with hypertension/sclerosis in the atherosclerosis risk in communities study. *Ophthalmology,* 106**,** 2269-2280.

IKRAM, M. K., DE JONG, F. J., VINGERLING, J. R., WITTEMAN, J. C. M., HOFMAN, A., BRETELER, M. M. B. & DE JONG, P. T. V. M. 2004. Are Retinal Arteriolar or Venular Diameters Associated with Markers for Cardiovascular Disorders? The Rotterdam Study. *Investigative Ophthalmology & Visual Science,* 45**,** 2129-2134.

IKRAM, M. K., VAN LEEUWEN, R., VINGERLING, J. R., HOFMAN, A. & DE JONG, P. T. V. M. 2005. Retinal Vessel Diameters and the Risk of Incident Age-Related Macular Disease: The Rotterdam study. *Ophthalmology,* 112**,** 548-552.

IKRAM, M. K., WITTEMAN, J. C. M., VINGERLING, J. R., BRETELER, M. M. B., HOFMAN, A. & DE JONG, P. T. V. M. 2006. Retinal Vessel Diameters and Risk of Hypertension. *Hypertension,* 47**,** 189-194.

JAN EVANGELISTA PURKYNĚ 1823. Commentatio de examine physiologico organi visus et systematis cutanei. *Breslau, Prussia: University of Breslau Press*.

JOSHI, G. & SIVASWAMY, J. Colour Retinal Image Enhancement Based on Domain Knowledge Computer Vision, Graphics & Image Processing, 2008. ICVGIP '08. Sixth Indian Conference on Digital Object Identifier, 2008. 591 - 598

KAIN, S., MORGAN, W. H. & YU, D.-Y. 2010. New observations concerning the nature of central retinal vein pulsation. *British Journal of Ophthalmology,* 94**,** 854-857.

KAUSHIK, S., KIFLEY, A., MITCHELL, P. & WANG, J. J. 2007. Age, Blood Pressure, and Retinal Vessel Diameter: Separate Effects and Interaction of Blood Pressure and Age. *Investigative Ophthalmology & Visual Science,* 48**,** 557-561.

KAWASAKI, R., CHE AZEMIN, M. Z., KUMAR, D. K., TAN, A. G., LIEW, G., WONG, T. Y., MITCHELL, P. & WANG, J. J. 2011. Fractal dimension of the retinal vasculature and risk of stroke: A nested case-control study. *Neurology,* 76**,** 1766-1767.

KAWASAKI, R., WANG, J. J., ROCHTCHINA, E., TAYLOR, B., WONG, T. Y., TOMINAGA, M., KATO, T., DAIMON, M., OIZUMI, T., KAWATA, S., KAYAMA, T., YAMASHITA, H. & MITCHELL, P. 2006. Cardiovascular Risk Factors and Retinal Microvascular Signs in an Adult Japanese Population: The Funagata Study. *Ophthalmology,* 113**,** 1378-1384.

KIFLEY, A., WANG, J. J., CUGATI, S., WONG, T. Y. & MITCHELL, P. 2007. Retinal Vascular Caliber, Diabetes, and Retinopathy. *American Journal of Ophthalmology,* 143**,** 1024-1026.

KIM, D. H., CHAVES, P. H. M., NEWMAN, A. B., KLEIN, R., SARNAK, M. J., NEWTON, E., STROTMEYER, E. S., BURKE, G. L. & LIPSITZ, L. A. 2011. Retinal Microvascular Signs and Disability in the Cardiovascular Health Study. *Arch Ophthalmol***,** archophthalmol.2011.360.

KLEIN, B. E. K., KLEIN, R., LEE, K. E. & DANFORTH, L. G. 2001. Drug use and five-year incidence of age-related cataracts: The Beaver Dam Eye Study. *Ophthalmology,* 108**,** 1670-1674.

KLEIN, R., KLEIN, B. E. K., KNUDTSON, M. D., WONG, T. Y. & TSAI, M. Y. 2006. Are Inflammatory Factors Related to Retinal Vessel Caliber?: The Beaver Dam Eye Study. *Arch Ophthalmol,* 124**,** 87-94.

KLEIN, R., KLEIN, B. E. K., MOSS, S. E. & WONG, T. Y. 2007. Retinal Vessel Caliber and Microvascular and Macrovascular Disease in Type 2 Diabetes: XXI: The Wisconsin Epidemiologic Study of Diabetic Retinopathy. *Ophthalmology,* 114**,** 1884-1892.

KNUDTSON, M. D., KLEIN, B. E. K., KLEIN, R., WONG, T. Y., HUBBARD, L. D., LEE, K. E., MEUER, S. M. & BULLA, C. P. 2004. Variation associated with measurement of retinal vessel diameters at different points in the pulse cycle. *British Journal of Ophthalmology,* 88**,** 57-61.

KNUDTSON, M. D., LEE, K. E., HUBBARD, L. D., WONG, T. Y., KLEIN, R. & KLEIN, B. E. 2003. Revised formulas for summarizing retinal vessel diameters. *Current Eye Research,* 27**,** 143-9.

KOFOED, P. K., SANDER, B., ZUBIETA-CALLEJA, G., KESSEL, L. & LARSEN, M. 2009. Retinal Vessel Diameters in Relation to Hematocrit Variation during Acclimatization of Highlanders to Sea Level Altitude. *Investigative Ophthalmology & Visual Science,* 50**,** 3960-3963.

KOTLIAR, K. E. & LANZL, I. M. 2011. Can Vascular Function Be Assessed by the Interpretation of Retinal Vascular Diameter Changes? *Investigative Ophthalmology & Visual Science,* 52**,** 635-636.

KUMAR, D. K., ALIAHMAD, B. & HAO, H., Retinal Vessel Diameter Measurement Using Unsupervised Linear Discriminant Analysis, *ISRN Ophthalmology,* vol. 2012, p. 7, 2012.

KUMAR, D. K., ALIAHMAD, B., HAO, H., CHE AZEMIN, M. Z. & KAWASAKI, R. 2013. A Method for Visualization of Fine Retinal Vascular Pulsation Using Nonmydriatic Fundus Camera Synchronised with Electrocardiogram. *ISRN Ophthalmology,* 2013**,** 9.

KYLSTRA, J., WIERZBICKI, T., WOLBARSHT, M., LANDERS, M. & STEFANSSON, E. 1986. The relationship between retinal vessel tortuosity, diameter, and transmural pressure. *Graefe's Archive for Clinical and Experimental Ophthalmology,* 224**,** 477-480.

LEE, K. E., KLEIN, B. E. K., KLEIN, R. & KNUDTSON, M. D. 2004. Familial Aggregation of Retinal Vessel Caliber in the Beaver Dam Eye Study. *Investigative Ophthalmology & Visual Science,* 45**,** 3929-3933.

LEGLER, U. & JONAS, J. B. 2009. Frequency of Spontaneous Pulsations of the Central Retinal Vein in Glaucoma. *Journal of Glaucoma,* 18**,** 210-212.

LEUNG, H., WANG, J. J., ROCHTCHINA, E., TAN, A. G., WONG, T. Y., HUBBARD, L. D., KLEIN, R. & MITCHELL, P. 2003a. Computer-assisted retinal vessel measurement in an older population: correlation between right and left eyes. *Clinical & Experimental Ophthalmology,* 31**,** 326-330.

LEUNG, H., WANG, J. J., ROCHTCHINA, E., TAN, A. G., WONG, T. Y., KLEIN, R., HUBBARD, L. D. & MITCHELL, P. 2003b. Relationships between Age, Blood Pressure, and Retinal Vessel Diameters in an Older Population. *Investigative Ophthalmology & Visual Science,* 44**,** 2900-2904.

LEVINE, D. N. 1998. Spontaneous Pulsation of the Retinal Veins. *Microvascular Research,* 56**,** 154-165.

LIEW, G., MITCHELL, P., LEEDER, S. R., SMITH, W., WONG, T. Y. & WANG, J. J. 2006a. Regular aspirin use and retinal microvascular signs: the Blue Mountains Eye Study. *Journal of Hypertension,* 24**,** 1329-1335.

LIEW, G., MITCHELL, P., ROCHTCHINA, E., WONG, T. Y., HSU, W., LEE, M. L., WAINWRIGHT, A. & WANG, J. J. 2011. Fractal analysis of retinal microvasculature and coronary heart disease mortality. *European Heart Journal,* 32**,** 422-429.

LIEW, G., WANG, J. J., MITCHELL, P. & WONG, T. Y. 2008. Retinal Vascular Imaging: A New Tool in Microvascular Disease Research. *Circulation: Cardiovascular Imaging,* 1**,** 156-161.

LIEW, G., WONG, T. Y., MITCHELL, P. & WANG, J. J. 2006b. Are Narrower or Wider Retinal Venules Associated With Incident Hypertension? *Hypertension,* 48**,** e10.

LIM, M., SASONGKO, M. B., IKRAM, M. K., LAMOUREUX, E., WANG, J. J., WONG, T. Y. & CHEUNG, C. Y. 2013. Systemic Associations of Dynamic Retinal Vessel Analysis: A Review of Current Literature. *Microcirculation,* 20**,** 257-268.

LINDLEY, R. I., WANG, J. J., WONG, M.-C., MITCHELL, P., LIEW, G., HAND, P., WARDLAW, J., DE SILVA, D. A., BAKER, M., ROCHTCHINA, E., CHEN, C., HANKEY, G. J., CHANG, H.-M., FUNG, V. S. C., GOMES, L. & WONG, T. Y. 2009. Retinal microvasculature in acute lacunar stroke: a cross-sectional study. *The Lancet Neurology,* 8**,** 628-634.

LOUWIES, T., PANIS, L. I., KICINSKI, M., DE BOEVER, P. & S, N. T. 2012. Retinal microvascular responses to short-term changes in particulate air pollution in healthy adults. *Environ Health Perspect***,** 1011-1016.

MAENHAUT, N., BOUSSERY, K., DELAEY, C. & VAN DE VOORDE, J. 2007. Control of Retinal Arterial Tone by a Paracrine Retinal Relaxing Factor. *Microcirculation,* 14**,** 39-48.

MASTERS, B. R. 2004. Fractal analysis of the vascular tree in the human retina. *Annu Rev Biomed Eng,* 6**,** 427-52.

MCCANNA, C. D., MYERS, C. E., LEE, M., DANFORTH, L. G., MOORE, E. L., MEUER, S. M., KLEIN, R. & KLEIN, B. E. K. 2013. Variability of Measurement of Retinal Vessel Diameters. *Ophthalmic Epidemiology,* 20**,** 392-401.

MCGEECHAN, K., LIEW, G., MACASKILL, P., IRWIG, L., KLEIN, R., KLEIN, B. E. K., WANG, J. J., MITCHELL, P., VINGERLING, J. R., DEJONG, P. T. V. M., WITTEMAN, J. C. M., BRETELER, M. M. B., SHAW, J., ZIMMET, P. & WONG, T. Y. 2009. Meta-analysis: Retinal Vessel Caliber and Risk for Coronary Heart Disease. *Annals of Internal Medicine,* 151**,** 404-413.

MCGRAW, K. O. & WONG, S. P. 1996. Forming Inferences About Some Intraclass Correlation Coefficients. *Psychological Methods,* 1**,** 30-46.

MORET, F., POLOSCHEK, C. M., LAGREZE, W. A. & BACH, M. 2011. Visualization of fundus vessel pulsation using principal component analysis. *Invest Ophthalmol Vis Sci,* 52**,** 5457-64.

MORGAN, W. H., HAZELTON, M. L., AZAR, S. L., HOUSE, P. H., YU, D.-Y., CRINGLE, S. J. & BALARATNASINGAM, C. 2004. Retinal venous pulsation in glaucoma and glaucoma suspects. *Ophthalmology,* 111**,** 1489-1494.

MURAMATSU, C., NAKAGAWA, T., SAWADA, A., HATANAKA, Y., HARA, T., YAMAMOTO, T. & FUJITA, H. 2011. Automated segmentation of optic disc region on retinal fundus photographs: Comparison of contour modeling and pixel classification methods. *Computer Methods and Programs in Biomedicine,* 101**,** 23-32.

MURRAY, C. D. 1926. The Physiological Principle of Minimum Work: I. The Vascular System and the Cost of Blood Volume. *Proc Natl Acad Sci U S A,* 12**,** 207-14.

NEIDER, M. 2004. Practical retinal photography and digital imaging techniques. *Archives of Ophthalmology,* 122**,** 941-941.

NEUBARUER, A. S., LUDTKE, M., HARITOGLOU, C., PRIGLINGER, S. & KAMPIK, A. 2008. Retinal Vessel Analysis Reproducibility in Assessing Cardiovascular Disease. *Optometry & Vision Science,* 85**,** E247-E254.

NEWSOM, R. S.B., SULLIVAN, P. M., RASSAM, S. M. B., JAGOE R. & KOHNER E. M. 1992. Retinal vessel measurement: comparison between observer and computer driven methods. *Graefe's Archive for Clinical and Experimental Ophthalmology,* 230**,** 221-225.

NIEMEIJER, M., ABRAMOFF, M. D. & VAN GINNEKEN, B. Automated localization of the optic disc and the fovea. Engineering in Medicine and Biology Society, 2008. EMBS 2008. 30th Annual International Conference of the IEEE, 20-25 Aug. 2008 2008. 3538-3541.

ORAM, J. J., MCWILLIAMS, J. C. & STOLZENBACH, K. D. 2008. Gradient-based edge detection and feature classification of sea-surface images of the Southern California Bight. *Remote Sensing of Environment,* 112**,** 2397-2415.

PAQUES, M., TICK, S., GENEVOIS, O., ADAM, P. & SAHEL, J. A. 2008. Retinal vessel pulse amplitude in health and disease. *Acta Ophthalmologica,* 86.

PARR, J. & SPEARS, G. 1974. General caliber of the retinal arteries expressed as the equivalent width of the central retinal artery. *Am J Ophthalmol***,** 472-477.

PATTON, N., MAINI, R., MACGILLIVARY, T., ASLAM, T. M., DEARY, I. J. & DHILLON, B. 2005. Effect of Axial Length on Retinal Vascular Network Geometry. *American Journal of Ophthalmology,* 140**,** 648.e1-648.e7.

PLUHACEK, F. & POSPISIL, J. 2010. *Digital Electro-optical Registration and Analysis Methods for Glaucoma Diagnostic*, Nova Science Publishers.

PRIES, A. R. & SECOMB, T. W. 2008. Blood Flow in Microvascular Networks. *In:* TUMA, R. F., DURAN, W. N. & LEY, K. (eds.) *Handbook of Physiology: Microcirculation.* Amsterdam: Elsevier.

QUIGLEY H.A., BROWN A.E., MORRISON J.D., DRANCE S.M. The Size and Shape of the Optic Disc in Normal Human Eyes. Arch Ophthalmol. 1990;108(1):51-57.

RESHEF, D. S. 1999. *Evaluation of generalized arteriolar narrowing expressed as central retinal artery/vein equivalents ratio (CRAVER) using ECG synchronised retinal photography.* PhD Thesis, Johns Hopkins University.

RETVIC 2008. Assessment of retinal vessle diameter using IVAN software. RetVIC Grading Protocol #04. R. V. I. C.

REZATOFIGHI, S. H., ROODAKI, A. & AHMADI NOUBARI, H. An enhanced segmentation of blood vessels in retinal images using contourlet. EMBS 2008, 2008. 3530-3533.

RIVA, C. E. & SCHMETTERER, L. 2008. Microcirculation of the Ocular Fundus. *In:* TUMA RF, DURAN WN & LEY K (eds.) *Handbook of Physiology: Microcirculation.* Amsterdam: Elsevier.

RONALD, K., BARBARA, E. K. K., SCOT, E. M., TIEN, Y. W. & SHARRETT, A. R. 2006. Retinal Vascular Caliber in Persons with Type 2 Diabetes: The Wisconsin Epidemiological Study of Diabetic Retinopathy: XX. *Ophthalmology,* 113**,** 1488-1498.

RYAN, S. J., SCHACHAT, A. P., WILKINSON, C. P., HINTON, D. R., SADDA, S. & WIEDEMANN, P. 2012. *Retina (5th edition)*, Elsevier Health Sciences.

SABANAYAGAM, C., SHANKAR, A., KOH, D., CHIA, K. S., SAW, S. M., LIM, S. C., TAI, E. S. & WONG, T. Y. 2009. Retinal Microvascular Caliber and Chronic Kidney Disease in an Asian Population. *American Journal of Epidemiology,* 169**,** 625-632.

SAINE, P. J., TYLER, M. E. & EDS 2002. *Ophthalmic Photography: Retinal Photography, Angiography, and Electronic Imaging*, Butterworth-Heinemann Medical.

SASONGKO, M., WANG, J. J., DONAGHUE, K. C., CHEUNG, N., BENITEZ-AGUIRRE, P., JENKINS, A., HSU, W., LEE, M.-L. & WONG, T. Y. 2010. Alterations in Retinal Microvascular Geometry in Young Type 1 Diabetes. *Diabetes Care*.

SASONGKO, M., WONG, T., NGUYEN, T., CHEUNG, C., SHAW, J. & WANG, J. 2011. Retinal vascular tortuosity in persons with diabetes and diabetic retinopathy. *Diabetologia,* 54**,** 2409-2416.

SASONGKO, M. B., HODGSON, L. A. B., WONG, T. Y., KAWASAKI, R., CHEUNG, C. Y., HSU, W., LI LEE, M., LAU, P. Q. F., MITCHELL, P. & WANG, J. J. 2012. Correlation and Reproducibility of Retinal Vascular Geometric Measurements for Stereoscopic Retinal Images of the Same Eyes. *Ophthalmic Epidemiology,* 19**,** 322-327.

SEIFERTL, B. & VILSER, W. 2002. Retinal Vessel Analyzer (RVA)--design and function. *Biomed Tech (Berl),* 47**,** 678-81.

SERR, H. 1937. Zur Analyse der spontanen Pulsercheinungen in den Netzhautgefassen. *Graefe's Arch. Ophthal***,** 487-505.

SHERRY, L. M., WANG, J. J., ROCHTCHINA, E., WONG, T. Y., KLEIN, R., HUBBARD, L. D. & MITCHELL, P. 2002. Reliability of computer-assisted retinal vessel measurement in a population. *Clinical & Experimental Ophthalmology,* 30**,** 179-182.

SILVA, R. 2013. *An Overview of PAL NTSC and SECAM Video Standards* [Online]. Available: http://hometheater.about.com/cs/consumerresources/a/aawhosyourpala.htm 2013].

SMITH, W., WANG, J. J., WONG, T. Y., ROCHTCHINA, E., KLEIN, R., LEEDER, S. R. & MITCHELL, P. 2004. Retinal Arteriolar Narrowing Is Associated With 5-Year Incident Severe Hypertension: The Blue Mountains Eye Study *Hypertension,* 44**,** 442.

SOFKA, M.; STEWART, C.V., "Retinal Vessel Centerline Extraction Using Multiscale Matched Filters, Confidence and Edge Measures," *Medical Imaging, IEEE Transactions on* , vol.25, no.12, pp.1531,1546, Dec. 2006

STANTON, A. V., WASAN, B., CERUTTI, A., FORD, S., MARSH, R., SEVER, P. P., THOM, S. A. & HUGHES, A. D. 1995. Vascular network changes in the retina with age and hypertension. *J Hypertens,* 13**,** 1724-8.

STEWART, C. V., CHIA-LING, T. & ROYSAM, B. 2003. The dual-bootstrap iterative closest point algorithm with application to retinal image registration. *Medical Imaging, IEEE Transactions on,* 22**,** 1379-1394.

SUN, C., WANG, J. J., MACKEY, D. A. & WONG, T. Y. 2009. Retinal Vascular Caliber: Systemic, Environmental, and Genetic Associations. *Survey of Ophthalmology,* 54**,** 74-95.

SWANSON, E. A., IZATT, J. A., LIN, C. P., FUJIMOTO, J. G., SCHUMAN, J. S., HEE, M. R., HUANG, D. & PULIAFITO, C. A. 1993. In vivo retinal imaging by optical coherence tomography. *Optics Letters,* 18**,** 1864-1866.

TAARNH J, N. C. B. B., LARSEN, M., SANDER, B., KYVIK, K. O., KESSEL, L., HOUGAARD, J. L. & S RENSEN, T. I. A. 2006. Heritability of Retinal Vessel Diameters and Blood Pressure: A Twin Study. *Investigative Ophthalmology & Visual Science,* 47**,** 3539-3544.

UMBAUGH, S. E. 2011. *Digital Image Processing and Analysis: Human and Computer Vision Applications with CVIPtools*, CRC Press.

VAN BELLE, G. 2008. *Statistical Rules of Thumb*, Wiley.

VON HELMHOLTZ, H. L. F. 1851. Beschreibung eines Augen-Spiegels. :A. Farstnerische Verlagsbuchhandlung.

WALKER, J. & ALMOND, P. (eds.) 2010. *Interpreting Statistical Findings: a guide for health professionals and students*: Open University Press, McGraw-Hill Education.

WALTER, T. & KLEIN, J.-C. 2001. Segmentation of Color Fundus Images of the Human Retina: Detection of the Optic Disc and the Vascular Tree Using Morphological Techniques Medical Data Analysis. *In:* CRESPO, J., MAOJO, V. & MARTIN, F. (eds.). Springer Berlin / Heidelberg.

WANG, J. J., LIEW, G., WONG, T. Y., SMITH, W., KLEIN, R., LEEDER, S. R. & MITCHELL, P. 2006a. Retinal vascular calibre and the risk of coronary heart disease-related death. *Heart,* 92**,** 1583-1587.

WANG, J. J., TAYLOR, B., WONG, T. Y., CHUA, B., ROCHTCHINA, E., KLEIN, R. & MITCHELL, P. 2006b. Retinal Vessel Diameters and Obesity: A Population-Based Study in Older Persons[ast]. *Obesity,* 14**,** 206-214.

WEINSTEIN, P. 1939. Significance of venous pulsation of the eyeground. *Br J Ophthalmol,* 23**,** 396-398.

WEISSTEIN, E. W. *Normal Distribution* [Online]. Available: MathWorld--A Wolfram Web Resource. http://mathworld.wolfram.com/NormalDistribution.html 2013].

WHITTAKER, E. T. & ROBINSON, G. (eds.) 1967. *Normal Frequency Distribution*: New York: Dover.

WILLIAMSON-NOBLE, F. A. 1952. Venous pulsation. *Trans. Ophthal. Soc. UK***,** 317-328.

WITT, N., WONG, T. Y., HUGHES, A. D., CHATURVEDI, N., KLEIN, B. E., EVANS, R., MCNAMARA, M., THOM, S. A. M. & KLEIN, R. 2006. Abnormalities of Retinal Microvascular Structure and Risk of Mortality From Ischemic Heart Disease and Stroke. *Hypertension,* 47**,** 975-981.

WONG, T., SHANKAR, A., KLEIN, R., KLEIN, B. K. & HUBBARD, L. D. 2005a. Retinal arteriolar narrowing, hypertension, and subsequent risk of diabetes mellitus. *Archives of Internal Medicine,* 165**,** 1060-1065.

WONG, T. Y. 2004. Is retinal photography useful in the measurement of stroke risk? *The Lancet Neurology,* 3**,** 179-183.

WONG, T. Y., DUNCAN, B. B., GOLDEN, S. H., KLEIN, R., COUPER, D. J., KLEIN, B. E. K., HUBBARD, L. D., SHARRETT, A. R. & SCHMIDT, M. I. 2004a. Associations between the Metabolic Syndrome and Retinal Microvascular Signs: The Atherosclerosis Risk in Communities Study. *Investigative Ophthalmology & Visual Science,* 45**,** 2949-2954.

WONG, T. Y., HUBBARD, L. D., KLEIN, R., MARINO, E. K., KRONMAL, R., SHARRETT, A. R., SISCOVICK, D. S., BURKE, G. & TIELSCH, J. M. 2002a. Retinal microvascular abnormalities and blood pressure in older people: the Cardiovascular Health Study. *British Journal of Ophthalmology,* 86**,** 1007-1013.

WONG, T. Y., ISLAM, F. M. A., KLEIN, R., KLEIN, B. E. K., COTCH, M. F., CASTRO, C., SHARRETT, A. R. & SHAHAR, E. 2006a. Retinal Vascular Caliber, Cardiovascular Risk Factors, and Inflammation: The Multi-Ethnic Study of Atherosclerosis (MESA). *Investigative Ophthalmology & Visual Science,* 47**,** 2341-2350.

WONG, T. Y., KAMINENI, A., KLEIN, R., SHARRETT, A. R., KLEIN, B. E., SISCOVICK, D. S., CUSHMAN, M. & DUNCAN, B. B. 2006b. Quantitative Retinal Venular Caliber and Risk of Cardiovascular Disease in Older Persons: The Cardiovascular Health Study. *Arch Intern Med,* 166**,** 2388-2394.

WONG, T. Y., KLEIN, R., KLEIN, B. E. K., MEUER, S. M. & HUBBARD, L. D. 2003. Retinal Vessel Diameters and Their Associations with Age and Blood Pressure. *Investigative Ophthalmology & Visual Science,* 44**,** 4644-4650.

WONG, T. Y., KLEIN, R., SHARRETT, A. R., DUNCAN, B. B., COUPER, D. J., KLEIN, B. E., HUBBARD, L. D. & NIETO, F. J. 2004b. Retinal arteriolar diameter and risk for hypertension. *Ann Intern Med,* 140**,** 248-55.

WONG, T. Y., KLEIN, R., SHARRETT, A. R., DUNCAN, B. B., COUPER, D. J., TIELSCH, J. M., KLEIN, B. E. & HUBBARD, L. D. 2002b. Retinal arteriolar narrowing and risk of coronary heart disease in men and women. The Atherosclerosis Risk in Communities Study. *Jama,* 287**,** 1153-9.

WONG, T. Y., KLEIN, R., SHARRETT, A. R., SCHMIDT, M. I., PANKOW, J. S., COUPER, D. J., KLEIN, B. E. K., HUBBARD, L. D. & DUNCAN, B. B. 2002c. Retinal Arteriolar Narrowing and Risk of Diabetes Mellitus in Middle-aged Persons. *Journal of the American Medical Association,* 287**,** 2528-2533.

WONG, T. Y., KNUDTSON, M. D., KLEIN, B. E. K., KLEIN, R. & HUBBARD, L. D. 2005b. Medication use and retinal vessel diameters. *American Journal of Ophthalmology,* 139**,** 373-375.

WONG, T. Y., KNUDTSON, M. D., KLEIN, R., KLEIN, B. E. K., MEUER, S. M. & HUBBARD, L. D. 2004c. Computer-assisted measurement of retinal vessel diameters in the Beaver Dam Eye Study: methodology, correlation between eyes, and effect of refractive errors. *Ophthalmology,* 111**,** 1183-1190.

WONG, T. Y., SHANKAR, A., KLEIN, R. & KLEIN, B. E. K. 2004d. Retinal Vessel Diameters and the Incidence of Gross Proteinuria and Renal Insufficiency in People With Type 1 Diabetes. *Diabetes,* 53**,** 179-184.

WOON WH, FITZKE FW, CHESTER GH & AL., E. 1990. The scanning laser ophthalmoscope: basic principles and applications. *J Ophthalmic Photography,* 12**,** 17-23.

XING, C., KLEIN, B. E. K., KLEIN, R., JUN, G., LEE, K. E. & IYENGAR, S. K. 2006. Genome-Wide Linkage Study of Retinal Vessel Diameters in the Beaver Dam Eye Study. *Hypertension,* 47**,** 797-802.

XU, J., CHUTATAPE, O., SUNG, E., ZHENG, C. & CHEW TEC KUAN, P. 2007. Optic disk feature extraction via modified deformable model technique for glaucoma analysis. *Pattern Recognition,* 40**,** 2063-2076.

YIP, W., CHEUNG, C. Y.-L., HAMZAH, H., HAN, C., HSU, W., LEE, M. L. & WONG, T. Y. 2012. Are Computer-assisted programs for measuring Retinal Vascular Caliber Interchangeable? *ARVO Abstract*

ZAMIR, M., MEDEIROS, J. & CUNNINGHAM, T. 1976. Optimality principles in arterial branching. *Journal of Theoretical Biology,* 62**,** 227-251.

ZAMIR, M., MEDEIROS, J. A. & CUNNINGHAM, T. K. 1979. Arterial bifurcations in the human retina. *The Journal of General Physiology,* 74**,** 537-548.

ZHU, X., RANGAYYAN, R. M., & ELLS, A. L. 2010. Detection of the Optic Nerve Head in Fundus Images of the Retina Using the Hough Transform for Circles.*Journal of Digital Imaging*, 23(3), 332–341.

Appendix

Appendix 1: Visualisation of Retinal Dynamic

The animated retinal dynamic can be viewed using ECG synchronised retinal photographs described in Chapter 7. The animation can be downloaded from online or thesis CD.

https://www.dropbox.com/s/2t3nwbbahp3yr7w/94.gif

https://www.dropbox.com/s/eun2cd776kwq5i0/101.gif

https://www.dropbox.com/s/j7cy1gwuc4lp0aq/120.gif

https://www.dropbox.com/s/476lh4t5zm77v6a/123.gif

https://www.dropbox.com/s/ad50a6dxczm5tbu/126.gif

https://www.dropbox.com/s/eb4z14yxaxc30xn/136.gif